UNIVERSIDAD DE MURCIA

ESCUELA INTERNACIONAL DE DOCTORADO

TESIS DOCTORAL

Antithrombin role beyond hemostasis.

Papel de la antitrombina más allá de la hemostasia.

D.ª Julia Peñas Martínez

2024

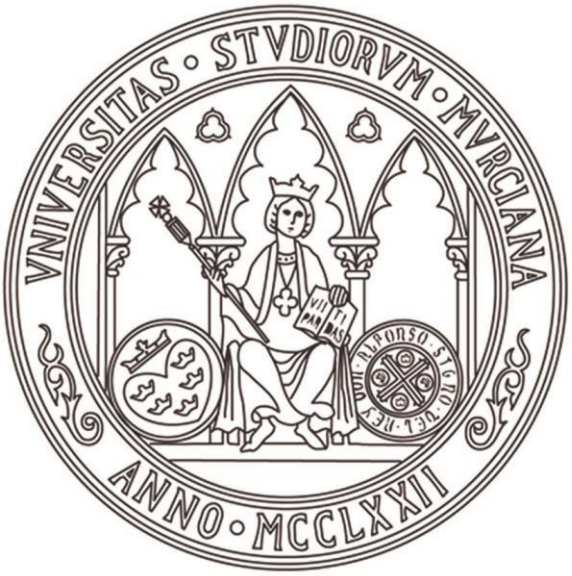

UNIVERSIDAD DE MURCIA

ESCUELA INTERNACIONAL DE DOCTORADO

TESIS DOCTORAL

Antithrombin role beyond hemostasis.

Papel de la antitrombina más allá de la hemostasia.

Autor: D.ª Julia Peñas Martínez

Director/es: D.ª Irene Martínez Martínez

Tutor: D. Vicente Vicente García

UNIVERSIDAD DE MURCIA

DECLARACIÓN DE AUTORÍA Y ORIGINALIDAD DE LA TESIS PRESENTADA EN MODALIDAD DE COMPENDIO O ARTÍCULOS PARA OBTENER EL TÍTULO DE DOCTOR

Aprobado por la Comisión General de Doctorado el 19-10-2022

D./Dña. Julia Peñas Martínez

doctorando del Programa de Doctorado en

Integración y modulación de señales en biomedicina

de la Escuela Internacional de Doctorado de la Universidad Murcia, como autor/a de la tesis presentada para la obtención del título de Doctor y titulada:

Antithrombin role beyond hemostasis / Papel de la antitrombina más allá de la hemostasia

y dirigida por,

D./Dña. Irene Martínez Martínez

D./Dña. Vicente Vicente García

DECLARO QUE:

La tesis es una obra original que no infringe los derechos de propiedad intelectual ni los derechos de propiedad industrial u otros, de acuerdo con el ordenamiento jurídico vigente, en particular, la Ley de Propiedad Intelectual (R.D. legislativo 1/1996, de 12 de abril, por el que se aprueba el texto refundido de la Ley de Propiedad Intelectual, modificado por la Ley 2/2019, de 1 de marzo, regularizando, aclarando y armonizando las disposiciones legales vigentes sobre la materia), en particular, las disposiciones referidas al derecho de cita, cuando se han utilizado sus resultados o publicaciones.

Además, al haber sido autorizada como compendio de publicaciones o, tal y como prevé el artículo 29.8 del reglamento, cuenta con:

- *La aceptación por escrito de los coautores de las publicaciones de que el doctorando las presente como parte de la tesis.*
- *En su caso, la renuncia por escrito de los coautores no doctores de dichos trabajos a presentarlos como parte de otras tesis doctorales en la Universidad de Murcia o en cualquier otra universidad.*

Del mismo modo, asumo ante la Universidad cualquier responsabilidad que pudiera derivarse de la autoría o falta de originalidad del contenido de la tesis presentada, en caso de plagio, de conformidad con el ordenamiento jurídico vigente.

En Murcia, a 19 de julio de 2024

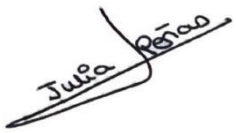

Fdo.: Julia Peñas Martínez

Esta DECLARACIÓN DE AUTORÍA Y ORIGINALIDAD debe ser insertada en la primera página de la tesis presentada para la obtención del título de Doctor.

Información básica sobre protección de sus datos personales aportados	
Responsable:	Universidad de Murcia. Avenida teniente Flomesta, 5. Edificio de la Convalecencia. 30003; Murcia. Delegado de Protección de Datos: dpd@um.es
Legitimación:	La Universidad de Murcia se encuentra legitimada para el tratamiento de sus datos por ser necesario para el cumplimiento de una obligación legal aplicable al responsable del tratamiento. art. 6.1.c) del Reglamento General de Protección de Datos
Finalidad:	Gestionar su declaración de autoría y originalidad
Destinatarios:	No se prevén comunicaciones de datos
Derechos:	Los interesados pueden ejercer sus derechos de acceso, rectificación, cancelación, oposición, limitación del tratamiento, olvido y portabilidad a través del procedimiento establecido a tal efecto en el Registro Electrónico o mediante la presentación de la correspondiente solicitud en las Oficinas de Asistencia en Materia de Registro de la Universidad de Murcia

A mi abuelos Julia y Pepe y a mis padres,

Ojito con la niña, ojito con la niña

AGRADECIMIENTOS

Creo que esta es la página que más me ha costado escribir de la tesis y con la que más he llorado...

En primer lugar, haber hecho la tesis doctoral ha sido un gran avance profesional para mí. Recuerdo en la carrera estudiar lo que era un western blot, una PCR o un ELISA y me parecían técnicas futurísticas con las que soñaba poder hacer algún día. Pero más recuerdo aún la increíble sensación de hacerlas por primera vez en el Centro Regional de Hemodonación (CRH), lo cual no habría sido posible si no hubiera estado rodeada de todos los magníficos investigadores e investigadoras que trabajan allí y que habéis hecho posible que pueda cumplir este sueño. Así que gracias por haberme estado siempre ahí, no solo a aprender cada técnica, a escribir, o a razonar científicamente hablando, si no a resolverme cada duda por el camino y a enseñarme lo que es el buen compañerismo.

Por otro lado, quiero daros a todos y todas las gracias por lo siguiente: durante todos estos años, levantarme e ir al CRH no era solo ir a trabajar, era estar con todos vosotros y vosotras, mi preciosa familia científica. Cada uno me habéis aportado algo precioso, y espero que quede plasmado en estas páginas:

Empiezo agradeciendo al Dr. Vicente no solo haberme dado la oportunidad de formar parte de este mundo, si no a enseñarme que el trabajo duro tiene su recompensa, conocido por todos ya como “la ley del meteoro”.

Quiero continuar con la patrona Irene. Luchadora como pocas y ejemplo de que familia e investigación pueden ir de la mano. Te agradezco la paciencia que has tenido conmigo y todo lo que me has enseñado, que abarca desde todos tus conocimientos de la antitrombina hasta convertirme en la investigadora que creo que he conseguido llegar a ser. Pero quiero hacer especial hincapié en todo lo que has luchado para que pudiera hacer la tesis contigo, cosa que estoy segura que cualquiera hubiera desistido mucho antes…así que mil gracias por todo.

En cuanto al resto de Sirenitos (equipo Irene) presentes y pasados, tengo que nombrar a David, Salva, Carmencita Ortega y Nataliya. David, espero que consigas alcanzar tu

Nirvana personal y el futuro profesional por el que tanto estás luchando. Carmencita, eres una máquina en cada aspecto de tu vida, no cambies. Salva y Nataliya… gran parte de mi formación fuisteis vosotros, qué paciencia divina tuvisteis, y cuánto lloré el día que os fuisteis... Sois maravillosos

Gracias al séquito de Anas (Marín, Zamora y Sánchez) de Pepe Rivera. De ellas decir que sois un show andante en el buen sentido y que espero que os vaya todo bien en la vida, porque cada una sois súper especiales, no lo olvidéis. Y de Pepe decir que hace tiempo le prometí que cuando le hiciera reír 5 veces expondría la tesis. Y estoy orgullosa de decir que lo he conseguido muchas más veces, aunque él no lo vaya a reconocer.

Gracias al equipo antitrombina: Belén, Uge, Esther, Javi, María PC, Pedro pc, Juanjo y Toñi. A Uge por los cafés y largas conversaciones en la esquina del mal, a Juanjo por sus constantes burradas con las que he llorado de la risa, y a Toñi por haber estado siempre siempre ahí en la más mínima duda que he tenido, o simplemente para darme un abrazo cálido.

A los miRNAs + team Sonia: Constant, Rocío, Sonia, Pedro papito, Salva, Laura, Alberto, Nuria… Si algo os caracteriza a la mayoría, es que se hable lo que se hable con vosotros, acaba a carcajada limpia. Así que por favor seguir así. Sonia, gracias de corazón, no solo por nuestras conversaciones infinitas, si no por haberme respondido cada duda, fuera la hora, momento y lugar que fuera. Eres una gran investigadora y persona, da gusto rodearse de gente como tú. Pin y Pon… espero poder meteros en el grupo de las carcajadas algún día jajajaja Salva, sigue sacando a relucir esa picaresca que te caracteriza y espero volver a llevarte a tu casa algún día, porque eso significará que seguimos viéndonos.

A Paqui agradecerle la oportunidad que me dio de publicar mi primer artículo con ella, y a enseñarme a lavar un ELISA golpeando con la fuerza suficiente para quitar el lavado sin llegar a romper el lavabo. A mi patrón Raúl, los 2 años y medio que trabajé contigo los sentí agobiantes en su momento, porque era llevar las secuencias de pacientes que necesitaban resultados cuanto antes junto a la tesis… Pero era hablar contigo, ponernos música mientras extraíamos muestras, o hablar de futuro y se me pasaba ese agobio y solo pensaba en la suerte que tenía de aprender al lado de semejante profesional. Y esa

última es la preciosa sensación que se me ha quedado de esos 2 años y pico. A Ernestito, meeeeeeeeehhhhh, el mejor compi de escritorio y de juegos de mesa. Qué bien que entraras justo solo un año después de mí, porque así he podido ver cómo has crecido personal y profesionalmente. Gracias en especial por tu paciencia con el BrdU y la estadística, parte de mi tesis no existiría sin tu ayuda. Y por último a Mari Luz, espero que algún día quieras reconocer cuánto nos parecemos en cuanto a forma de ser, y espero que lo reconozcas porque tienes una personalidad envidiable de luchadora y graciosa.

Gracias a mis Pedros…creo que es políticamente incorrecto escribir lo que pienso sobre vosotros aquí así que, esa parte me la salto y os digo primero lo mucho que os quiero a los 3. A Pedro papito por aguantarme desde primera hora de la mañana que iba a buscarlo para el café, porque sin él, casi que prefería no tomármelo, y por los cotis que tanto nos gustan a ambos. A Pedro pc por acompañarme a comprar, por la confianza que me has dado para conocer lo bello que eres, y por las conversaciones infinitas durante fiestas interminables. Y a Pedro pistolas, la gran incorporación del CRH, y a quien siento como un hermanito pequeño. Por sus imitaciones que espero que no decaigan, por nuestras constantes risas y bromas, hasta nuestros "piques", por acompañarme 24/7 y simplemente por ser como eres, eres un "maquinista".

Gracias a Reyes y sus "varitas mágicas" compartidas, Silvia, María José, Candela, todo serología y enfermería, Darío, Ginés, Juan Fran, Alberto, Ana Jiménez, Tania, Marina y Marisa. Todos y todas formáis parte de ese sentimiento de alegría y emoción que siento al entrar en el CRH.

Especial mención quiero hacer a mi mamá y papá del laboratorio, Rosa y Padilla, y a mi hermanita Vero. Quiero mucho a todo el mundo, pero lo que siento por vosotros es devoción. No sé cómo agradeceros vuestra grata existencia, los despreñamientos, los buenos días princhecho, o las conversaciones infinitas…los cafés eternos, toda la ayuda personal y profesional, el cariño que me habéis transmitido. Sois gente maravillosa, tanto por dentro, como por fuera, y los 3 valéis millones, que nada ni nadie os haga pensar lo contrario.

A mis Tricantinas, a las Carapapas, a los Girasoles, a los Monos y las monas (a Marisa como mi representante científica en especial) y a mis compis de carrera favoritas

(Rosalba, Sara, José y Paula). Todas habéis tenido la paciencia de escucharme café/cerveza en mano cuando he tenido algún momento de bajón durante estos años o con algún rollo de algún resultado que me hacía ilusión contaros. Qué lujo saber que con pedíroslo aparecéis para apoyarme estéis donde estéis.

A mi Manolo, solo decirte que gracias por ser "mi suerte", y ya tú y yo sabemos todo el amor que eso abarca. Y gracias a tu familia (la cual considero mi familia también), sobre todo por los arroces de los domingos, que me llenaban de fuerza gastronómica y anímicamente para el lunes empezar a tope la semana.

Y por último, quiero dedicarles esta tesis a la gente que más quiero en este mundo, que son mis padres y mis abuelos Pepe y Julia. A mi mamá Josefina, gracias por ser mi personal shopper y por haberme cogido el teléfono todos los santos días que te he llamado después del CRH. Me enorgullece decir que no solo eres mi mami, sino también una de mis mejores amigas. A mi padre le agradezco no solo sus visitas esporádicas al CRH que me amenizaban el día, si no el ejemplo que es a seguir como gran trabajador y luchador por su familia, espero que algún día consiga hacerte transmitir y que te creas la valiosa persona y padre que eres. Y a mis abuelos, escribo y me pongo a llorar…si ya he tenido suerte con la madre y el padre que me han tocado, tener unos "segundos padres" como habéis sido vosotros es un lujo que no mucha gente puede decir. Gracias por existir y haber estado en cada paso de mi vida personal y profesional. Abuelo, espero que estés donde estés, sigas estando orgulloso de mí. Os quiero

INDEX

ABBREVIATURES 1
RESUMEN 3
SUMMARY 9
MAIN INTRODUCTION 15
1. The hemostatic system 15
1.1 Primary hemostasis 15
1.2 Secondary hemostasis or the coagulation cascade 15
1.3 Fibrinolysis 16
2. Antithrombin 16
2.1 Structure of antithrombin 17
2.2 Mechanism of action 18
2.3 Conformations of antithrombin 20
2.4 Antithrombin deficiency 21
2.5 Antithrombin beyond haemostasis 22
2.5.1 Anti-inflammatory antithrombin 22
2.5.2 Antiapoptotic antithrombin 23
2.5.3 Antiviral antithrombin 23
2.5.4 Antiangiogenic antithrombin 24
2.5.5 Antitumoral antithrombin 25
3. Glioblastoma multiforme 25
3.1 Definition of glioma and classification 25
3.2 Current treatment for glioblastoma 26
3.3 Pathological characteristics of glioblastoma 27
3.3.1 Inter- and intratumoral heterogeneity 27
3.3.2 Tumour infiltration and invasion 28
3.3.3 Presence of glioma stem cells 29
3.3.4 Presence of the blood–brain barrier 29
3.3.5 High vascularization of glioblastoma (angiogenesis) 30
4. Corollary 32
OBJECTIVES 33

CHAPTER 1. Characterization of the antitumor functions of prelatent antithrombin on glioblastoma multiforme cells 35
1. Introduction 37
2. Material and methods 38
2.1 Purification of native and prelatent antithrombin 38
2.2 Characterization of native and prelatent antithrombin 39
2.3 Cell culture 39
2.4 Enteropeptidase inhibition by prelatent AT and complex formation 40
2.5 Wound healing assay 41
2.6 Matrigel invasion assay 41
2.7 Real Time-PCR and Immunoblotting of Selected Cancer Signalling Proteins . 42
2.8 Statistics 42
3. Results 43
3.1 Prelatent antithrombin characterization 43
3.2 Prelatent AT is able to inhibit enteropeptidase 44
3.3 Native and prelatent antithrombin inhibits migration and invasion of glioblastoma multiforme cells 45
3.4 Prelatent antithrombin downregulates the expression or function of different cancer signalling molecules 49
4. Discussion 52
CHAPTER 2. Study of the cellular mechanisms underlying the antitumor effect of native and prelatent conformations of antithrombin on glioblastoma cell lines 57
1. Introduction 59
2. Material and methods 59
2.1 Cell culture 59
2.2 Transcriptomic analysis. Microarray expression 60
2.3 Functional validation of miRNAs and angiogenesis assay 61
2.4 Cell cycle and proliferation assay 62
3. Results 63
3.1 Prelatent antithrombin regulates the expression of different protumoral proteins 63
3.2 Antithrombin regulates the expression of various miRNAs 65
3.3 Cell cycle and proliferation assay 68
4. Discussion 73

CHAPTER 3. Identification of the potential receptor of antithrombin in glioblastoma multiforme cells and validation of the in vitro results in a preclinical model based on the use of organoids and in samples of glioblastoma multiforme patients..... 77

1. Introduction 78

2. Material and methods 84

2.1 Crosslinking and immunoprecipitation assay 84

2.2 Proteomic analysis by TripleTOF 6600 LC-MS/MS System 84

2.2.1 Protein digestion 84

2.2.2 Protein Quantification by SWATH-MS (Sequential Window Acquisition of all Theoretical Mass Spectra) Analysis 84

2.3 Receptor blocking: cytometry 85

2.4 Organoids generation 86

2.5 Glioma stem cells generation 87

2.6 *In vitro* 3D invasion assay 88

2.7 Validation of dystonin expression by Real-Time qPCR 88

3. Results 89

3.1 Identification of the receptor of AT on GBM cells: Dystonin 89

3.2 Native and prelatent antithrombin can inhibit 3D glioblastoma-neurospheres invasion on human brain organoids 94

3.3 Validation of dystonin expression in glioblastoma cell lines and patients' samples 95

4. Discussion 97

CONCLUSIONS 101

BIBLIOGRAPHY 103

FIGURES & TABLES INDEX

Figure 1. Primary and secondary hemostasis…….....17
Figure 2. Structure of antithrombin…….18
Figure 3. Interaction of native antithrombin with different heparins……..20
Figure 4. Angiogenesis in glioblastoma (GBM)…….31
Figure 5. Characterization of native and prelatent antithrombin. ……...43
Figure 6. Evaluation of the interaction between antithrombin (AT) and enteropeptidase (EP)……..45
Figure 7. Dose-response curve of prelatent antithrombin (AT) and percentage of wound healing…….46
Figure 8. Antithrombin inhibits U87 glioblastoma cells migration…….47
Figure 9. Antithrombin inhibits U87 glioblastoma cells invasion……..48
Figure 10. VEGFA expression on U87 cells after prelatent antithrombin (AT) treatment compared to control (buffer A)……49
Figure 11. pSTAT3, pAKT, and pERK1/2 expression on U87 glioblastoma cells…….50
Figure 12. VEGFA, pSTAT3, pAKT, and pERK1/2 expression on U251 glioblastoma cells……..51
Figure 13. Principal component analysis (PCA) of transcripts obtained from U87 cells treated with buffer A (control) (circles) or prelatent antithrombin (squares)……..63
Figure 14. Main pathways altered in cancer after U87 glioblastoma cells treatment with prelatent antithrombin……..64
Figure 15. Scheme of the steps followed for the first bioinformatics analysis and selection of the different miRNAs……...65
Figure 16. Manhattan plot of different databases……66
Figure 17. Cord plot representation of the Reactome database results……...67
Figure 18. Measurement of miRNAs expression by qRT-PCR after transfection with miRNA mimics……67
Figure 19. Effect of the selected miRNA expression on angiogenesis in endothelial cells……..68
Figure 20. Effect of native and prelatent antithrombin (AT) on cell cycle (left) and proliferation (right) in U87 (A) and U251 (B) glioblastoma cell lines……...70

Figure 21. Cyclins and regulatory proteins involved in the cell cycle progression expressed on U87 glioblastoma cells after treatment with antithrombin (AT)……...71
Figure 22. Cyclins and regulatory proteins involved in the cell cycle progression expressed on U251 glioblastoma cells after treatment with antithrombin (AT)…….72
Figure 23. Summary of most frequent molecular alterations in gliomas……80
Figure 24. Subclassification of primary GBM based on sequential genetic changes observed in the pathogenesis……...81
Figure 25. Principal component analysis (PCA) plot illustrating the protein relationship between U87 immunoprecipitated samples incubated with native or prelatent antithrombin (AT) *vs*. controls……....90
Figure 26. Schematic representation of the predominant *DST* isoforms…….92
Figure 27. Effect of native and prelatent antithrombin (AT) in the presence or absence of anti-dystonin antibody (DST) and compared to control on cell cycle (A, C-F) and proliferation (B) in U87 cell line…….93
Figure 28. Organoids development…….94
Figure 29. Three-dimensional model of glioblastoma multiforme invasion to test the antitumor effect of antithrombin (AT)…….95
Figure 30. Dystonin isoforms expression……96

Table 1. Enteropeptidase activity……45
Table 2. Results of the Parket Genomics Suite software…….64
Table 3. Altered genes after treatment with prelatent (prelat.) antithrombin (AT) which were related to cell cycle…….69
Table 4. Grading of diffuse gliomas according to histological features……..79
Table 5. Primers and probes for *DST* isoforms detection……88
Table 6 Pre-amplification PCR run method……89
Table 7. qPCR run method……..89
Table 8. Proteomics study. Results obtained by SWATH-MS of crosslinked and immunoprecipitated U87 lysates incubated with native antithrombin, prelatent or buffer A (control samples)…….91

ABBREVIATURES

AT: Antithrombin

BBB: Blood–brain barrier

Buffer A: 20 mM sodium phosphate, 20 mM NaCl, 0.1 mM ethylenediaminetetraacetic acid, pH 7.4 buffer

CCNE2: Cyclin E2

CNS: Central nervous system

EGFR or **EGFRvIII**: Epidermal growth factor receptor wild type or with mutation variant III

EP: Enteropeptidase

FC: Fold-change

FI, **FIII**, **FV**, **FVII**, **FIX**, **FX**, **FXI**, **FXII**, **FXIII**: Inactive factors of the coagulation I, III, V, VII, IX, X, XI, XII, XIII

FIa, **FIIIa**, **FVa**, **FVIIa**, **FIXa**, **FXa**, **FXIa**, **FXIIa**, **FXIIIa**: Active factors of the coagulation I, III, V, VII, IX, X, XI, XII, XIII

FIIa: Factor coagulation II or thrombin

GBM: Glioblastoma multiforme

GFP: Green fluorescent protein

GSCs: Glioma stem cells

HIF-1: Hypoxia-inducible factor-1

HIV: Human immunodeficiency virus

IDH: Isocitrate dehydrogenase

iPSCs: Induced pluripotent stem cells

K_D: Dissociation constant

LMWH: Low molecular weight heparin

LRP1: Low-density lipoprotein receptor-related protein 1

NF-κB: Nuclear factor κB

NIM: Neural induction medium

PCA: Principal component analysis

PGI2: Prostacyclin or prostaglandin I2

Rb: Retinoblastoma protein

RCL: Reactive center loop

RFP: Red fluorescent protein

SDS-PAGE: Sodium dodecyl sulfate polyacrylamide gel electrophoresis

STAT3: Signal transducer and activator of transcription 3

Sulpho-EGS: Ethylene glycolbis(sulfosuccinimidylsuccinate)

SWATH-MS: Sequential Window Acquisition of all Theoretical Mass Spectra

TMZ: Temozolomide

TTSP: Type II transmembrane serine protease

U251: U-251 MG Glioblastoma cell line

U87: U-87 MG Glioblastoma cell line

VEGFA: Vascular endothelial growth factor A

VTE: Venous thromboembolism

RESUMEN

La antitrombina es una glicoproteína principalmente secretada por el hígado que pertenece a la superfamilia de las serpinas, que son inhibidores de serín proteasas, entre las que se encuentran algunas proteínas de la cascada de la coagulación. De hecho, la antitrombina es el principal inhibidor fisiológico de dicha cascada. La antitrombina presenta una gran flexibilidad estructural que le permite tanto inhibir a las proteasas de la coagulación, como presentar distintas conformaciones: nativa, activada por heparina, rota, latente y prelatente. Las dos últimas conformaciones, en las que el loop reactivo se internaliza en la lámina beta central, son adoptadas *in vitro* al incubar la antitrombina nativa a temperaturas elevadas. A diferencia de la conformación latente, la prelatente se caracteriza por mantener su capacidad inhibitoria, pero con una menor afinidad por la heparina que la conformación nativa, y se presenta *in vivo* en concentraciones muy bajas. Más allá de su función en la hemostasia, se ha demostrado que la antitrombina puede presentar función anti-angiogénica, anti-inflamatoria, anti-apoptótica y anti-viral. Hace unos años, nuestro grupo demostró que la antitrombina activada por heparina también puede tener función anti-tumoral sobre células de glioblastoma. Este efecto anti-tumoral parece estar mediado por la inhibición que ejerce la antitrombina sobre la proteasa enteropeptidasa, pero además otras proteínas podrían estar participando en el papel antitumoral de la antitrombina.

El glioblastoma pertenece a los gliomas de grado IV, que son los gliomas más avanzados y con peor pronóstico. De hecho, el glioblastoma es el tumor maligno primario más agresivo y letal del sistema nervioso central en adultos, aunque con una incidencia global menor de 10 por cada 100000 personas. A pesar de los agresivos tratamientos que conlleva (cirugía, radio- y quimioterapia), la mediana de supervivencia sigue siendo de 12-15 meses tras el diagnóstico. Esto se debe a diversos factores como su elevada inter- e intra- heterogeneidad, su gran capacidad invasiva, a la incapacidad de ciertos fármacos de atravesar la barrera hematoencefálica o a la presencia de células madre de glioma. La baja tasa de supervivencia de este tumor hace necesario desarrollar nuevas estrategias terapéuticas, y la antitrombina, dados sus efectos pleiotrópicos y la diversidad en sus conformaciones, podría ser una gran candidata como nuevo tratamiento en el glioblastoma.

Ante la urgente necesidad de identificar nuevos tratamientos para el glioblastoma, los objetivos de esta tesis han sido: 1. Caracterizar la función antitumoral de la antitrombina prelatente sobre células de glioblastoma multiforme. 2. Estudiar el mecanismo celular subyacente a la función antitumoral de la antitrombina nativa y prelatente sobre células de glioblastoma multiforme. 3. Identificar el potencial receptor de la antitrombina en células de glioblastoma multiforme y validar los resultados *in vitro* en un modelo preclínico basado en el uso de organoides y muestras de pacientes con glioblastoma multiforme.

Para llevar a cabo esta tesis doctoral se purificó antitrombina prelatente a partir de plasma humano mediante dos pasos de cromatografía de afinidad por heparina tras incubar antitrombina nativa a 60ºC y durante 30 horas. Tras cada purificación, se caracterizaron las conformaciones nativa y prelatente evaluando mediante western blot la capacidad de formación de complejo con el FXa o la trombina, tanto en ausencia como presencia de heparina, así como la afinidad por heparina (determinación de la constante de disociación) mediante medida de emisión de fluorescencia. Previo a cada ensayo, se trataron las células U87 y/o U251 con 2.16 µM de antitrombina nativa, prelatente, o con buffer A (buffer de elución de la antitromina prelatente durante su purificación compuesto por 20 mM, NaCl 20 mM y EDTA 0.1 mM, pH 7,4; muestras control), durante 11 horas.

En el primer capítulo de esta tesis doctoral quisimos caracterizar la función antitumoral de la antitrombina sobre células de glioblastoma U87. Para ello, evaluamos su interacción con enteropeptidasa. Así, mediante ensayos cromogénicos y western blot se determinó que la antitrombina prelatente, al igual que la nativa, es capaz de inhibir a la enteropeptidasa. Sin embargo, en presencia de heparina, la antitrombina nativa mostró un efecto inhibidor cuatro veces mayor que el de la conformación prelatente. Tras un ensayo de dosis-respuesta mediante un ensayo de migración mediante la técnica de *wound healing*, se determinó que la concentración óptima de antitrombina para ejercer su efecto antitumoral es de 2.16 µM, equivalente a la concentración plasmática de la proteína. Además, empleando a estas dosis las técnicas de *wound healing* y usando *transwells* cubiertos con matrigel determinamos, respectivamente, que la antitrombina prelatente es capaz de reducir la migración e invasión de las células U87 de glioblastoma de forma significativa en ausencia de heparina, y en el caso de la migración, de forma más eficiente que la conformación nativa, a una concentración 1.38

veces menor. Este efecto de la antitrombina prelatente no se ve potenciado por la presencia de heparina. También, mediante RT-qPCR y/o western blot determinamos que la antitrombina prelatente es capaz de inhibir la expresión de diferentes proteínas implicadas en la progresión de las células de glioblastoma U87. Por un lado, la antitrombina prelatente es capaz de inhibir la expresión de VEGFA tanto a nivel de proteína como de ARNm. Estos resultados refuerzan el papel anti-angiogénico previamente descrito para la conformación prelatente, y además demuestran el mecanismo implicado. Y por otro lado, comprobamos que la antitrombina prelatente es capaz de inhibir de forma estadísticamente significativa la expresión de *STAT3*, así como la fosforilación de pSTAT3α y de pERK1/2, pero no de pAKT, lo que se ha asociado, junto con la inhibición de VEGFA, con una menor resistencia al tratamiento en el glioblastoma multiforme. Estos resultados en la inhibición de la expresión de las distintas proteínas mencionadas tras el tratamiento con antitrombina prelatente no se observaron en la línea celular U251 de glioblastoma.

Una vez demostrado *in vitro* el potencial papel antitumoral de la antitrombina prelatente sobre células de glioblastoma U87, en el segundo capítulo quisimos estudiar el mecanismo celular subyacente a dicha función antitumoral. Para ello, realizamos un array de expresión (Clariom D human array) tras tratar a las células U87 con antitrombina prelatente o con buffer A (20 mM, NaCl 20 mM y EDTA 0.1 mM, pH 7,4; muestras control). El análisis de componentes principales separó las muestras control y las muestras tratadas con antitrombina prelatente en función de los transcritos expresados. Tras considerar diferencias estadísticamente significativas aquellos valores de expresión con un p-value < 0,001 y fold change ± 1,5, obtuvimos que 2477 genes se encontraban sobreexpresados, mientras que 6760 estaban infraexpresados. Numerosas rutas de señalización relacionadas con cáncer se encontraban inhibidas. Entre ellas, destacamos la vía del VEGFA o de angiogénesis. Tras un amplio análisis bioinformático, de 35 miRNAs alterados en el array, seleccionamos 3 de ellos dada su relación con la ruta del VEGFA o angiogénesis. Para evaluar su implicación en dicho proceso, transfectamos células U87 con los 3 miRNAs de forma individual o conjunta, y realizamos un experimento de angiogénesis tras co-cultivarlas con células endoteliales. Tras confirmar la alta eficiencia de transfección mediante qPCR, observamos que, aunque las imágenes de microscopía sugerían que el miR-A reducía la angiogénesis, el análisis mostraba que ninguno de los miRNAs evaluados alteran este proceso. Estos

resultados deberán ser repetidos empleando otro análisis informático o analizando otros miRNAs resultantes del array de expresión. Otra de las rutas alteradas en el array de expresión fue el ciclo celular, dado que diversos genes de ciclinas y proteínas reguladoras del ciclo celular se encontraban inhibidas (FC, p-valor): *CDK4* (-1.64, $2.60x10^{-5}$), *CCNE2* (-2.06, $2.65x10^{-6}$), *RB1* (-1.58, $1.37x10^{-6}$) y *E2F4* (-2.03, $1.09x10^{-7}$). Mediante citometría de flujo, midiendo incorporación de los compuestos BrdU y 7AAD, observamos un significativo mayor número de eventos en las fases G2-M y G0-1 y una inhibición significativa de la fase S del ~50% respecto al control tras el tratamiento de las U87 con antitrombina nativa y prelatente. Además, la proliferación celular también disminuyó un 40.63% en comparación con las muestras control, aunque este resultado solo fue significativo con la forma nativa. También, mediante western blot, validamos la inhibición de la proteína E2F4 y de la fosforilación de pRb en las U87 tras el tratamiento con antitrombina nativa. Sin embargo, no se observó inhibición significativa del ciclo, proliferación celular y expresión de proteínas relacionadas tras el tratamiento de la línea celular U251.

Finalmente, en el tercer capítulo de esta tesis doctoral quisimos identificar el potencial receptor de la antitrombina en células de glioblastoma multiforme y validar los resultados *in vitro* en un modelo preclínico basado en el uso de organoides y muestras de pacientes con glioblastoma multiforme. En primer lugar, realizamos un ensayo de crosslinking e inmunoprecipitación para determinar al receptor de la antitrombina nativa y prelatente en células U87. Tras realizar proteómica cuantitativa, los resultados mostraban una elevada interacción de la antitrombina, tanto nativa como prelatente, con la proteína distonina. La distonina, pertenece a la familia de las plaquinas, que son proteínas de unión entre la membrana plasmática y el citoesqueleto. Mediante citometría de flujo, midiendo incorporación de 7AAD y BrdU y tras bloquear la interacción entre ambas proteínas usando un anticuerpo policlonal anti-distonina, también determinamos que la distonina está implicada en la inhibición de la proliferación tumoral de las células U87. También quisimos evaluar en un modelo preclínico la capacidad anti-invasiva de la antitrombina. Para ello, por un lado generamos organoides-RFP (*red fluorescence protein*) de cerebro humano sano a partir de células madre pluripotentes inducidas, y por otro, generamos neuroesferas-GFP (*green fluorescence protein*) 275 a partir de células aisladas de la biopsia al diagnóstico de un paciente con glioblastoma. Las neuroesferas 275-BIS-GFP se generaron a partir

de células asiladas de la biopsia en la recaída del mismo paciente. Organoides de 25 días se incubaron con las neuroesferas y se trataron durante 10 días alternos con 10 µM de antitrombina nativa, prelatente o con buffer A (20 mM, NaCl 20 mM y EDTA 0.1 mM, pH 7,4; muestras control). Los resultados se analizaron mediante inmunofluorescencia y se midió la capacidad de invasión de las neuroesferas empleando el software Fiji. De forma preliminar, demostramos que tanto la antitrombina nativa como antitrombina prelatente redujeron parcialmente la capacidad de invasión de las neuroesferas 275 sobre organoides de cerebro sano. Esta inhibición fue notablemente mayor en el caso de las neuroesferas 275-BIS en comparación con el control, dado que tanto la antitrombina nativa como la prelatente impidieron completamente la invasión de las neuroesferas en recaída sobre los organoides. Este mayor efecto en las neuroesferas derivadas del paciente en recaída con respecto a las neuroesferas realizadas a partir de la biopsia al diagnóstico podría explicarse por el diferente patrón de expresión molecular entre estos estadios de la enfermedad. Finalmente, evaluamos también el potencial de la distonina como biomarcador pronóstico mediante RT-qPCR en las líneas celulares U87, U251, 275 y 275 BIS, así como en 10 muestras parafinadas de pacientes con gliomas de bajo grado (I-II) y pacientes con glioma de alto grado (III-IV). Aunque los resultados muestran una mayor expresión de la isoforma 2 de la distonina en las células U87, 275 BIS y en los pacientes de alto grado, esta medida deberá optimizarse empleando otras técnicas, como podría ser la PCR digital.

La presente tesis doctoral demuestra el efecto antitumoral *in vitro* de las antitrombinas nativa y prelatente. Ambas presentan propiedades antitumorales sorprendentemente versátiles sobre células de glioblastoma U87. Estas se asocian con reducción de la migración e invasión tumoral, con menor resistencia al tratamiento, parada del ciclo celular y menor proliferación, y con su función anti-angiogénica previamente ya descrita. El mecanismo subyacente a la función antitumoral de la antitrombina podría explicarse por su capacidad inhibitoria sobre proteasas como la enteropeptidasa, sobre el agente pro-angiogénico VEGFA, o sobre la proteína oncogénica STAT3. También hemos demostrado que la antitrombina prelatente regula la expresión de varios miRNAs implicados en la angiogénesis en glioblastoma, señalando el potencial uso de imitadores sintéticos de miRNA como terapia antitumoral. Además, los resultados transcriptómicos demuestran la capacidad de la antitrombina para inhibir diversas vías tumorales implicadas en la progresión del glioblastoma. Por otro lado, la identificación de la

distonina como receptor de la antitrombina en este tumor, podría ayudar a diseñar terapias dirigidas. Hasta ahora, hemos conseguido demostrar el papel anti-proliferativo de la distonina, aunque podría estar implicada además en otros procesos. Del mismo modo, será necesario evaluar el potencial pronóstico de los niveles de expresión de la distonina mediante otras técnicas como la PCR digital en muestras parafinadas. Finalmente, el sistema 3D presentado en esta tesis recapitula la heterogeneidad, patrones de invasión de las células madre de glioma, y microambiente tumoral del glioblastoma, pudiendo emplearse como un modelo de estudio preclínico que permita realizar estudios de terapia personalizada. Con este modelo, hemos demostrado de forma preliminar que las antitrombinas nativa y prelatente son capaces de inhibir la invasión tumoral de células madre de glioma derivadas de un paciente con glioblastoma, observando un mayor efecto en las neuroesferas del paciente en recaída respecto a las neuroesferas al diagnóstico. La capacidad inhibitoria de la antitrombina sobre las U87 y 275 BIS frente a las U251 y 275, refuerza la elevada heterogeneidad de este tumor y su consecuente necesidad de desarrollar técnicas más personalizadas para estudiar al glioblastoma. De validarse nuestros resultados *in vivo*, éstos apoyan las potenciales propiedades terapéuticas de la antitrombina prelatente en el glioblastoma.

SUMMARY

Antithrombin is a glycoprotein mainly secreted from the liver belonging to the serpin superfamily, which are serine proteases inhibitors. Among these serine proteases, some proteins of the coagulation cascade are found. Indeed, antithrombin is the main physiological of the coagulation cascade. Antithrombin has a great structural flexibility that allows it to both inhibit its target coagulation proteases, and also to adopt different conformations, which are: native, heparin-activated, cleaved, latent and prelatent. The latter two conformations, in which the reactive loop is internalized in the central β-sheet, are adopted *in vitro* by incubating native antithrombin at elevated temperatures. In contrast to the latent conformation, the prelatent conformation is characterized by maintaining its inhibitory capacity, but with a lower affinity for heparin than the native form, and is presented *in vivo* at very low concentrations. In addition to its role in hemostasis, antithrombin has been shown to have antiangiogenic, anti-inflammatory, antiapoptotic and antiviral functions. Specifically, our group first demonstrated that heparin-activated antithrombin may also have antitumor functions on glioblastoma cells. This antitumor effect appears to be mediated by the capacity of antithrombin to inhibit the serine protease enteropeptidase, but other proteins may also be involved in the antitumor role of antithrombin.

Glioblastoma is a tumor that belongs to grade IV gliomas, which are the most advanced gliomas with the worst prognosis. In fact, glioblastoma is the most aggressive and lethal primary malignant tumor of the central nervous system in adults, although with a global incidence of less than 10 per 100,000 people. Despite the aggressive treatments involved (surgery, radio- and chemotherapy), the median survival time is still 12-15 months after diagnosis. This is due to several factors such as its high inter- and intra-heterogeneity and invasiveness, the inability of certain drugs to cross the blood-brain barrier or the presence of glioma stem cells, among other factors. The low survival rate of this tumor makes it necessary to develop new therapeutic strategies, and antithrombin, given its pleiotropic effects and the diversity of its conformations, could be a great candidate as a new treatment for glioblastoma.

Given the urgent need to identify new treatments for glioblastoma, the objectives of this thesis were: 1) Characterization of the antitumor functions of prelatent antithrombin on

glioblastoma multiforme cells; 2) Study of the cellular mechanisms underlying the antitumor effect of native and prelatent conformations of antithrombin on glioblastoma cell lines; 3) Identification of the potential receptor of antithrombin in glioblastoma multiforme cells and validation of the *in vitro* results in a preclinical model based on the use of organoids and in samples of glioblastoma multiforme patients.

In order to carry out this doctoral thesis, prelatent antithrombin was purified from human healthy donor's plasma by applying two heparin affinity chromatography steps after incubation of native antithrombin at 60°C for 30 hours. After each purification, the native and prelatent conformations were characterized by western blotting to assess the ability to complex with FXa or thrombin, both in the absence and presence of heparin, as well as their affinity for heparin (determination of the dissociation constant) by fluorescence emission measurement. Prior to each assay, U87 and/or U251 cells were treated with 2.16 µM native or prelatent antithrombin, or buffer A (prelatent antithrombin elution buffer during its purification consisting of 20 mM sodium phosphate, 20 mM NaCl and 0.1 mM EDTA, pH 7.4; control samples), for 11 hours.

In the first chapter of this doctoral thesis we aimed to characterize the antitumor function of antithrombin on U87 glioblastoma cells. Therefore, we evaluated its interaction with enteropeptidase. Thus, using chromogenic and western blot assays, we determined that prelatent antithrombin, like native antithrombin, is able to inhibit enteropeptidase. However, in the presence of heparin, native antithrombin showed an inhibitory effect four times greater than that of the prelatent conformation. Following the dose-response assay performed through a migration assay using the wound healing technique, the optimal concentration of antithrombin to exert its antitumor effect was determined to be 2.16 µM, equivalent to the plasma concentration of the protein. Furthermore, by applying this dose in the technique wound healing and using matrigel-covered transwells, we respectively determined that prelatent antithrombin is able to significantly reduce migration and invasion of U87 glioblastoma cells in the absence of heparin, and in the case of migration, more efficiently than the native conformation, at a 1.38-fold lower concentration. This effect of prelatent antithrombin is not enhanced by the presence of heparin. Also, by RT-qPCR and/or western blot we determined that prelatent antithrombin is able to inhibit the expression of different proteins involved in the progression of U87 glioblastoma cells. On the one hand, we determined that prelatent antithrombin is able to inhibit VEGFA expression in U87 cells both at protein

and mRNA levels. These results reinforce the previously described anti-angiogenic role of the prelatent conformation, as well as the mechanism involved in. And on the other hand, we found that prelatent antithrombin is able to statistically significantly inhibit STAT3 expression, as well as phosphorylation of pSTAT3α and pERK1/2, but not pAKT, which has been associated, together with VEGFA inhibition, with reduced resistance to treatment in glioblastoma multiforme. These results in the inhibition of the expression of different proteins mentioned above after treatment with prelatent antithrombin were not observed in the U251 glioblastoma cell line.

Once the potential antitumour role of prelatent antithrombin on U87 glioblastoma cells was demonstrated in vitro, in the second chapter we aimed to study the cellular mechanism underlying this antitumour function. For this purpose, we performed an expression array (Clariom D human array) after treating U87 cells with prelatent antithrombin or buffer A (20 mM sodium phosphate, 20 mM NaCl and 0.1 mM EDTA, pH 7.4; control samples). A principal component analysis separated control and prelatent antithrombin-treated samples on the basis of expressed transcripts. After considering statistically significant differences those expression values with a p-value < 0.001 and fold change ± 1.5, we found that 2477 genes were overexpressed, while 6760 were underexpressed, which are the majority. Numerous cancer-related signaling pathways were inhibited. Among them, we highlight the VEGFA or angiogenesis pathway. After an extensive bioinformatics analysis which included an over-representation analysis with the g:Profiler software and the Reactome biological pathway database, out of 35 miRNAs altered in the array, 3 miRNAs were selected to be studied given their involvement in the VEGFA or angiogenesis pathway. To assess their involvement in this process, we transfected U87 cells with the 3 miRNAs individually or together, and performed an angiogenesis assay after co-culture with endothelial cells. After confirming the high transfection efficiency by qPCR, we observed that, although microscopy images suggested that miR-A reduced angiogenesis, computational analysis showed that none of the miRNAs tested alter this process. These results will have to be repeated using another computational analysis or by analysing other miRNAs resulting from the expression array. Among the altered pathways after prelatent antithrombin treatment, we also observed that different cyclin and regulatory protein genes involved in the cell cycle were inhibited (FC, p-value): *CDK4* (-1.64, 2.60×10^{-5}), *CCNE2* (-2.06, 2.65×10^{-6}), *RB1* (-1.58, 1.37×10^{-6}) and *E2F4* (-2.03, $1.09 \times 10^{-}$

[7]). By flow cytometry and measuring incorporation of 7AAD and BrdU compounds we demonstrated that both native and prelatent antithrombin significantly inhibited the S-phase to almost half in the U87 cells. A significantly increased number of events in G2-M and G0-1 phases was also observed. In addition, cell proliferation also decreased by 40.63% compared to the control samples, although this result was only significant with the native form. We also validated by western blot the inhibition of E2F4 protein and pRb phosphorylation in U87 cells after treatment with native antithrombin, both proteins involved in the entry of cells into the S phase of the cell cycle. However, no significant inhibition of cell cycle, cell proliferation and related protein expression was observed after treatment of the U251 cell line.

Finally, in the third chapter of this doctoral thesis we aimed to identify the potential receptor of antithrombin in glioblastoma multiforme cells and validate the results *in vitro* in a preclinical model based on the use of organoids and samples from glioblastoma multiforme patients. First of all, we performed a crosslinking and immunoprecipitation assay to determine the receptor of native and prelatent antithrombin in U87 cells. Quantitative proteomics results showed a high interaction of both native and prelatent antithrombin with the protein dystonin. Dystonin belongs to the family of plakins, which are binding proteins between the plasma membrane and the cytoskeleton. By flow cytometry, measuring incorporation of 7AAD and BrdU and after blocking the interaction between both proteins using a polyclonal anti-dystonin antibody, we also determined that dystonin is involved in the inhibition of the tumor proliferation of U87 cells. We also aimed to evaluate the anti-invasive capacity of antithrombin in a preclinical model. To this end, on the one hand, we generated organoids-RFP (red fluorescence protein) from healthy human brain from induced pluripotent stem cells. And on the other hand, we generated 275-GFP (green fluorescence protein) neurospheres from cells isolated from the biopsy at diagnosis of a patient with glioblastoma. 275 BIS-GFP neurospheres were generated from cells isolated from the biopsy at relapse of the same patient. Twenty-five day old organoids were incubated with the neurospheres and treated for 10 alternate days with 10 µM native or prelatent antithrombin or buffer A (control). The results were analyzed by immunofluorescence and the invasiveness of the neurospheres was measured using Fiji software. Preliminary we demonstrated that both native and prelatent antithrombin partially reduced the invasiveness of 275 neurospheres on human healthy brain

organoids. However, this inhibition was markedly greater in the case of 275 BIS neurospheres compared to the control, as both native and prelatent antithrombin completely prevented the invasion of the relapsed neurospheres on the organoids. This greater effect on neurospheres derived from the relapsed patient compared to neurospheres extracted from the biopsy at diagnosis, could be explained by the different molecular expression pattern between these stages of the disease. Finally, we also evaluated the potential of using dystonin as a prognostic biomarker by RT-qPCR in U87, U251, 275 and 275 BIS cell lines, as well as in 10 paraffin-embedded samples from patients with low-grade gliomas (I-II) and patients with high-grade gliomas (III-IV). Although the results show an increased expression of dystonin isoform 2 in U87, 275 BIS cells and in high-grade patients, this measure should be optimized using other techniques, such as digital PCR.

This doctoral thesis demonstrates the *in vitro* antitumor effect of native and prelatent antithrombin. Both show surprisingly versatile antitumor properties on U87 glioblastoma cells, which are associated with reduced tumor migration and invasion, reduced treatment resistance, cell cycle arrest and proliferation, and their previously described anti-angiogenic function. The mechanism underlying the antitumor function of antithrombin could be explained by its inhibitory capacity on proteases such as enteropeptidase, on the proangiogenic agent VEGFA, or on the oncogenic protein STAT3. We have also shown that prelatent antithrombin upregulates the expression of several miRNAs involved in angiogenesis in glioblastoma, thus enhancing the potential use of synthetic miRNA mimics as antitumor therapy. In addition, the transcriptomic results demonstrate the ability of antithrombin to inhibit several tumor pathways involved in glioblastoma progression. Furthermore, the identification of dystonin as the receptor of antithrombin in this tumor could help to design targeted therapies. So far, we have been able to demonstrate the antiproliferative role of dystonin, although it could be involved in other processes. Similarly, the study of dystonin as a potential prognostic biomarker will be assessed by other techniques such as digital PCR on paraffin-embedded samples. Finally, the 3D system presented in this doctoral thesis recapitulates the heterogeneity, invasion patterns of glioma stem cells, and tumor microenvironment of glioblastoma, and can be used as a preclinical study model for personalized therapy studies. With this model, we have preliminarily demonstrated that native and prelatent antithrombin are able to inhibit tumor invasion of glioma stem cells derived from a

glioblastoma patient, observing a greater effect on the neurospheres from the relapsed patient compared to the neurospheres extracted at diagnosis. The inhibitory capacity of antithrombin on U87 and 275 BIS *vs*. U251 and 275 reinforces the high heterogeneity of this tumor and the consequent need to develop more personalized techniques to study glioblastoma. If validated *in vivo*, our results support the potential therapeutic properties of prelatent antithrombin in glioblastoma.

MAIN INTRODUCTION

1. The hemostatic system

The hemostatic system is the physiological defense mechanism that is activated after trauma or injury in order to stop a major bleeding. Although, this system is always activated, as the deposition and dissolution of fibrin in the endothelium is a continuous phenomenon, it is ready to greatly accelerate its function when a hemorrhage or vascular occlusion occurs. In general, it can be divided into 3 phases, which are summarized as follows: primary hemostasis, secondary hemostasis and fibrinolysis[1].

1.1 Primary hemostasis

Primary hemostasis begins after vessel injury. At this point, vasoconstriction occurs and the extracellular matrix of the damaged area exposes different platelet ligands such as von Willebrand factor and collagen. Thus, platelets reach the damaged area and, by adhering to the matrix, become activated. This activation consists of a conformational change of the αIIbβ3 integrin, which allows binding sites for fibrinogen, collagen, von Willebrand factor and fibronectin to be exposed and induce aggregation. In addition, platelets release various agonists to enhance more platelets' activation and aggregation and the eventual formation of a provisional platelet thrombus that stops the bleeding[1].

1.2 Secondary hemostasis or the coagulation cascade

Secondary hemostasis is activated either by the intrinsic or extrinsic pathway. The intrinsic pathway consists of factors I, II, IX, X, XI and XII, and is activated by exposed endothelial collagen. Meanwhile, the extrinsic pathway consists of factors I, II, VII and X, and is activated by tissue factor which is exposed to the bloodstream. Both pathways converge in the activation of the active factor X (FXa), which represents a final common pathway involving factors I, II, V, VIII and X. To notice, during secondary hemostasis, multiple plasma proteins and coagulation factors are activated. Except for factors I, V, VIII and XIII, the rest of them circulate in the bloodstream as zymogens, and are activated as serine proteases to cleave the next zymogen. Due to this continuous activation of zymogens, the secondary hemostasis is commonly known as the coagulation cascade[1].

After FXa activation, thrombin or active factor II (FIIa) is activated and interacts with the fibrinogen to form fibrin monomers, which combine with each other and bind platelets. This results in a fibrin matrix that stabilizes the platelet plug or clot and prevents blood from leaking out[1].

Figure 1 illustrates primary hemostasis and the complex coagulation cascade, with the main elements involved. To control an excessive activation of the coagulation cascade, natural anticoagulants such as antithrombin (AT) and protein C are available. Highlighted in purple, we pointed out AT, as it plays a crucial role in this process. AT exerts its inhibitory function at different levels in order to maintain hemostasis.

1.3 Fibrinolysis

Once the tissue has been repaired, plasminogen is activated and converted into plasmin, and then plasmin degrades fibrin to ultimately dissolve the clot and restore blood flow[1].

2. Antithrombin

AT is a glycoprotein mainly secreted from the liver and secreted into the plasma that belongs to the serpin (acronym: serine protease Inhibitors) superfamily, which are serine proteases inhibitors. Thus, it regulates the proteolytic activity of proteases of both the extrinsic and intrinsic pathways, being the main physiological inhibitor of the coagulation cascade[2]. In fact, AT deficiency significantly increases the risk of suffering a thromboembolic event. The molecular and biochemical characterization of AT deficiency has allowed expanding the knowledge about the inhibitory mechanism of this protein, as well as its structural characteristics[3–5].

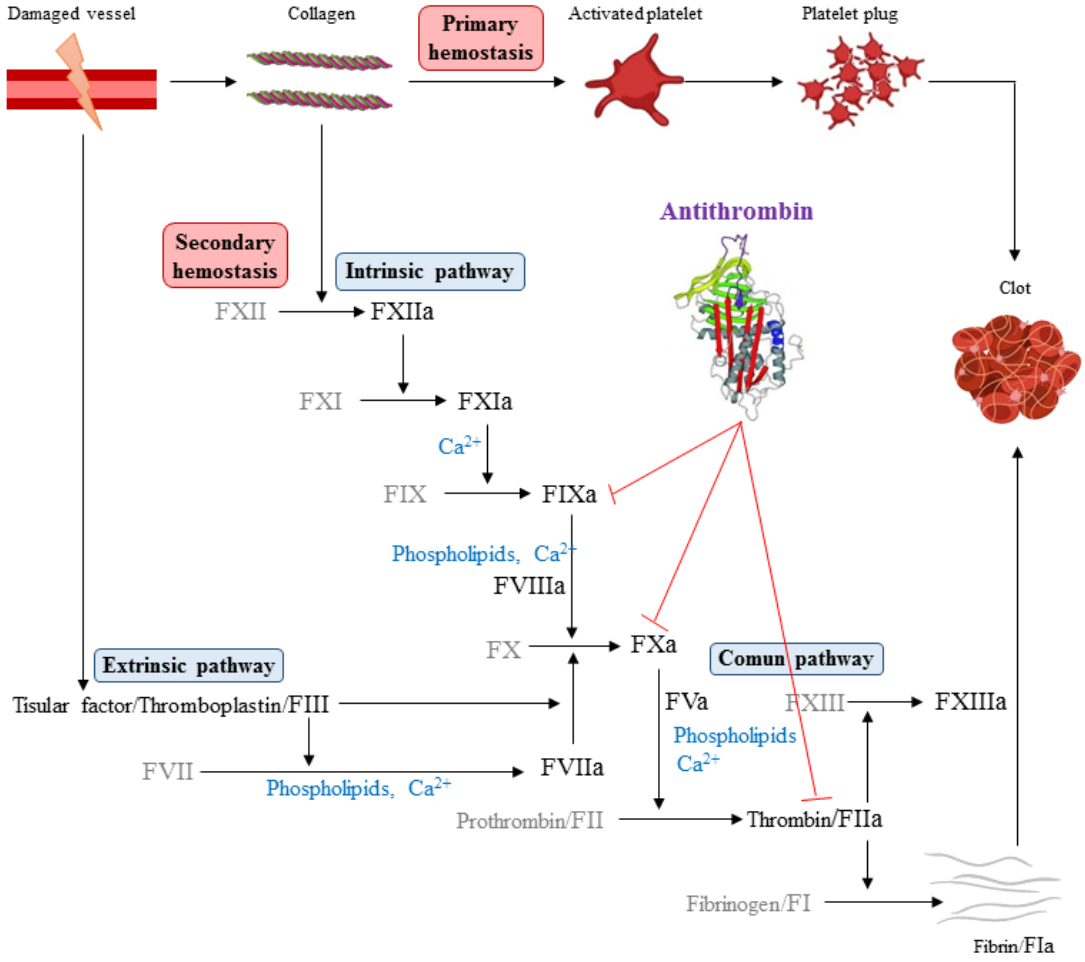

Figure 1. Primary and secondary hemostasis. In this diagram, the steps that occur in both primary and secondary hemostasis are schematically shown, leading ultimately to clot formation.

2.1 Structure of antithrombin

AT is mainly synthesized in the liver as a single-chain glycoprotein with 432 amino acids, 3 disulfide bonds and 4 glycosylation sites. In plasma it is found at 0.125 mg/ml (2.16 μM) and has a half-life of 3 days. AT presents 4 potential N-glycosylation sites. In general, for this type of post-translational modification to occur, a consensus sequence is required: Asparagine-X-(X being any amino acid except Proline)-Serine or Threonine (Asn-X-Ser or Asn-X-Thr, respectively). For AT, 3 of the 4 N-glycosylation sites have the sequence Asn-X-Thr and their glycosylation rate is 100%, while the sequence Asn-X-Ser, is only glycosylated 50% of the time. This leads to the existence of two circulating glycoforms in plasma: α-AT, which has 4 N-glycans and has a molecular weight of ~58 kDa, and β-AT, which has 3 N-glycans, so its molecular weight is 56

~kDa. Although they have the same secretion rate, only 10% of β-AT and 90% of α-AT are detected in plasma. This is because the absence of a glycan results in a higher clearance of the protein, but it also increases the affinity for heparin by 2 to 4 times[3,6,7].

In general, serpins are characterized by a high structural homology. They all present 3 β-sheets (A-C), 7 to 9 α-helices (A-I) and a reactive center loop (RCL) that extends from P15 to P5' and connects the larger 5-stranded β-sheet (A) to the smaller 3-stranded β-sheet (C) (Figure 2). The RCL has an amino acid sequence complementary to the active site of its target proteases. Despite their name, not all serpins are inhibitory, as some of them have roles in hormone transport or even sperm development, among other functions[8].

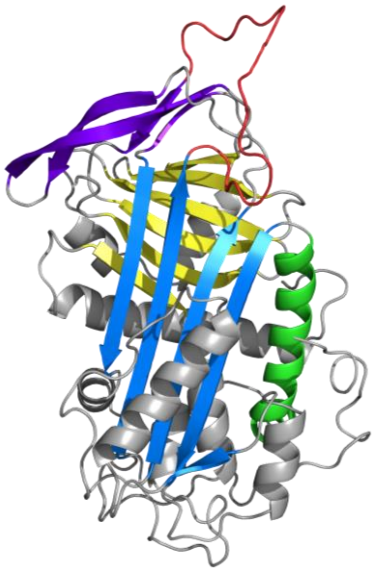

Figure 2. Structure of antithrombin. Antithrombin is shown with the A β-sheet in blue, B β-sheet in yellow and C β-sheet in purple. The reactive center loop (RCL) is shown in red. The D α-helix is shown in green. Image generated with The PyMOL Molecular Graphics System, Version 2.5 Schrödinger, LLC software (PDB: 1AZX).

2.2 Mechanism of action

AT has a great structural flexibility that allows it to both inhibit its target coagulation serine proteases and to present different conformations. This is because the serpin superfamily has a metastable structure that is not folded in its thermodynamically most stable conformation, but is kinetically trapped in a higher free energy state. This structural feature is required for its inhibitory mechanism, and its structural stability is achieved only when the RCL is inserted as a fourth strand into the β A-sheet of the serpin. The insertion of the RCL by binding to the active center of a target protease and/or by spontaneous conversion results in the so-called latent conformation[2].

Regarding its mechanism of action, like other serpins, AT exerts a "suicide inhibition mechanism" on its targets. Primary, when the catalytic pocket (Ser-195) of the target protease recognizes the RCL (P1-Arg 393) of AT as a substrate, they interact and the RCL remains cleaved, thus generating a covalent acyl intermediate "target protease-AT RCL" called a Michaelis-type enzyme inhibitor complex. The cleavage of the RCL causes great instability in AT. In order to acquire an energetically more favorable conformation, AT incorporates the N-terminal of the RCL into the central β-sheet A, whereby the RCL pulls the acylated target protease to the opposite pole of the serpin, about ~70 Å from its original position, leaving its active center disrupted and inactive. This mechanism resembles a mouse trap, where AT is the trap and the protease is the cheese, and is called a suicide inhibition mechanism since protease and inhibitor are irreversibly inactivated[9].

AT can inhibit several coagulation proteases, being its main targets thrombin and FXa[2]. However, the effectiveness in its reactivity depends on the interaction with heparin. Heparin, which is a sulphated glycosaminoglycan, is the main cofactor of AT. When they interact through several basic residues located in the D-helix of AT, this binding causes an activating conformational change consisting in the generation of an extra turn of the D-helix, the compression of the central sheet strands and, consequently, the expulsion of the RCL. This change accelerates the inhibition of target proteases by more than 1000-times, as the exosite of the RCL becomes more accessible[10].

The mechanism by which heparin increases AT's inhibition rate depends on the type of heparin (Figure 3). In the case of FXa and FIXa inhibition, low molecular weight heparin (LMWH) or pentasaccharide heparin is required. Thus, when they bind to AT, a cryptic exosite located on strand 3 of the C-sheet of AT becomes available and specifically interacts with an autolysis loop located on FXa and FIXa. However, thrombin lacks such an autolysis loop, so a high molecular weight heparin called unfractioned heparin is required to link thrombin and the D-helix of AT as a ternary complex, allowing its inhibition[2]. LMWH are obtained from unfractionated heparins by chemical degradation or enzymatic digestion, while the pentasaccharide is obtained by chemical synthesis. Due to the effectiveness in the activation of AT, heparins are used as anticoagulant therapy in a variety of diseases: deep vein thrombosis and pulmonary embolism, acute coronary syndrome, atrial fibrillation, cardiopulmonary bypass, extracorporeal circulation, hemodialysis, and central or peripheral venous catheters[11].

LMWH are preferentially used as they are easier to monitor, since unfractionated heparins can interact with other molecules.

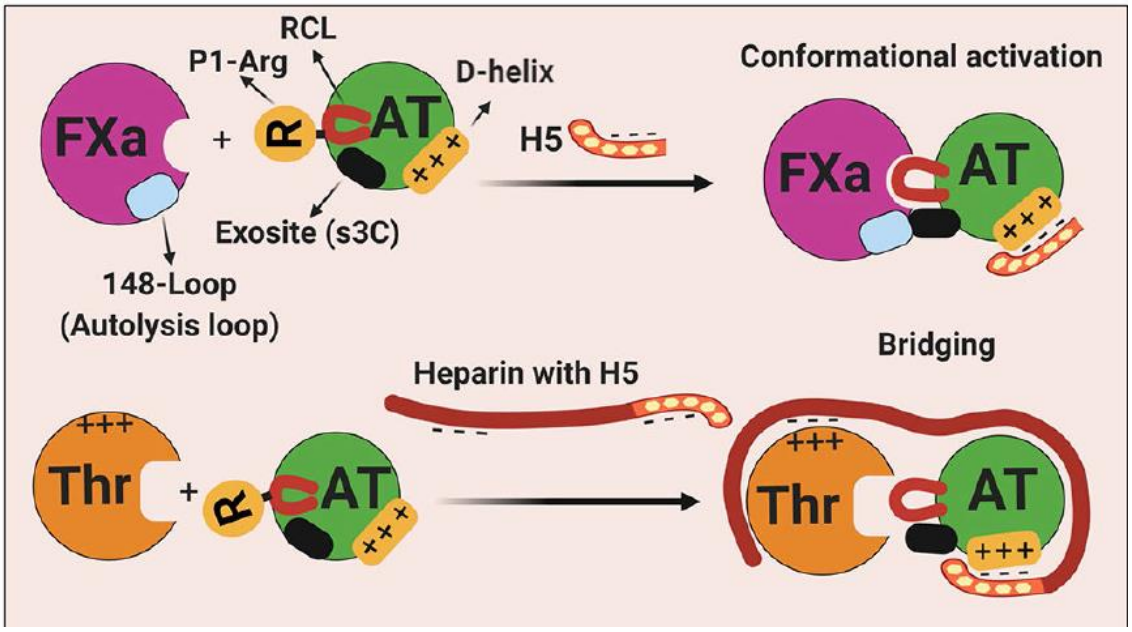

Figure 3. Interaction of native antithrombin with different heparins. (Top) Binding of heparin pentasaccharide (H5) on D-helix of the AT results in expulsion of the RCL and exposure of the cryptic exosite s3C, which interacts with the basic residue 148 of FXa, also called the autolysis loop. (Bottom) Unfractioned heparin (heparin with H5) binds both thrombin and D-helix of AT to promote the inhibition of the protease by a bridging mechanism. AT, antithrombin; FXa, factor Xa; H5, pentasaccharide; RCL, reactive center loop; s3C, strand 3 of β-sheet C; Thr, thrombin. Image extracted from Rezaie, A.R. *et al*[2].

2.3 Conformations of antithrombin

Due to the high structural flexibility of AT mentioned above, the protein presents different conformations: native, heparin-activated, prelatent, latent and cleaved[2].

The native conformation is thermodynamically unstable and has little inhibitory capacity. This is the conformation that circulates in our organism, since it allows maintaining the required hemostatic balance. Only when endothelial damage occurs and heparan sulfate glycosaminoglycans are exposed, or when heparin is released by mast cells, AT becomes activated to exerts its function at the appropriate site[10]. When native AT binds to its cofactor heparin, it triggers a conformational change that accelerates the inhibition of target proteases by about 1000-times, since its RCL becomes more accessible. In contrast, the latent and cleaved conformations are the most hyperstable conformations but lack inhibitory capacity, because the RCL is internalized within the central β-sheet, showing 6 central β-sheet instead of 5. This conformational change also

occurs when AT forms complexes with its target proteases upon inhibition. Indeed, when this inhibition is inefficient, the target protease escapes, but AT remains cleaved and also incorporates the RCL into the central β-sheet[12]. AT polymers are usually produced intracellularly due to mutations or *in vitro* by applying high temperatures (above 60°C) for a short period of time (10 to 30 minutes). In the case of the latent conformation, it is adopted when protein is senescent, although some mutations in AT may also increase its circulating concentration. It is also possible to generate the latent conformation *in vitro* by applying temperatures around 42°C for at least one week[13]. Despite lacking the inhibitory capacity of native AT, the latent and cleaved conformations have been shown to be antiangiogenic[14]. The prelatent conformation was first described by Larsson and colleagues when, after heating native AT at 60ºC, they observed this new form that had an affinity for heparin mid-way between the latent and native conformations, hence being called prelatent[15]. In fact, prelatent AT is found at very low concentrations in plasma, since it is in constant equilibrium between native and latent concentrations[16]. Moreover, the prelatent form is particularly interesting in as much as it is the most antiangiogenic form of all, a very important process in many tumors such as melanoma, breast cancer, colorectal cancer or glioblastoma multiforme (GBM)[17]. In addition, unlike the inactive conformations, it also retains a certain inhibitory capacity of the coagulation proteases[15].

2.4 Antithrombin deficiency

AT is described as the main inhibitor of the coagulation cascade as its deficiency has been shown to significantly increase the risk of suffering a thrombotic event. AT deficiency is a rare disease with low prevalence and an autosomal dominant inherited genetic component. For its detection, thrombophilia studies are performed, where both the levels and activity of AT present in the patient's plasma are measured. Other clotting factors such as protein C or prothrombotic polymorphisms like factor V Leiden or prothrombin are also measured in this screening. Congenital AT deficiency is classified into type I and type II. Type I occurs in heterozygosis, with complete loss of the mutated AT in circulation. Therefore, only 50% of AT is detected in plasma. Homozygous cases also occur, however, this is lethal at embryonic level as it causes massive subcutaneous hemorrhages. Type II is characterized by mutations in the AT gene (*SERPINC1*) and is classified into three subtypes. It can present mutations in the RCL (Type IIa), in the heparin binding site (Type IIb), or present multiple or pleiotropic

alterations that can affect the aforementioned sites and/or plasma concentration (Type IIc). The antigenic levels of AT with this type of mutations will be higher than 50%, but the functionality of AT will be lower than this value. In this case, homozygosity is rare but compatible with life[18,19].

2.5 Antithrombin beyond haemostasis

Beyond its role in hemostasis, it has been described that AT presents antiangiogenic, anti-inflammatory, antiapoptotic, antiviral and antitumor functions.

2.5.1 Anti-inflammatory antithrombin

All studies related to the anti-inflammatory role of AT have shown that this function is due to its D-helix interaction with different vascular heparan sulfate proteoglycans[20]. In addition, several clinical trials have confirmed the anti-inflammatory role of AT in patients with severe sepsis[21–23].

In 1990, it was first demonstrated that AT was able to induce the production of the anti-inflammatory prostacyclin, also known as prostaglandin I2 (PGI2), by its interaction with heparin-like glycosaminoglycan[24,25]. Furthermore, it was shown that the anti-inflammatory function of AT is due to its interaction with syndecan-4. This binding promotes the release of prostacyclins, thus inhibiting the production of inflammatory cytokines and tumor necrosis factor in monocytes and blocking neutrophil chemotaxis. They also demonstrate that exogenous heparin competes with syndecan-4 for its binding site to AT, thus concomitant administration of heparin and AT blocks the anti-inflammatory function of the serpin[26,27]. These results are consistent with those obtained in the different clinical trials mentioned above[21–23], where the administration of heparin did not improve patient mortality, but the administration of AT alone did. Also in 2002[28], it was demonstrated in cultured human monocytes and endothelial cells that AT blocks nuclear factor κB (NF-κB) activation and signaling, a transcription factor involved in inflammation. They also showed that this effect was performed by the interaction of AT with syndecan-4, as described by Kaneider *et al*[26].

However, in 2019, Praveen Papareddy *et al* demonstrated that the anti-inflammatory effect of AT is restricted to the β-AT isoform. In this study, they generated heterozygous mice expressing the α-AT or β-AT isoform, and exposed them

to lipopolysaccharide or infected them with lethal doses of *Escherichia coli*. While no differences were observed with α-AT, the β-AT isoform was able to prevent the death of mice after lethal doses were injected, as well as less inflammatory response and less severe organ damage. In this article, they also demonstrated that the anti-inflammatory function of the protein is performed by binding to different proteins on monocytes (CD13, CD300f and LRP-1) and thus blocking the NF-κB inflammatory response[29].

2.5.2 Antiapoptotic antithrombin

The antiapoptotic function of AT was first described after its administration in a rat model of obstructive jaundice diminished hepatocytes apoptosis. This ability was related to the capacity of AT to inhibit PGI2, as mentioned above, since the authors hypothesize that this could be due to the fact that PGI2, in turn, is able to inhibit leukocyte activation by inhibiting tumor necrosis factor, which would justify the antiapoptotic role of AT[30]. AT has also been shown to exert a protective role against liver damage in a murine model by decreasing liver transaminase levels, liver injury size, leukocyte infiltration and the amount of apoptotic Bcl-2 protein. However, the mechanism by which AT exerts this protective role was not explored[31].

2.5.3 Antiviral antithrombin

In 2002 it was shown for the first time that CD8+ T-cells produced during human immunodeficiency virus (HIV) infection release a modified form of AT capable of inhibiting viral replication. In addition, they also showed that native, heparin-activated and prelatent conformations were able to perform this antiviral function, while the latent form did not[32]. Later, another studied demonstrated that the antiviral role of AT not only in HIV but also in patients with hepatitis C virus infection was related to its capacity to block the NF-κB activation in CD4+ T-cells produced after the virus infection[33]. One of the most common comorbidities in patients with HIV is infection with hepatitis C virus. These patients usually progress to an end-stage liver disease, with decompensated cirrhosis being one of the primary causes of hospitalization and death. The latter aspect was investigated by Mohammed Asmal *et al*. In this study, they showed that AT also decreases the expression of overexpressed liver genes as a result of viral regulation, such as the matrix metalloproteinase 10 gene, which is also involved in the host cells inflammatory response to the virus, again demonstrating the anti-

inflammatory capacity of the serpin. Moreover, by combining AT administration with interferon α2 treatment, they also observed a reduction in the expression of genes related to liver cirrhosis or hepatocarcinoma[34].

2.5.4 Antiangiogenic antithrombin

Angiogenesis is the process by which new blood vessels are formed to supply oxygen and nutrients to cells. In various tumors, it has been observed that areas of malignant cells are highly vascularized compared to healthy areas, as the cells need this process to proliferate, survive and promote tumor progression[17].

The antiangiogenic role of AT has been studied in different *in vitro* and *in vivo* models of cancer such as pancreatic cancer, small cell lung cancer or GBM, among others[14,35–37]. This ability seems to be related to the conformation of AT, since it is only produced when the serpin has the RCL inserted, thus exposing certain epitopes that interact with the appropriate components of endothelial cell membranes[15]. In fact, Zhang, W., *et al*. performed mutagenesis assays on heparin binding sites of the latent and cleaved conformations, and observed that the antiangiogenic function of AT was lost. Thus, activation of native AT by heparin prevents this conformation from exhibiting this function[38]. Therefore, only the inactive conformations latent and cleaved, as well as the prelatent form, exhibit antiangiogenic function, unlike the native and polymeric conformations[14].

Several mechanisms of angiogenesis inhibition have been described for AT. For example, it has been described that AT may induce endothelial cell apoptosis, as well as the inhibition of cell proliferation by blocking focal adhesion formation and focal adhesion kinase activity[39]. Furthermore, a microarray study was conducted following treatment of primary umbilical cord vein endothelial cells with latent and cleaved AT. More than half of the under-expressed genes had pro-angiogenic functions in endothelial cells, while most of the over-expressed genes were antiangiogenic, promoting apoptosis and cell cycle arrest, and inhibiting tumor growth and metastasis, which would justify the antiangiogenic function of AT[40]. Additionally, it has been demonstrated that thrombin is able to promote the production of soluble vascular endothelial growth factor (VEGF), one of the most angiogenic growth factors studied. Therefore, the prelatent conformation of AT could also be exerting its antiangiogenic

role by inhibiting thrombin and hence impeding thrombin to release the angiogenic factor, while the inactive conformations of AT would not[36]. Also, AT is able to block the formation of ternary signaling complexes between the proangiogenic factors, such as human basic fibroblast growth factor and VEGF, and their receptors and heparan sulfate coreceptors on endothelial cells, thereby impeding growth factor signaling[41].

2.5.5 Antitumoral antithrombin

Finally, AT has been shown to exhibit antitumor function through inhibition of enteropeptidase (EP), which is a type II transmembrane serine protease (TTSP). Furthermore, it was shown that U-87 MG (U87) GBM cells silenced for EP expression significantly reduce their ability to migrate and invade, confirming the role of this protease in these tumorigenic processes. Finally, heparin-activated AT treatment of these EP-silenced cells further reduced these processes, especially in the case of invasion, indicating that other serine proteases besides EP may be under the control of AT[37].

3. Glioblastoma multiforme

3.1 Definition of glioma and classification

The central nervous system (CNS) is composed of both neurons and glia or neuroglia cells. The “glioma” term derives from Greek, meaning “glue”, as it was originally thought that these cells functioned only as support for neurons. However, today, it is known that they insulate, defend, and nourish neurons, thus playing a key role in their survival, which is very important, since neurons cannot be replaced. Glioma refers to all types of intra-axial tumors that originate from CNS glia cells[42]. Most gliomas are characterized by diffuse infiltrative growth of tumor cells in the preexistent parenchyma of the CNS, therefore also called diffuse gliomas[43]. Historically, gliomas have been classified on the basis of similar histological features, including astrocytomas (including high-grade astrocytomas called glioblastomas), brain stem gliomas, ependymomas, oligodendrogliomas, gliomas of the optic pathway, and mixed gliomas[44]. However, this histological classification provided no information on the malignancy of the tumor, no molecular basis, and therefore no possibility to design new drugs or more targeted treatments. In consequence, molecular information was added to the histological

diagnosis in 2014[45] and this allowed the World Health Organization to classify gliomas into grades I to IV in 2016[46].

Grade I gliomas present low proliferation rate and can be treated with complete surgery alone. For example, the most frequent glioma in children, the pilocytic astrocytoma, is a grade I neoplasm that usually shows limited infiltrative growth and does not progress to malignancy. Grade II gliomas are invasive and frequently recur despite their low proliferative potential. Grade III gliomas are usually histologically confirmed malignant tumors with rapid mitotic division anaplasia. Finally, grade IV is the most advanced grade with the worst prognosis, and it refers to GBM. In turn, GBM was divided into 3 groups according to the isocitrate dehydrogenase (*IDH*) gene. Ninety percent of cases are primary, occurring de novo in elderly patients and present wild type *IDH*. The other 10% progress from lower grade astrocytomas, are more prevalent in younger patients, and present the *IDH* gene mutated, with better prognosis. There is a third group where the gene status could not be determined[47]. Furthermore, through the study of genomic, transcriptomic and epigenetic profiles of the tumor, another subclassification into classical, mesenchymal, neural and proneural has been made possible, with the aim of developing more personalized treatments[48]. GBM affect primarily the cerebral hemispheres of adult brains and they are much less common in children, where they affect specifically the brainstem region[49].

GBM is the most aggressive and frequent lethal primary tumor of the CNS in adults, with no cure actually. Although is a rare tumor with global incidence of less than 10 per 100,000 people[50], according to U.S. National Cancer Institute, it represents 15.4% of all primary brain tumors and about 60%-75% of all astrocytomas. GBM is characterized by a median survival within the range of 12-15 months after diagnosis despite the aggressive multi-modality treatments[51]. In contrast, patients with grade II gliomas usually survive for more than 10 years, although they often progress to a higher grade and, therefore, to a worse prognosis of glioma[43].

3.2 Current treatment for glioblastoma

Standard treatment of GBM is based on as complete a surgery as possible, followed by concomitant radiotherapy and chemotherapy for 6 weeks. First and foremost, the removal of the tumor is attempted. Complete resection of the tumor has been shown to

increase survival, whereas with minimal residual tumor remaining, recurrence often occurs and in a more aggressive form[52]. Secondly, the tumor area is irradiated with 2 Gy per day, 5 days per week (60 Gy total). Chemotherapy is based on the administration of 75 mg/m^2 temozolomide (TMZ) per day. Afterward, TMZ alone is administrated every 4 weeks at 150-200 mg/m^2 per day for 5 consecutive days[53]. Recurrence usually occurs 6-9 months after diagnosis and in 90% of cases occurs at the edge of surgical resection. At the time of recurrence, survival is 3-6 months. No protocol has yet been validated in the treatment of recurrent GBM. An increase in TMZ doses does not lead to a gain in survival, but induces more toxicity, including necrosis of healthy tissue. Long-term side effects of radiation exposure (including neurocognitive, psychosocial, endocrine...) are present months or years after treatment and cause problems in the rare people who survive, as the effect of these side effects increases over time. In most cases, patients with recurrent GBM are included in clinical trials. Otherwise, several second-line therapeutic molecules are proposed, mainly alkylating agents (lomustine, carmustine, fotemustine, carboplatin or procarbazine), a microtubule destabilizing agent (vincristine) or an antiangiogenic drug (bevacizumab)[54].

3.3 Pathological characteristics of glioblastoma

This dismal patient outcome is due to the different characteristics that define GBM. Among them, the following aspects are found: 1) the evolution of intrinsic and acquired treatment resistance clones; 2) its high heterogeneity; 3) its high capacity for tumor infiltration and invasion of vital brain structures, 4) the presence of glioma stem cells; 5) the presence of the blood-brain barrier; or 6) its high vascularity; among others[54].

3.3.1 Inter- and intratumoral heterogeneity

The term "multiforme" comes from the first histopathological descriptions of this tumor, as it was observed that it presented diverse morphological features and the presence of several heterogeneous cell populations. Yung, W. K. *et al* demonstrated that different clones isolated from a single GBM tumor displayed a wide range of sensitivity to chemotherapeutics[55]. This high heterogeneity leads to treatment failure, as several of the existing treatments are developed against a specific target, preventing all patients from benefiting from them in the case of presenting this mutated target. This has been the case of a treatment tested in a clinical trial conducted at the Vall d'Hebron Institute

of Oncology. The treatment consists of a bispecific antibody that binds T-cells via CD3 on the one hand, and GBM cells via the mutated variant III of the epidermal growth factor receptor (EGFRvIII) on the other, so that the former destroy the latter by cytotoxic attack. The difficulty of this strategy has not only been to find targets that are expressed on the surface of tumor cells and are not shared by healthy cells, but also that the EGFRvIII mutation is only found in 50% of patients with GBM, preventing GBM patients with wild-type EGFR from benefiting from this promising treatment[56].

Another factor involved in the heterogeneity that characterizes this tumor is the presence of glioma stem cells (GSCs). These cells are capable of self-renewal and give rise to non-tumorigenic but phenotypically diverse daughter cells with limited division properties that can differentiate and compose the bulk of the tumor, thus hindering the proper delivery of targeted radiotherapy or preventing chemotherapy from reaching tumor cells[57].

In short, the heterogeneity of this tumor continues to be one of the most important bottlenecks in the therapeutic progress of this tumor. For this reason, multi-treatment in glioblastoma is currently necessary.

3.3.2 Tumour infiltration and invasion

GBM has a high capacity to infiltrate healthy tissue through the perivascular space around blood vessels, and through the parenchyma surrounding the tumor, which contains neuronal and glia cells[58]. Invasion occurs by vessels co-option, a process by which vessels move into and along pre-existing blood vessels in order to gain access to the vasculature instead of generating new vessels, or through the white matter and subarachnoid space. In addition, these cells are also capable of returning to the initial tumor site[59]. For this process to occur, several changes in the tumor cell are necessary, such as changes in energy metabolism, cytoskeleton, cell adhesion and extracellular matrix remodeling[60].

This feature is clinically relevant in the treatment of GBM. On the one hand, it prevents complete resection of the tumor, which has already been shown to favor a more aggressive future recurrence with lower overall survival[52]. Furthermore, it prevents the radiotherapy focusing, as it impedes the radiation from reaching GBM cells that have invaded more distant from the tumor. Regarding the patients, invasion of

various brain structures often results in pathophysiological squeals for them. For example, if invasion occurs in the temporal or parietal area, speech function may be impaired and patients often suffer from epileptic episodes[60].

3.3.3 Presence of glioma stem cells

One of the main characteristics of GBM is its ability to migrate through brain tissue and its very high capacity to invade areas outside the tumor mass, thus preventing complete resection of the tumor and, therefore, favoring future recurrence[59]. The second characteristic is that it presents a great inter- and intra-tumoral heterogeneity[57]. These characteristics involve GSCs, which are characterized by their ability to self-renew (ability to divide while maintaining its de-differentiated state, i.e. its stem cell state), persistent proliferation, and are able to initiate and recapitulate the heterogeneity of the initial tumor once it has been removed. In addition, they may have other properties such as the ability to differentiate into various types of cancer cells within the tumor, which has been shown to contribute to both GBM progression and resistance to treatment[61]. In fact, it has been demonstrated that GSCs can escape the action of TMZ and radiotherapy[62]. Regarding this, it has been speculated that it may be due to their quiescent status, resulting in ineffectiveness of chemotherapies targeting the cell cycle. This is because of their high expression of membrane transporters, which would flush out chemotherapeutic agents, or because of a defective regulation of apoptosis, with would increase the expression of survival factors and the ability to adapt under stress conditions[54]. The presence of GSCs can be explained by malignant transformation of non-tumor neural stem cells and/or dedifferentiation of tumor cells into tumor stem cells after radio- or chemotherapy[63].

3.3.4 Presence of the blood–brain barrier

The blood-brain barrier (BBB) is a structure constructed of endothelial cells, pericytes and astrocytes around the blood vessels of the brain that acts as a filter, 'screening out' substances and cells that can migrate from the blood into the CNS. Likewise, the presence of this BBB makes it difficult for different chemotherapeutic agents to enter the tumor core[64]. Several studies have shown that both TMZ and bevacizumab (a second-line chemotherapy agent) cross the BBB[65,66]. This is explained by the fact that during tumor progression, the BBB has been shown to become more

permeable. However, it has also been demonstrated that there are also clinically significant tumor sites with an intact BBB in all GBMs, preventing drugs with poor permeability from providing therapeutic exposures in these tumor sites[67].

This is a major challenge in the treatment of GBM as, while in other tumors chemotherapy is administered systemically, in GBM the presence of the BBB makes this process difficult. Therefore, several types of minimally invasive delivery targeting the tumor core have been developed. Among these therapies are, for example, laser interstitial thermal therapy, stereotactic injections, convection-enhanced delivery, catheters or intra-arterial delivery[68].

3.3.5 High vascularization of glioblastoma (angiogenesis)

A pathological feature of GBM is that it is highly vascularized (Figure 4). Hypoxia is the main trigger of this event, as it activates hypoxia-inducible factor-1 (HIF-1) which, in turn, controls the release of various proangiogenic factors from the tumor cells that end up being produced in excess without balance, such as VEGF[69,70]. These factors bind to their receptors on the endothelial cell membrane, thus triggering the activation of matrix metalloproteases that eventually degrade the extracellular matrix. Therefore, as the endothelial cells migrate and proliferate, they increase vascular permeability, since as they migrate, they form a new endothelial tube, around which a basement membrane is formed, resulting in a new stable vessel. The process described above, that is, the formation of new vessels from pre-existing ones, is the most well-studied mechanism for tumors to generate vasculature and it is called angiogenesis[71,72].

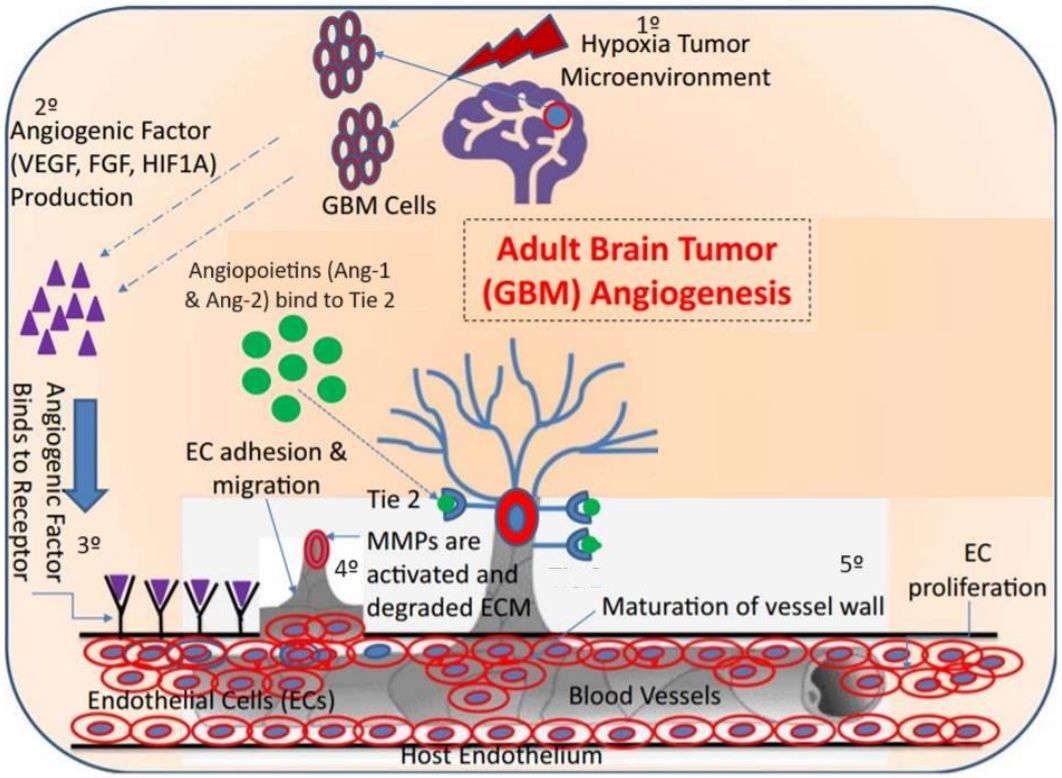

Figure 4. Angiogenesis in glioblastoma (GBM). Under a hypoxic microenvironment, GBM cells release the major angiogenic factors such as VEGF, FGF, HIF1α, and Ang-1 and Ang-2. These angiogenic factors bind to their receptors on endothelial cells and then start to initiate the endothelial cell proliferation and migration. During the endothelial cell proliferation and migration processes, the extracellular matrix starts to degrade, and the endothelial cells are assembled into a tube/vessel-like structure. In the end, the new blood vessel wall is formed, which is constructed by the recruitment of pericytes to cover the endothelial cells from its outside to form a new blood vessel formation. Image adapted from Ahir, B. K., *et al*[71].

It has been shown that only 3-6 glioma cells are needed to fill the space between two adjacent microvessels. Thus, GBM cells can reach out to already well-perfused blood vessels without the need to the angiogenesis pathway. Vessel co-opting GBM cells benefit from both their oxygen and nutrients supply and the specific microenvironment of the vascular niche. In addition, infiltrating GBM cells that employ vascular co-option use the vasculature as a scaffold to invade normal CNS tissue. Clinically, studies have shown that vessel co-option occurs in GBM patients in the peritumor regions, and that is increased in patients following antiangiogenic treatment (Bevacizumab). Thus, vessel co-option has been proposed as a resistance mechanism to antiangiogenic therapy[73].

4. Corollary

AT has been shown to have various functions beyond the inhibition of certain proteases in the coagulation cascade. These other functions depend on either its inhibitory activity of serine proteases or its ability to bind to other proteins through its heparin-binding domain. Its various conformations have also been shown to have different effectiveness in the described functions beyond the control of hemostasis. Among these described functions, the anti-tumoral function of AT has been the least explored. Therefore, exploring the anti-tumor functions of AT, mainly in GBM, a tumor for which effective strategies to increase patient survival have not yet been found, seems interesting. It is important to delve into the potential of AT as a new treatment in GBM based on its pleiotropic effects on tumor cells, as well as investigate the role of less studied conformations such as prelatent AT.

OBJECTIVES

Chapter 1) Characterization of the antitumor functions of prelatent antithrombin on glioblastoma multiforme cells

Chapter 2) Study of the cellular mechanisms underlying the antitumor effect of native and prelatent conformations of antithrombin on glioblastoma cell lines.

Chapter 3) Identification of the potential receptor of antithrombin in glioblastoma multiforme cells and validation of the *in vitro* results in a preclinical model based on the use of organoids and in samples of glioblastoma multiforme patients.

CHAPTER 1. Characterization of the antitumor functions of prelatent antithrombin on glioblastoma multiforme cells

1. Introduction 37
2. Material and methods 38
2.1 Purification of native and prelatent antithrombin 38
2.2 Characterization of native and prelatent antithrombin 39
2.3 Cell culture 39
2.4 Enteropeptidase inhibition by prelatent AT and complex formation 40
2.5 Wound healing assay 41
2.6 Matrigel invasion assay 41
2.7 Real Time-PCR and Immunoblotting of Selected Cancer Signalling Proteins . 42
2.8 Statistics 42
3. Results 43
3.1 Prelatent antithrombin characterization 43
3.2 Prelatent AT is able to inhibit enteropeptidase 44
3.3 Native and prelatent antithrombin inhibits migration and invasion of glioblastoma multiforme cells 45
3.4 Prelatent antithrombin downregulates the expression or function of different cancer signalling molecules 49
4. Discussion 52

Peñas-Martínez, J.; Luengo-Gil, G.; Espín, S.; Bohdan, N.; Ortega-Sabater, C.; Ródenas, M.C.; Zaragoza-Huesca, D.; López-Andreo, M.J.; Plasencia, C.; Vicente, V.; Carmona-Bayonas, A.; Martínez-Martínez, I. Anti-Tumor Functions of Prelatent Antithrombin on Glioblastoma Multiforme Cells. Biomedicines 2021, 9, 523. https://doi.org/10.3390/biomedicines9050523

1. Introduction

The first antitumor mechanism of action described for AT was through inhibition of the TTSP superfamily known as enteropeptidase. TTSP are regulated by endogenous protease inhibitors, especially by inhibitors with Kunitz domains and by serpins. These proteases are involved in the degradation and remodeling of the extracellular matrix. Their deregulation has been observed in certain tumors, thus facilitating tumor growth, invasion of surrounding tissues, and establishment of metastatic colonies[74,75].
It has recently been shown that native and heparin activated AT may also have a potential antitumor function by inhibiting EP. Physiologically, EP is expressed at the brush border of the duodenal mucosa where it is involved in the degradation of the extracellular matrix and in converting pancreatic trypsinogen to trypsin, an essential step for the initiation of proteolytic reactions of digestive enzymes in the small intestine[74]. However, its expression has also been observed in the brain, where high concentrations of the serine protease have been shown to drastically decrease the survival of hippocampal neurons[76].

The antitumor mechanism of AT was described as follows: when AT and EP interacts, the RCL of AT is broken, generating a peptide that would be bound to the active center of EP and act as an irreversible inhibitor. The identification of the peptide would be very useful, as it could act as an antitumor drug. However, further studies are needed to confirm this hypothesis[37]. Moreover, silencing of the gene coding for EP (*TMPRSS15*) significantly reduces migration and invasion of U87 cells[37].

On the other hand, as indicated above, in 2001 Larsson *et al*. demonstrated that treatment of native AT with an elevated temperature similar to that used to prepare latent AT, caused a limited conformational change in serpin that generated a new form of AT. This new form was characterized by showing a potent antiangiogenic function and antitumor activity which, unlike latent AT, retained its protease binding ability and had a higher affinity for heparin than the latent form but lower than native AT. Therefore, they decided to denote this new form as prelatent AT[15]. Afterwards, Karlsson *et al*. in 2004 improved the purification of prelatent AT by applying two steps of heparin affinity chromatography, harnessing the intermediate heparin affinity of this conformation. They also used citrate in the incubation buffer for its lipotropic effect, which influences the hydrophobic interactions of proteins, decreasing aggregation and

denaturation of AT during heat treatment[77,78]. As for the biochemical characterization of prelatent AT, Steve Olson *et al*. further explored on this and determined that prelatent AT shared certain characteristics with native AT, such as its ability to inhibit the target proteases of the coagulation cascade, and others in which it differed, such as its affinity for heparin and melting temperature[16].

Regarding GBM, is the most aggressive and lethal primary malignant tumor of the CNS in adults and, despite aggressive multi-modality treatments (surgery, radiotherapy, chemotherapy (temozolomide)), the median overall survival remains within the range of 12–15 months since diagnosis and has failed to increase in recent years. Therefore, GBM remains a poor prognosis tumour, where urgently necessary to discover new targets and develop new drugs that increase the survival of GBM patients, improve their quality of life, and minimize the side effects of different treatments[79,80]. The main objective of this chapter was to evaluate the previously unstudied antitumor functions of prelatente AT on GBM cells.

2. Material and methods

2.1 Purification of native and prelatent antithrombin

The following protocol was used in all chapters in order to purify native and prelatent AT. Native AT was purified as previously described[81]. Briefly, α-AT was purified from a pool of human plasma from four healthy subjects by two steps of heparin affinity chromatography using HiTrap Heparin columns (GE Healthcare) and an ÄKTA Purifier (GE Healthcare). A gradient from 0 to 3 M NaCl in 50 mM Tris-HCl, pH 7.4 was applied for the elution of native α-AT. Finally, proteins were eluted using a gradient from 0 to 1 M NaCl and desalted using dialysis tubing (Sigma-Aldrich, D0530-100FT). The purity of proteins was evaluated by silver staining of 8% sodium dodecyl sulfate polyacrylamide gel electrophoresis (SDS-PAGE), as indicated elsewhere[82]. Proteins were stored at -80ºC. In this study, we did not use β-AT isoform. Prelatent AT was generated by first concentrating 13 mg of native α-AT purified from human plasma at 60ºC for 30 hours in 0.5 M sodic citrate, 10 mM Tris-HCl, pH 7.4 buffer. Then, it was purified by two steps of heparin affinity chromatography using HiTrap Heparin columns (GE Healthcare) and an ÄKTA Purifier (GE Healthcare), slightly modifying the linear gradient previously described[16], as follows: 0.1–0.88 M NaCl gradient from 5–35 min, and hold at 0.88 M NaCl for 20 min. Finally, the prelatent AT obtained was dialyzed

using dialysis tubing in 20 mM sodium phosphate, 20 mM NaCl, 0.1 mM ethylenediaminetetraacetic acid, pH 7.4 buffer (buffer A), and concentrated in 1 mL using the Vivaspin^{TM} 20 system (Sartorius, 10670333). Its concentration and purity were evaluated by silver staining.

2.2 Characterization of native and prelatent antithrombin

The following protocol was used in all chapters after every purification, in order to confirm the native and prelatent conformations.

The dissociation constant (K_D) for the interaction between AT and heparin was determined as described previously[83]. Briefly, the increase of intrinsic fluorescence of native and prelatent AT (50 nM) after pentasaccharide Fondaparinux (0–8 μM) titrations (Arixtra) was measured at room temperature (25ºC) under physiologic ionic strength (I) of 0.30 in 20 mM sodium phosphate, 0.25 M NaCl, 0.1 mM ethylenediaminetetraacetic acid, polyethylene glycol 8000 0.1%, pH 7.4. A 2 ml quartz cuvette (10 mm path length) (Agilent technologies) was used, and fluorescence was monitored on a Cary Eclipse Fluorescence Spectrophotometer (Agilent), with excitation at 280 nm and emission at 340 nm, using bandwidths of 3.5 nm for both excitation and emission. Fluorescence emission intensity was calculated as the average of 100 measurements saved at 1-s intervals for each heparin addition. Data were analyzed using SigmaPlot 11.0 software (Systat Software Inc., accessed on 5 May 2018) and adjusting the results by non-linear regression to a 2-paremeter hyperbolic equation to estimate the K_D for antithrombin-heparin interactions.

Formation of covalent complexes between native or prelatent AT and FXa or FIIa was evaluated by incubating for 15 minutes at 37 °C the AT conformations with Fondaparinux pentasaccharide (0.14 mM) or unfractionated heparin (3.3 mM) and, next and respectively, with FXa (1 μM) or FIIa (9.50 μM) for 45 minutes at 37 °C. The same assay was carried out but in the absence of heparin. Complexes were evaluated by 8% SDS-PAGE under reducing conditions and silver staining.

2.3 Cell culture

The following protocol was used in all chapters for the culture of the GBM cell lines. Human GBM cell lines U-87 MG (U87) and U-251 MG (U251) were purchased from

American Type Culture Collection and European Collection for Authenticated Cell Cultures, respectively. The U87 cell line was authenticated by Bioidentity (Elche, Spain) by STR, according to the American National Standards Institute. STR profiling was carried out following the ANSI/ATCC ASN-0002-2011 guidance, Authentication of Human Cell Lines: Standardization of STR Profiling. For the U251 cell line, manual DNA extraction was performed and the PowerPlex® 16 System (Promega, Madrid, Spain) was used for STR analysis. STR profiles were analyzed by GeneMapper 5 software and the cellosaurus STR database (CLASTR) search tool of the Cellosaurus database (ExPASy) (https://web.expasy.org/cellosaurus/, accessed on 13 February 2020). U87 and U251 cells were treated with 10 µg/mL cyclins (BM Cyclin, Sigma-Aldrich, 10799050001) for the decontamination of possible mycoplasmas. U87 and U251 cells were grown in DMEM medium containing 1 g/L or 4.5 g/L glucose, respectively (Gibco Thermo Fisher, 11570406 and 11594416, respectively) and both supplemented with 10% fetal bovine serum (Gibco Thermo Fisher), 1% sodium pyruvate (Gibco Thermo Fisher), 1% non-essential amino acids (Gibco Thermo Fisher, 11140050), 1% L-GlutaMAX (Gibco Thermo Fisher), and 0.1% gentamicin (Gibco Thermo Fisher, 15750-037). Cells were maintained in T-75 tissue culture flasks (Fisher scientific, 353136) and grown in 5% CO_2 at 37ºC, in a humidified incubator.

2.4 Enteropeptidase inhibition by prelatent AT and complex formation

The formation of covalent complexes between AT and EP was evaluated by 8% SDS-PAGE under non-reducing and reducing conditions, and western blot, after incubating native or prelatent AT (0.17 µM) with EP (4.98 µM) (Sigma-Aldrich), for 1 hour, at 37ºC, in the presence or absence of 0.11 mM low molecular weight heparin (LMHW) (0.11 mM) (Bemiparin, Laboratorios Farmacéuticos Rovi). For detection by western blot, a rabbit anti-human AT antibody was employed (Sigma-Aldrich, A9522), followed by horseradish peroxidase-conjugated donkey anti-rabbit IgG (Amersham, NA9340). Detection was performed using the ECL kit (Thermo scientific, 32106).

The interaction between AT and EP was evaluated by chromogenic assays as previously described[37]. Briefly, native or prelatent AT (0.5 µM), were incubated in the presence or absence of LMWH (33 µM) (Bemiparin, Laboratorios farmacéuticos Rovi) and EP (0.55 µM) (Sigma-Aldrich), in TCNB buffer (50 mM Tris-HCl, 10 mM $CaCl_2$, 150 mM NaCl, 0.05% Brij-35, pH 7.5), in a 96-well plate for 1 h, at 37ºC in a total volume of

100 µL. After adding the chromogenic substrate Z-Lys-SBzl (200 µM), the absorbance at 405 nm was measured on a microplate reader. Triplicate assays were performed for each condition.

2.5 Wound healing assay

To determine the concentration at which AT exerts its greatest antitumor effect on U87 cells, we performed a wound healing assay. U87 cells were cultured as confluent monolayers in a polystyrene microplate 6-well (Falcon, 353934). Then, cells were wounded by removing a 300–500 µm-wide strip of cells across the well with a standard 200 µl pipette tip, and washed twice to remove non-adherent cells. Increasing concentrations of prelatent AT were incubated with cells for 11 hours: (1) Control: buffer A, (2) 0.86 µM, (3) 1.72 µM, (4) 2.16 µM, (5) 2.59 µM, (6) 3.02 µM. Images were taken using a Leica DMI6000 B microscope. Finally, wound healing was quantified using ImageJ software as the median percentage of the remaining cell-free area compared to the area of the initial wound (n=3).

Once the AT administration concentration was determined, the migration capacity of U87 cells was assessed following the same wound healing experiment after 11 hours of incubation with these conditions: (1) control: medium supplemented with buffer A; (2) 3.88 µM native AT; (3) 2.16 µM prelatent AT; (4) 200 U/mL LMWH (enoxaparin, Sanofi-Aventis); (5) 3.88 µM native AT and 200 U/mL LMWH, (6) 2.16 µM prelatent AT and 200 U/mL LMWH. Triplicate assays were performed for each condition, and results were expressed relative to the control condition.

2.6 Matrigel invasion assay

The experiment was performed at 37ºC for 6h using 24-well transwell inserts coated with Matrigel (BD Biosciences). U87 cells ($7x10^4$ cells) suspended in 400 µL of serum-free medium were seeded into the upper chamber and 500 µL of serum-supplemented medium was added in the lower chamber. The following six treatments were analyzed against untreated cells: (1) control (cells with serum-free medium); (2) 12.93 nM native AT; (3) 12.93 nM prelatent AT; (4) 200 U/mL LMWH (enoxaparin, clexane, Sanofi-Aventis); (5) native AT and LMWH, and (6) prelatent AT and LMWH. Images were taken using a Leica DMI6000 B microscope. Cells that migrated and invaded the membrane were counted after fixing with methanol and staining with crystal violet.

Images were analyzed with Fiji-ImageJ 1.52i software.

2.7 Real Time-PCR and Immunoblotting of Selected Cancer Signalling Proteins

U87 cells were incubated with prelatent AT (2.16 μM) or buffer A (n = 8/group). After 11 h of incubation, total RNA was isolated using Trizol® Reagent (Invitrogen) following manufacturer's instructions. The RNA concentration and 260/280 ratio were determined by using a NanoDrop spectrophotometer (Thermo Scientific). From total RNA, a 200-ng sample was reverse transcribed to cDNA according to the manufacturer's instructions (SuperScript First Strand, Invitrogen). PCR reactions were carried out using TaqMan® Gene Expression probes: vascular endothelial growth factor A (*VEGFA*): hs00900055_m1; signal transducer and activator of transcription 3 (*STAT3*): hs00374280_m1; on a LC480 real-time PCR (Roche) in triplicate for each sample. *GAPDH* (hs99999905_m1) expression was used as the endogenous reference control as its expression was not affected by the prelatent AT treatment. The fold difference for each sample was obtained using the 2-ΔCt method.

Concurrently, cells were lysed and samples separated by 8% SDS-PAGE under reducing conditions to evaluate pAKT, pERK1/2, pSTAT3, and VEGFA protein expression (n=4). Bands were detected by western blot following standard immunoblotting procedures using polyvinylidene difluoride membrane. Primary anti-human antibodies (1:1000 dilution) were pAKT (Invitrogen), pERK1/2 (9101S, Cell Signaling Technologies), pSTAT3(Tyr705) (9145, Cell Signaling Technologies), and VEGFA (ab46154, Abcam) made in rabbit. Secondary IgG antibodies were horseradish peroxidase-coupled and visualized by the ECL kit detection. Protein expression of GAPDH (3683, Cell Signaling Technologies) was used as the endogenous reference control.

2.8 Statistics

The Kruskal–Wallis test was applied to evaluate genetic expression and percentage data according to different AT conformations. Pairwise comparisons were evaluated by means of post hoc Dunn tests adjusted with the Benjamini–Hochberg method.

3. Results

3.1 Prelatent antithrombin characterization

Every time native and prelatent AT were purified, the conformations were confirmed by two methods: affinity for heparin by dissociation constant (K_D) determination (Figure 5A), and by complexes formation with FX and FIIa in the presence or absence of pentasaccharide or unfractioned heparin, respectively, by 8% SDS-PAGE under reducing conditions (-DTT) and silver staining (Figure 5B).

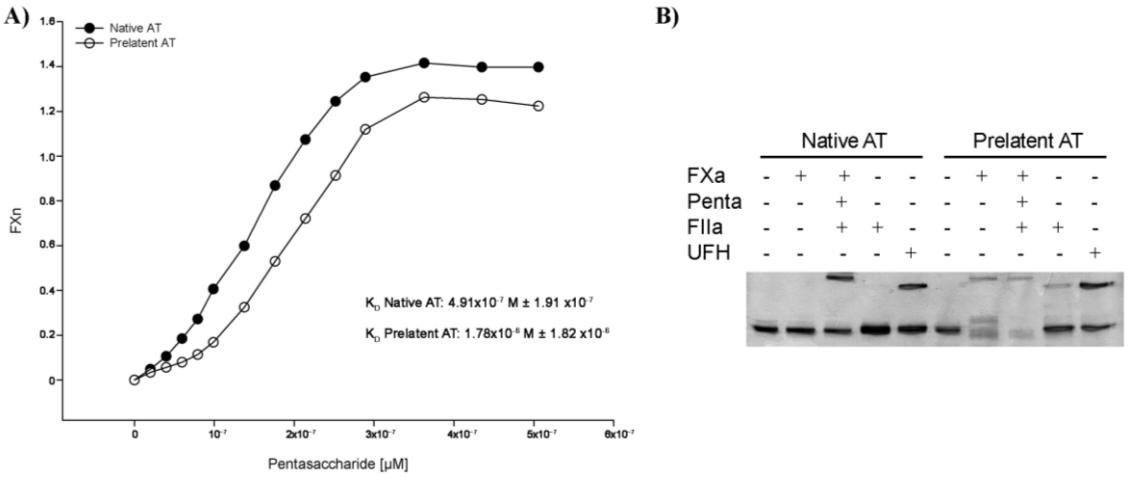

Figure 5. **Characterization of native and prelatent antithrombin**. A) Heparin-antithrombin (AT) binding assay. Dissociation constant determination. Plot of intrinsic tryptophan fluorescence intensity of native and prelatent AT *vs*. increasing heparin concentration. Black and white circles represent the best-fit curves calculated with non-linear regression to a 2-paremeter hyperbolic equation. B) Complex formation of native or prelatent AT with factor Xa (FXa) and factor IIa (FIIa), in the presence or absence of pentasaccharide (Penta) or unfractioned heparin (UFH), respectively, by 8% SDS-PAGE under reducing conditions and silver staining.

We began by confirming the previously known inhibitory profile of the prelatent AT and its affinity for heparin, lower than native AT (K_D prelatent AT-heparin: $1.78x10^{-6}$ M ± 1.82 $x10^{-6}$ M vs K_D native AT-heparin: $4.91x10^{-7}$ M ± $1.91x10^{-7}$ M) (Figure 5A).

As shown in Figure 5B, in the absence of heparin, the native conformation was only able to complex with the clotting factors in the presence of heparin. However, the presence of prelatent AT-protease complexes were observed both in the presence and absence of heparin. It has been previously reported that the prelatent conformation exhibits anticoagulant function, but this is not superior to that exerted by the native form[16]. We attribute these results to the fact that, during purification, some heparin may

be coming off the affinity columns. In view of these results, all assays performed during this doctoral thesis were always compared with a control treated with buffer A (20 mM sodium phosphate, 20 mM NaCl, 0.1 mM ethylenediaminetetraacetic acid, pH 7.4 buffer) which we flowed through the columns in the same way as we purified the prelatent conformation, in order to ensure that it showed the same traces of heparin that might be present in the purified AT.

3.2 Prelatent AT is able to inhibit enteropeptidase

After characterization of the prelatent AT, we evaluated the inhibitory capacity of this conformation on EP, and in comparison with native AT. As seen in Figure 6A, the electrophoresis under reducing conditions revealed no covalent complex formation with any of the AT conformations, since no bands were detected around 90 kDa, which would be the estimated molecular weight for the complex between AT and EP. However, under non-reducing conditions (Figure 6B), in all reactions with EP we observed a band of broken AT band in all reactions with AT, with less migration than intact AT. These results are in agreement with those previously published for heparin-activated AT[37]. Therefore, as the prelatent AT behaved the same as the native conformation in both electrophoresis, both forms of AT could be exerting the same inhibitory effect on EP. Electrophoresis was conducted under reducing (Figure 6A) and non-reducing conditions (Figure 6B), since DTT it is known to affect the electrophoretic migration of cleaved AT[37].

Therefore, as both conformations generated the same cleavage on EP, we evaluated the residual enzymatic activity of this serine protease in the presence of the different AT, both in the presence and absence of LMWH by chromogenic assay. As shown in Table 1, both conformations slightly inhibited EP activity. However, in the presence of heparin, the inhibitory effect was 4-times higher for native AT, and only 1.2-times higher for prelatent AT.

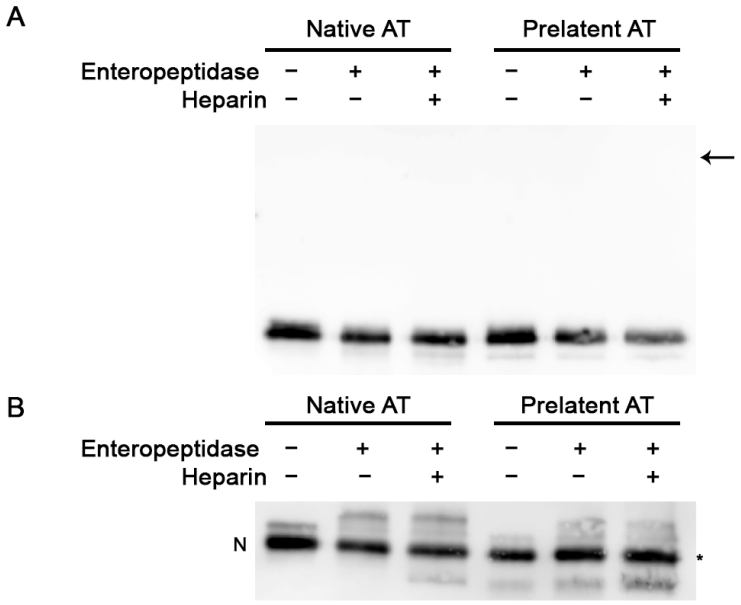

Figure 6. **Evaluation of the interaction between antithrombin (AT) and enteropeptidase (EP)**. SDS-PAGE, 8%, under reducing (+DTT) (6A) and non-reducing (-DTT) (6B) conditions, revealed by western blot with anti-AT antibody.1) Native AT; 2) Native AT + EP; 3) Native AT + EP + LMWH; 4) Prelatent AT; 5) Prelatent AT + EP; 6) Prelatent AT + EP + LMWH. Broken AT bands are indicated by an asterisk (*).

Table 1. **Enteropeptidase activity**. Maximum velocity at 405 nm (Vmax405) (mOD/min) of the interactions between native or prelatent antithrombin (AT) with enteropeptidase (EP), in the presence and absence of low molecular weight heparin (heparin) (n=3).

Table 1. Enteropeptidase activity	
Condition	**$Vmax_{405}$ (mOD/min)**
Enteropeptidase	3.357 ± 0.311
Native AT + Enteropeptidase	2.714 ± 0.679
Prelatent AT + Enteropeptidase	2.976 ± 1.209
Native AT + Enteropeptidase + Heparin	0.536 ± 0.258
Prelatent AT + Enteropeptidase + Heparin	2.571 ± 0.619

3.3 Native and prelatent antithrombin inhibits migration and invasion of glioblastoma multiforme cells

Given that the native and prelatent conformations of AT are able to inhibit EP, which is expressed in the plasma membrane of U87 GBM cells, we decided to evaluate the inhibitory capacity of prelatent AT on tumor migration and invasion of this cells in comparison with native AT, both in the presence and absence of heparin. For this purpose, we first performed a dose-response curve assay, in order to determine the concentration of AT required for the greatest antitumor effect. Surprisingly, we obtained

a value of 2.16 µM (Figure 7), equivalent to the plasma concentration of AT in plasma.

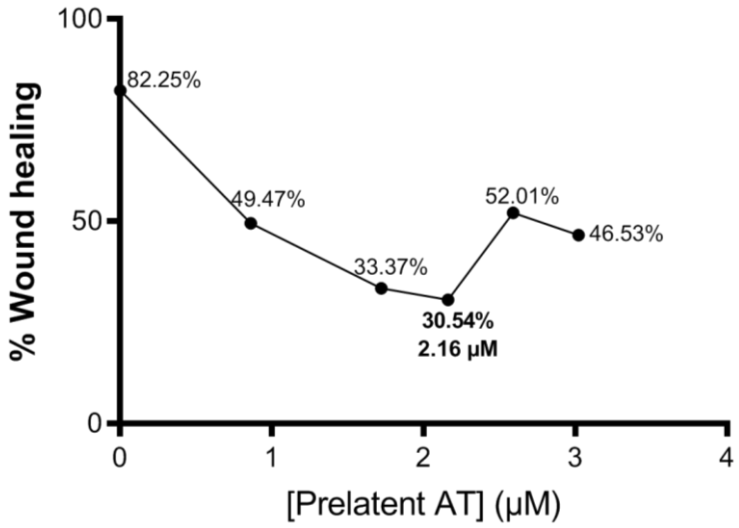

Figure 7. Dose-response curve of prelatent antithrombin (AT) and percentage of wound healing. Cells were treated with different concentrations of prelatent AT for 11 hours. The results are expressed as the percentage of remaining wound area.

Tumor migration was assessed using the wound healing technique. As shown in Figure 8, prelatent AT was able to reduce tumor migration significantly compared to the control (mean percentage of confluence, 55% vs. 72%, p-value <0.001), and more efficiently than native AT (55% vs. 68%, p<0.01), while native AT and the control revealed no differences (60% vs 72%, respectively, p=0.326). In addition, the prelatent AT-heparin complex did not enhance the inhibition, whereas native AT exerted a greater inhibitory effect when interacting with its cofactor.

We also measured the effect of prelatent AT on tumor invasion using matrigel-coated transwells. Prelatent AT was also able to reduce the invasion of U87 cells (Figure 9). Although significant results (p<0.001) were only obtained after treatment with native AT and LMWH, both conformations (native and prelatent), in the presence and absence of LMWH, were able to inhibit the invasion of GBM cells.

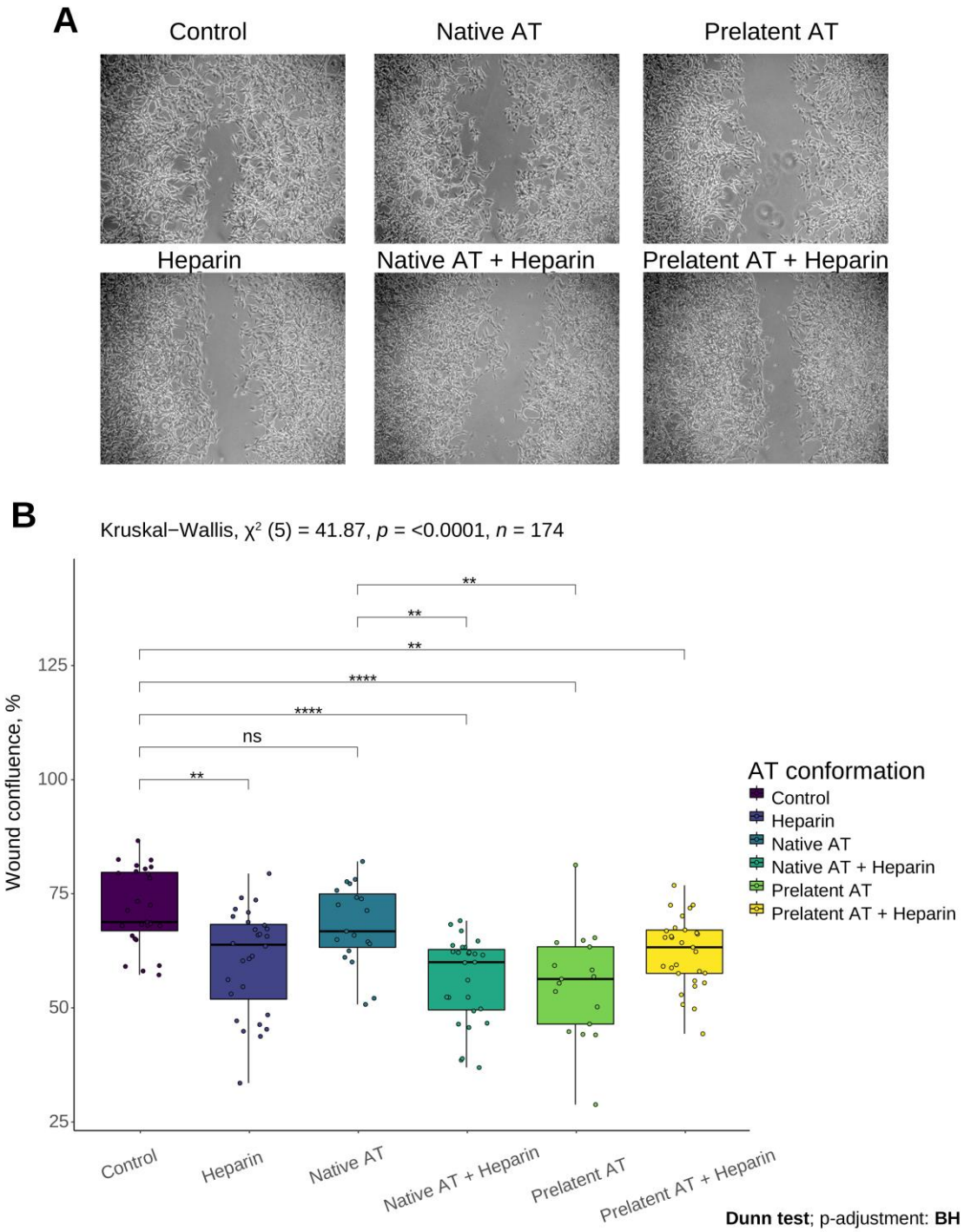

Figure 8. Antithrombin inhibits U87 glioblastoma cells migration. The migratory capacity of U87 cells was assessed by wound healing after 11 hours of incubation with low molecular weight heparin (heparin), native or prelatent antithrombin (AT), and each AT in the presence of heparin. Each condition was evaluated in triplicate, and 5 different images were processed for each assay. (A) Microscopy images. (B) Cell confluence (%). * $p<0.05$; ** $p<0.01$; **** $p<0.0001$; ns = not significant.

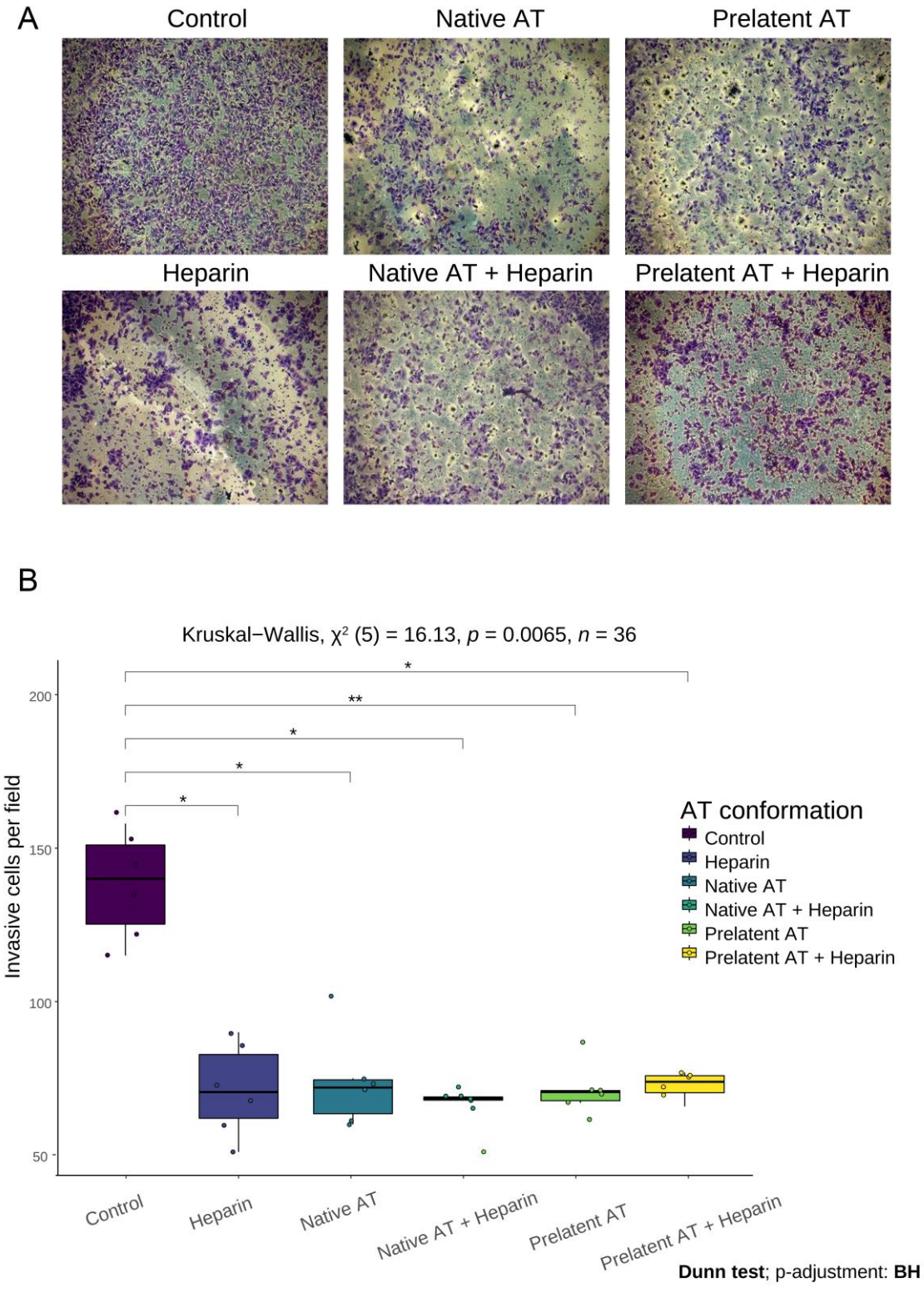

Figure 9. **Antithrombin inhibits U87 glioblastoma cells invasion.** Invasion was assessed by transwell assay after incubation of U87 cells for 6 hours with low molecular weight heparin (heparin), native or prelatent antithrombin (AT), and each AT in the presence of heparin. Each condition was evaluated in triplicate, and 3 different images were processed for each assay. (A) Microscopy images. (B) Number of invasive cells per field. (%). * $p<0.05$; ** $p<0.01$; BH = Benjamini–Hochberg procedure.

3.4 Prelatent antithrombin downregulates the expression or function of different cancer signalling molecules

On the one hand, the prelatent conformation of AT is the most antiangiogenic of all[15]. On the other hand, a pathological feature of GBM is that it is highly vascularized[84]. One of the mechanisms involved in the vascularization of GBM is the release of angiogenic factors, such as VEGF, by the tumor cells themselves, which increases vascular permeability and promotes cell migration[69]. Therefore, we studied the effect of prelatent AT on VEGFA expression in U87 cells and compared it with native AT. As shown in Figure 10, prelatent AT was able to statistically significantly inhibit this factor at both mRNA and protein levels in U87 GBM cells.

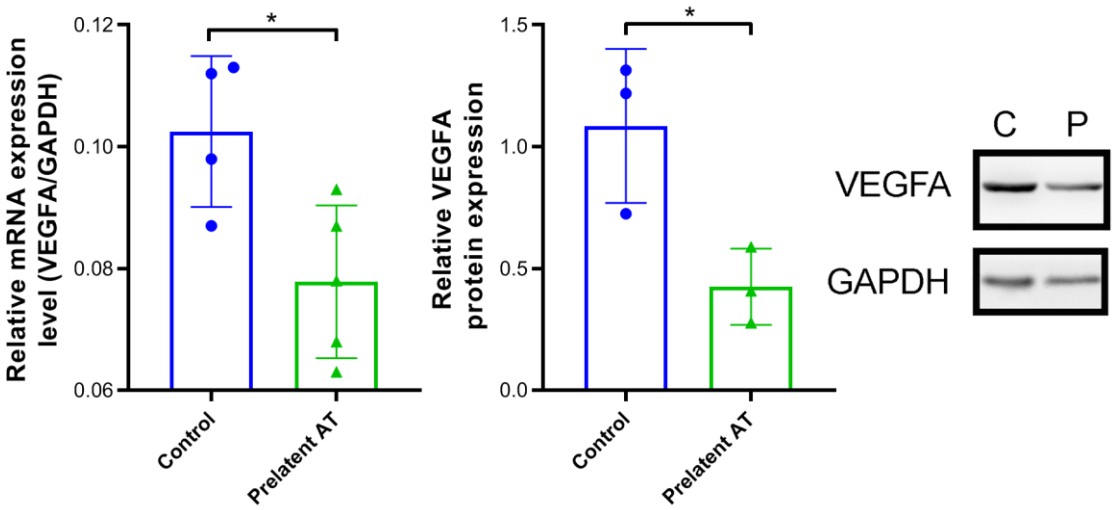

Figure 10. **VEGFA expression on U87 cells after prelatent antithrombin (AT) treatment compared to control (buffer A)**. A) Relative expression of *VEGFA* to *GAPDH* mRNA (2-ΔCt). Each condition was evaluated in triplicate, and 5 different samples per group were analyzed. * $p < 0.05$. B) Electrophoresis and western blot of VEGFA in lysates of U87 cells treated with buffer A (C) or prelatent (P) AT. GAPDH expression was detected as loading control. * $p < 0.05$.

We also examined the expression of STAT3 and pSTAT3, pERK1/2 and pAKT whose expression is crucial in cancer signaling pathways and have become potential targets for GBM treatment[51,85,86]. As shown in Figures 11A, prelatent AT treatment significantly reduced *STAT3* expression by half (p=0.026), and at the protein level, it also inhibited pSTAT3-α phosphorylation (p=0.019), which is the isoform that can act as an oncogene[87]. On the other hand, prelatent AT reduced ERK1/2 phosphorylation, although not statistically significantly, and this reduction did not appear to be mediated by the AKT pathway, whose activation remained unaffected (Figure 11B).

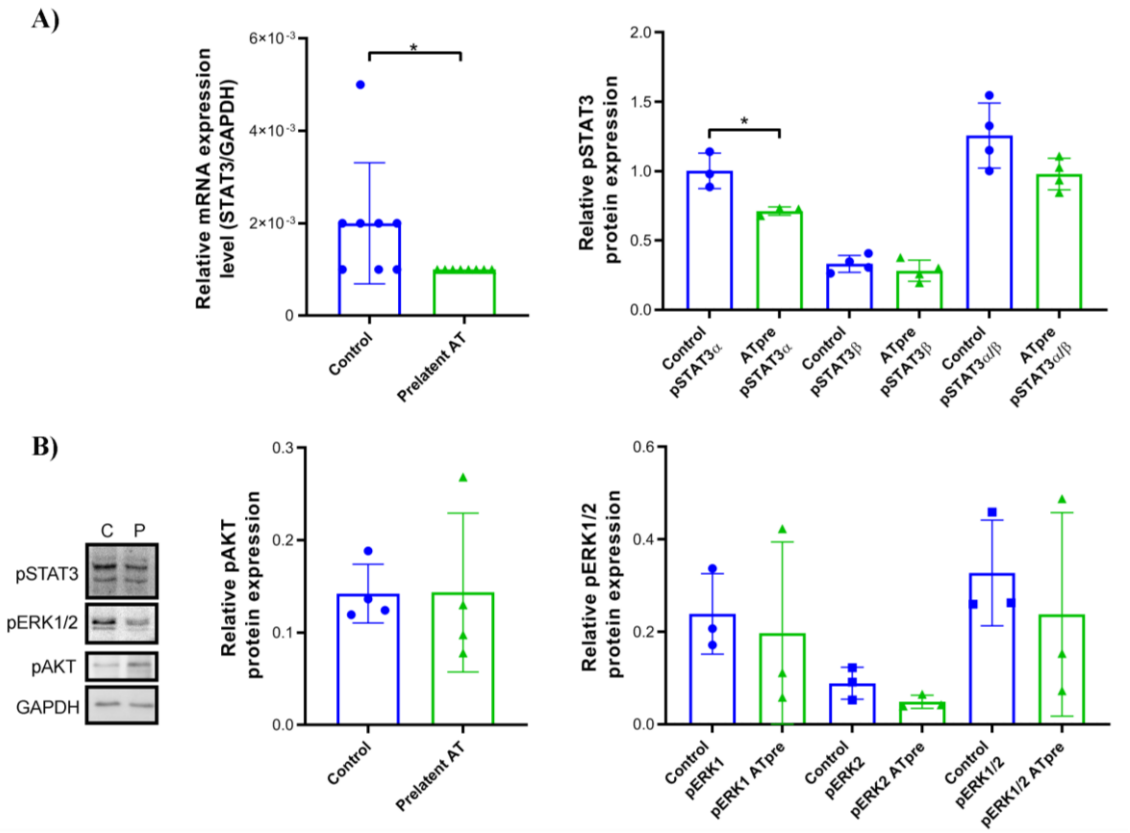

Figure 11. **pSTAT3, pAKT, and pERK1/2 expression on U87 glioblastoma cells**. A) (Left) Relative expression of *STAT3* to GAPDH mRNA (2-ΔCt). Each condition was evaluated in triplicate, and 5 different samples per group were analyzed. * $p < 0.05$. (Right) Electrophoresis and western blot of pSTAT3 in lysates of U87 cells treated with buffer A (C, control) or prelatent antithrombin (P, ATpre). GAPDH expression was detected as loading control. B) Electrophoresis and western blot of pAKT (left) and pERK1/2 (right) in U87 cells treated with buffer A (control) or prelatent antithrombin (ATpre). GAPDH expression was detected as loading control. AT: antithrombin. * $p < 0.05$.

Finally, we also evaluated the effect of prelatent AT treatment on a different GBM cell line. However, treatment of U251 cells with prelatent AT did not significantly modified the expression of these signal transduction factors (Figure 12), as it happened with U87 cells (Figure 11).

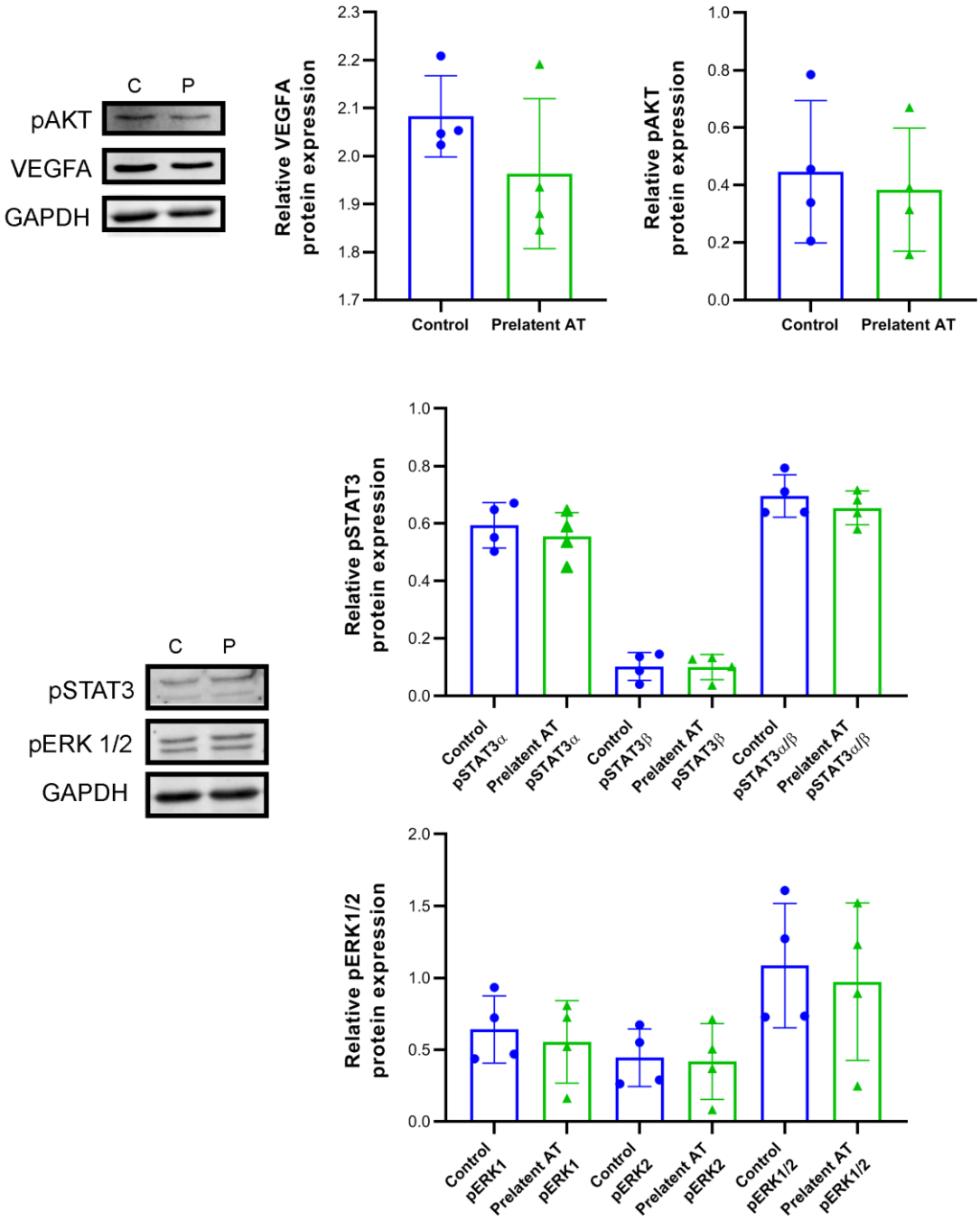

Figure 12. **VEGFA, pSTAT3, pAKT, and pERK1/2 expression on U251 glioblastoma cells**. A) Electrophoresis and western blot of VEGFA and pAKT in lysates of U251 cells treated with buffer A (C, control) or prelatent antithrombin (P). GAPDH expression was detected as loading control. B) Electrophoresis and western blot of pSTAT3 and pERK1/2 in lysates of U251 MG cells treated with buffer (C, control) or prelatent antithrombin (P). GAPDH expression was detected as loading control. AT: antithrombin.

4. Discussion

AT is the main inhibitor of the coagulation cascade, but the diversity of conformations that AT can adopt (native, heparin-activated, cleaved, latent and prelatent) could in turn indicate a functional diversity for this protein[28,31,34,40]. In fact, heparin-activated AT has recently been described to exhibit antitumor function[37] by inhibiting the protease activity of EP, a TTSP. Tumor cells often take advantage of the deregulation of certain proteases to promote metastasis. This is because proteases involved in extracellular matrix remodeling allow cells to access the bloodstream and thus reach other tissues and organs[88,89]. Although EP had never been related to tumorigenicity, our group demonstrated that its silencing reduced the migration and invasiveness of tumor cells, thus directly linking its expression to these processes. Furthermore, treatment of EP-expressing cells with AT also reduced migration and invasion, and in the case of invasion, incubation of EP-silenced cells with AT almost completely reduced invasion. This showed that other proteases besides EP are involved in extracellular matrix degradation and are under the control of AT[37]. This adds to the fact that a new conformation of AT, called prelatent AT, which is physiologically present in our blood at very low levels, exhibits special abilities, such as its high antiangiogenic capacity[15].

On the other hand, GBM is the most common malignant brain tumor in adults and carries a poor prognosis overall. Despite intense research, little progress has been made in recent years[54]. This implies the need to elucidate new mechanisms and treatments that fuel the next generation of clinical trials.

The main drawback of working with prelatent AT is its purification. It is a tedious process, as it requires 10-12 days, whereas the native conformation is purified in 2 days. On the other hand, despite starting from approximately 13 mg of native AT for its transformation to prelatent, the yield is very low, which hinders its large-scale production. In addition, a double heparin affinity purification is performed to prevent contamination of the prelatent fraction with native form, which leads to an additional, albeit small, loss of concentration.

Since prelatent and native AT are conformationally different, we evaluated whether this could favor interaction with EP. Our results show that prelatent AT is also able to inhibit EP, although this inhibition is less efficient than that exerted by the native conformation in the presence of heparin. We also found that the prelatent AT is not able

to form covalent complexes with EP, probably being cleaved at the Arg 393 residue, as is the case with the native conformation[37].

Our results also confirm that prelatent AT has multiple effects on U87 cells, being capable of reducing the expression of VEGFA and STAT3, which normally form an up-regulation transcriptional circuit in GBM[15,90]. Concomitantly, prelatent AT is able of decreasing the activation of ERK1/2, a factor whose high expression has been associated with tumor progression and resistance to antitumor therapies[85]. However, our results suggest that the regulation exerted by prelatent AT on ERK1/2 is not mediated by the AKT pathway. In summary, this array of capacities makes prelatent AT a potential ally in antiangiogenic treatment strategies, either by enhancing them or delaying mechanisms of evasive resistance.

Microvascular proliferation comprises one of the hallmarks of GBM, as opposed to low-grade glioma. Several factors have been implicated in generating the rich vascular network of these tumors[70]. Glial neo-angiogenesis is a highly complex tumor process with several intertwined steps. Thus, tumor hypoxia is one trigger, with the induction of HIF-1 and the expression of several associated transcription factors, and components of the extracellular matrix[69]. This leads to the imbalance between anti- and proangiogenic factors such as VEGF, transforming growth factor-β, epidermal growth factor, and others. These factors act as receptors on endothelial cells, which are recruited. This recruitment, in turn, entails the degradation of the endothelial cell basement membrane and extracellular matrix by various matrix metalloproteinases[71]. The process culminates in capillaries sprouting from preexisting blood vessels, and the transcriptional activation of the *VEGFA* gene in GBM cells is one of the main factors involved in[69]. In the phase III Avaglio randomized controlled trial, the addition of bevacizumab (a VEGFA-inhibiting monoclonal antibody) in combination with radio- and chemotherapy, enhanced progression free-survival in patients with GBM (10.6 months vs. 6.2 months; hazard ratio, 0.64; 95% confidence interval, 0.55 to 0.74; $p < 0.001$)[91]. Nevertheless, no differences were seen in overall survival due to an increased migration/invasion as a common mechanism of resistance, which correlates with a diffuse progression[92]. If validated *in vivo*, the co-repression shown here of the VEGFA factor in U87 cells would endorse the role of prelatent AT in controlling resistance to antiangiogenics.

STAT3 is part of a particularly interconnected circuit, with multiple roles in tumor progression, evasion of the immune response, antiapoptotic activity, angiogenesis, etc[93].

The co-option of reactive astrocytes of the tumor microenvironment by means of STAT3 signaling fosters the implantation and survival of metastasis by modulating the immune system[94]. Up-regulation of the pSTAT3 pathway has been correlated with the development of evasive resistance to bevacizumab in individuals with GBM[95]. For the inhibition of this pathway in GBM, it has been shown that the small molecule napabucasin inhibits both *in vitro* and in mice the proliferation, invasion and self-renewal of GSCs through direct inhibition of STAT3[96]. A phase II clinical trial combining napabucasin with TMZ in patients with recurrent GBM was completed last year. However, the results have not yet been published[97].

STAT3 has also been shown to induce VEGF transcription[90]. In addition, ERK1/2 has also been shown to promote tumor progression and mediate resistance to antitumor therapies[85]. Indeed, the combination of inhibiting STAT3 and ERK1/2 has been proposed as a means to prevent the radioresistance that often occurs in GBM tumors[86]. On the other hand, AKT is a serine/threonine kinase whose pathway interacts at multiple points with the ERK1/2 pathway[98]. Moreover, AKT is often mutated in GBM patients, leading to increased pAKT levels and consequent uncontrolled tumor growth, evasion of apoptosis and increased tumor invasion[51]. Our results showed that prelatent AT was able to statistically significantly reduce *STAT3* expression by half, and at protein level, it also significantly inhibited pSTAT3α, which is the isoform that acts as an oncogene[87]. On the other hand, prelatent AT reduced pERK1/2 phosphorylation, although not statistically significantly, and this reduction did not appear to be mediated by the AKT pathway, since the expression of this protein was not affected after prelatent AT treatment.

Interestingly, when AT was incubated with U87 cells, which express EP on the membrane surface, we observed a stronger effect of prelatent AT on the inhibition of cell migration compared to native AT. Moreover, this effect was not enhanced in the presence of heparin and was even greater than that exerted by heparin-activated AT. This could be explained by the lower affinity of prelatent AT for heparin compared to native AT. Regarding tumor invasion, the prelatent AT did not exert a greater inhibition than the native conformation either in the presence or absence of heparin. Therefore, although the effect of prelatent AT on EP was not as potent as that exerted by native AT, the effect on migration could be explained, at least in part, by the inhibition of the TTSP EP[37], and/or by the concomitant inhibition of several points in this complex

network, such as VEGF, STAT3 and ERK1/2[86]. We cannot rule out that other proteins involved in these tumorigenic processes should be under the control of AT.

In summary, in this first chapter, we have described the surprisingly versatile mechanisms by which a special conformation of AT is able to take on antitumor abilities at several levels in U87 cells. Among these mechanisms is the inhibition of invasion, migration and angiogenesis processes, and a potential reduction of treatment resistance through the modulation of critical signaling pathways in glial cells, such as VEGFA and STAT3.Therefore, the antitumor effect of AT should be explored in the treatment of GBM.

CHAPTER 2. Study of the cellular mechanisms underlying the antitumor effect of native and prelatent conformations of antithrombin on glioblastoma cell lines

1. Introduction 59
2. Material and methods 59
2.1 Cell culture 59
2.2 Transcriptomic analysis. Microarray expression 60
2.3 Functional validation of miRNAs and angiogenesis assay 61
2.4 Cell cycle and proliferation assay 62
3. Results 63
3.1 Prelatent antithrombin regulates the expression of different protumoral proteins 63
3.2 Antithrombin regulates the expression of various miRNAs 65
3.3 Cell cycle and proliferation assay 68
4. Discussion 73

1. Introduction

As described above, GBM is the most aggressive and common lethal primary CNS tumor in adults, whose median survival rate is 12-15 months after diagnosis. In recent years, many studies have focused on improving this survival rate and the quality of life of these patients. Some of them target GSCs, attempting to target the signaling pathways involved in their self-renewal, or induce their differentiation to sensitize them to therapies, or inhibit resistance pathways. Others focus on inhibiting cell growth and migration, where most trials focus on inhibiting the EGFR receptor. In addition, there are also assays focusing on inhibition of apoptosis and cell cycle or angiogenesis[54]. However, the large number of altered tumorigenic pathways makes more specific treatments inefficient.

Therefore, it would be worthwhile to identify a multitarget drug. Regarding this, different functions that would be beneficial in the treatment of GBM have been related to AT[15,37,80]. The interaction of AT with different heparan sulphates on the cell membrane of specific cells allows it to exhibit anti-inflammatory function[21]. The inflammatory system is usually a biological response to eliminate the tumor. However, this proinflammatory environment that is triggered ends up being detrimental to the treatment of the tumor, as it releases proliferative, anti-apoptotic or proangiogenic growth factors, among others[99]. Furthermore, in the first chapter of this doctoral thesis, it has been shown that the previously established antiangiogenic function of AT[15] could also be exerted by the inhibition of the main factor involved in this process, VEGF. On the other hand, we have shown that it has an antitumor role, as both native and prelatent AT are able to inhibit the migration and invasion of U87 cells[80]. In addition, treatment of U87 cells silenced for the EP gene (*TMPRSS15*) with heparin-activated AT further reduced the invasion of these cells, indicating that other molecules and signaling pathways may be under the control of AT[37].

Hence, the aim of this second chapter was to investigate the impact of prelatent and native AT on different tumorigenic pathways in GBM using an expression array.

2. Material and methods

2.1 Cell culture

U87 cell line and cultures were purchased and prepared as described in chapter 1. The

human EA. hy926 endothelial cell line was a kind gift from Dr. C.-J. S. Edgell (University of North Carolina, USA). EA.hy926 cells were grown in DMEM medium containing 4.5 g/L glucose (Gibco Thermo Fisher, 11594416) and supplemented with 10% fetal bovine serum (Gibco Thermo Fisher), 1% sodium pyruvate (Gibco Thermo Fisher), 1% L-Glutamine (Gibco Thermo Fisher) and 1% streptomycin/penicillin (Gibco Thermo Fisher). Cells were maintained in T-75 tissue culture flasks (Fisher scientific, 353136) and grown in 5% CO_2 at 37ºC in a humidified incubator.

2.2 Transcriptomic analysis. Microarray expression

U87 cells were incubated with prelatent AT (2.16 μM) or buffer A (n = 8/group). After 11 h of incubation, total RNA was isolated using Trizol® Reagent (Invitrogen) following manufacturer's instructions. The RNA concentration and 260/280 ratio were determined by using a NanoDrop spectrophotometer (Thermo Scientific). The amount and quality of the RNA was checked by Bioanalyzer 2100 (Agilent Technologies). For each sample, ss-cDNA was synthesized from 100 ng of total RNA using the GeneChip WT Pico Reagent kit (Affymetrix ThermoFisher Scientific, P/N 703262), according to the protocol supplied by manufacturer. The amount and quality of ss-cDNA was checked by Nanodrop 2000 (ThermoFisher Scientific) and Bioanalyzer. ss-cDNA targets were cleaned up and after fragmentation and terminal labelling, 5.5 μg of fragmented and biotinylated ss-DNA were included in the hybridization mix, using the GeneChip Hybridization, Wash and Stain (Affymetrix ThermoFisher Scientific, P/N 900720), according to recommendations of manufacturer. The resulting preparations were hybridized to ®Clariom D Human Array (Affymetrix, ThermoFisher Scientific, P/N 902922), which includes more than 540,000 transcripts from 6,765,000 probes that provide a comprehensive coverage of the whole transcriptome. This array confidently detects genes, exons, and alternative splicing events that give rise to coding and long noncoding RNA isoforms and even detects rare and low-expressing transcripts otherwise missed by common sequencing practices.

After scanning, microarrays data were processed using Affymetrix Expression Command Console (Affymetrix). Data analysis was then performed with RMA (Robust Multiarray Average) allowing that raw intensity values were background corrected, log2 transformed and then quantile normalized to obtain an individual intensity value for each probe set. TAC software (Transcriptome Analysis Console, ThermoFisher

Scientific) and Partek Genomics Suite and Partek Pathways software (Partek Incorporated, St. Louis, USA) were used for the statistical analysis. The molecular interaction, reaction and relation networks that showed differentially expressed genes were then analyzed using KEGG Pathways Kyoto Encyclopedia of Gene and Genomes. The criterion for selection of differentially expressed genes was a fold-change (FC) ± 1.5, considering a significance level of p-value < 0.001. Exploratory data analysis was performed by principal component analysis (PCA). KEGG pathway database was used to represent the altered molecular interaction networks after treatment.

2.3 Functional validation of miRNAs and angiogenesis assay

First, a bioinformatic analysis was performed to select the miRNAs for study. The Partek Genomics Suite software revealed that the expression of 586 genes coding for microRNAs were altered after U87 cells treatment with prelatent AT. Additionally, using the Partek Genomics Suite software, a list of 379 miRNAs that could potentially be altered based on their target genes altered in the microarray was obtained. Finally, to select the miRNAs candidates, the following filters were applied: A) The microRNA should appear altered with both analyses; B) The miRNA gene must be inversely expressed with its target; C) p-value < 0.001 for both the miRNA genes and their targets. A list of 35 miRNAs with 511 targets was obtained. An over-representation analysis was conducted using the g: Profiler software. Information from the Reactome biological pathway was selected to finally choose 3 miRNAs: miR-A, miR-B and miR-C.

These three miRNAs were purchased from ABI Applied Biosystems. $4x10^4$ U87 cells were transfected with chemically modified double-stranded RNAs that mimic endogenous miRNAs (mimic): 5 nM miRNA mimic-A, 5 nM miRNA mimic-B and/or 10 nM miRNA mimic-C by using the siPORT™ NeoFX™ Transfection Agent (Invitrogen, AM4510). Then, transfected cells were cultured in 24-well plates containing U87 medium for 48 hours and incubated in a humidified atmosphere at 37ºC, 5% CO_2. 5 nM mirVana mimic scrambled miRNA (Ambion, 4464058) with no target was used as negative control.

After 48 hours of transfection, co-culture of EA.hy926 and U87 transfected cells was assayed to determine the effect of selected miRNAs on vessel formation. Briefly, both

cell lines were added to a 96-well plate ($1.5x10^4$ cells each cell line in 100 µl of medium deprived of fetal bovine serum to each well) previously treated with 9 µ L of Matrigel. The conditions studied were as follows: 1) 10 µM D,L-sulforaphane; 2) U87 transfected with has-miR-A; 3) U87 transfected with has-miR-B; 4) U87 transfected with has-miR-C; 5) U87 cells transfected with miR-A, -B and –C; 6) U87 transfected with scrambled miRNA. Each condition was tested in quintuplicate. D,L-sulforaphane was used as a positive control of angiogenesis inhibition in this assay[100]. The lengths of endothelial tubes formed in each well was quantified from captured images using Angiogenesis Analyzer for ImageJ. The statistical analysis was performed with a One-way ANOVA test using the GraphPad Prism 8.0.2 software.

Simultaneously, after 48 hours, U87 transfected cells were employed to measure the expression of the different miRNAs in each transfection. For that, total RNA was isolated using Trizol® Reagent (Invitrogen) following manufacturer's instructions. The RNA concentration and 260/280 ratio were determined by using a NanoDrop spectrophotometer (Thermo Scientific). From total RNA, a 100-ng sample was reverse transcribed to cDNA according to the manufacturer's instructions (Multiscribe, 4368814, ThermoFisher Scientific). PCR reactions were carried out using TaqMan® Gene Expression probes in duplicate for each sample. *U6* (#001973, ThermoFisher Scientific) expression was used as the endogenous reference control. The fold difference for each sample was obtained using the 2-ΔCt method. Data was expressed as changes relative to the values of the cells transfected with the scramble, taken as 100%.

2.4 Cell cycle and proliferation assay

To evaluate the proliferative capacity of U87 and U251 cell lines under the effect of prelatent AT (2.16 µM) or buffer A, $8x10^5$ cells were grown in a polystyrene microplate 6-well (n=3/group). After 11 hours of treatment, cells were labeled with 10 µM 5-Bromo-20-deoxyuridine (BrdU) (BD Biosciences, 552598) for 4 hours. Then, the APC BD BrdU flow kit (552598, BD Biosciences) was used to fix and permeabilize cells prior to DNAse treatment and staining with anti-BrdU-APC. Total DNA was stained with 7-aminoactinomycin D to evaluate cell death. Finally, data were obtained using a BD Accuri C6 flow cytometer device (Ann Arbor) and analyzed with FlowJo 10.3 software. The experiment was performed in triplicate.

3. Results

3.1 Prelatent antithrombin regulates the expression of different protumoral proteins

Due to the wide spectrum of prelatent AT effects beyond hemostasis, we decided to investigate those genes that could be over- or underexpressed using transcriptomic analysis. In the PCA (Figure 13) we observed that the samples differentiate into 2 populations based on the expressed transcripts (control *vs.* prelatent AT treatment). The genes overexpressed in U87 cells after prelatent AT treatment were 2,477, while 6,760 were underexpressed (p-value < 0.001, fold change ± 1.5).

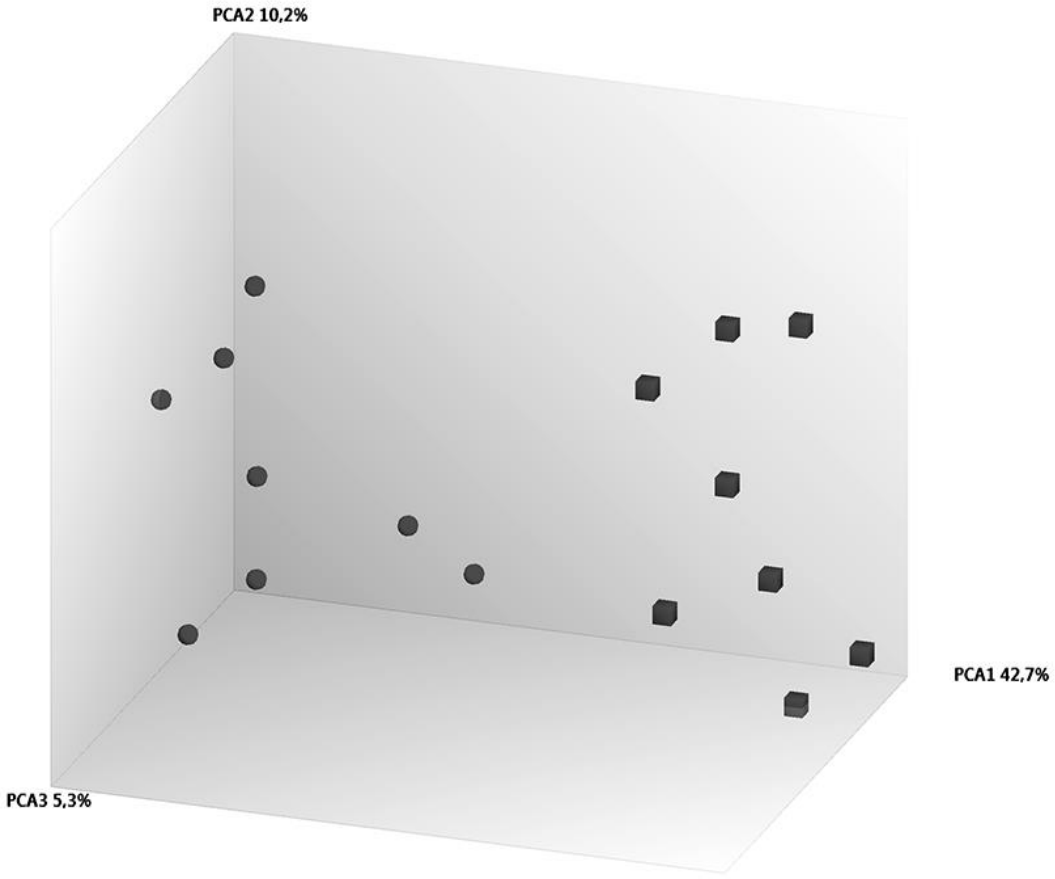

Figure 13. Principal component analysis (PCA) of transcripts obtained from U87 cells treated with buffer A (control) (circles) or prelatent antithrombin (squares).

Numerous cancer-related signaling pathways in U87 cells were disrupted after prelatent AT treatment. In Figure 14, under-expressed genes in these pathways are shown in green, while over-expressed genes are shown in red. Table 2 displays the results of the expression array of the different proteins validated in this chapter and already related to GBM[101].

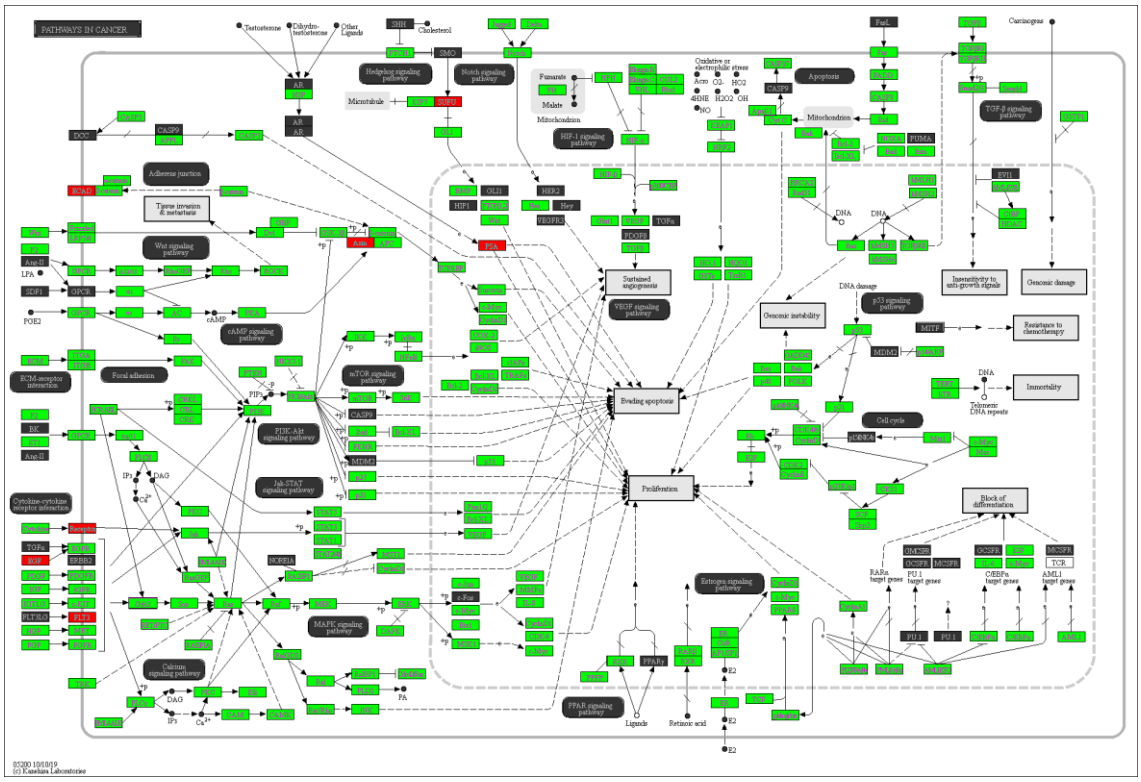

Figure 14. **Main pathways altered in cancer after U87 glioblastoma cells treatment with prelatent antithrombin**. Solid line between genes/molecules indicates direct regulation, while dashed lines indicates possible indirect regulation. Circle indicates a group of similar molecules. After treatment with antithrombin and compared to control, the genes in red are overexpressed, while the genes in green are underexpressed [Kanehisa Laboratories, 2019].

Table 2. **Results of the Parket Genomics Suite software.** Prelat: prelatent AT.

Table 2. Results of the Parket Genomics Suite software.			
Gene symbol	**Gene name**	***p*-value** (prelat.*vs* control)	**Fold-change** (prelat. *vs* control)
EGFR	*Epidermal growth factor receptor*	$9{,}34 \times 10^{-6}$	-1.82
IDH1	*Isocitrate dehydrogenase 1 ($NADP^+$)*	$3{,}96 \times 10^{-4}$	-1.57
IDH2	*Isocitrate dehydrogenase 2 ($NADP^+$), mitochondrial*	$5{,}72 \times 10^{-5}$	-1.82
MDM4	*Mouse double minute 4*	$3{,}58 \times 10^{-4}$	-1.80
MET	*Hepatocyte growth factor receptor*	2.50×10^{-5}	-1.61
NIF	*Neurofibromin 1*	$1{,}35 \times 10^{-4}$	-2.23
PIK3R1	*Phosphoinositide-3-kinase, regulatory subunit 1 (alpha)*	$5{,}41 \times 10^{-4}$	-2.23
STAT3	*Signal transducer and activator of transcription 3*	2.17×10^{-7}	-2.02
VEGFA	*Vascular endothelial growth factor A*	1.63×10^{-4}	-1.79

Among the main altered cancer-pathways, we first highlighted the inhibition of the VEGF-A factor (Table 2). These results agree with those shown in chapter 1, where we demonstrated that prelatent AT can inhibit VEGFA expression (Figure 10).

3.2 Antithrombin regulates the expression of various miRNAs

Also related to the microarray expression, we observed a powerful effect of prelatent AT in regulating the expression of 586 genes coding for microRNAs in U87 cells. Additionally, using the Partek Genomics Suite software, we obtained a list of 379 miRNAs that could be potentially altered based on their target genes altered in the microarray. Finally, to select our miRNAs candidates, we followed the filters indicated in Materials and Methods. We finally obtained a list of 35 miRNAs with 511 targets (Figure 15).

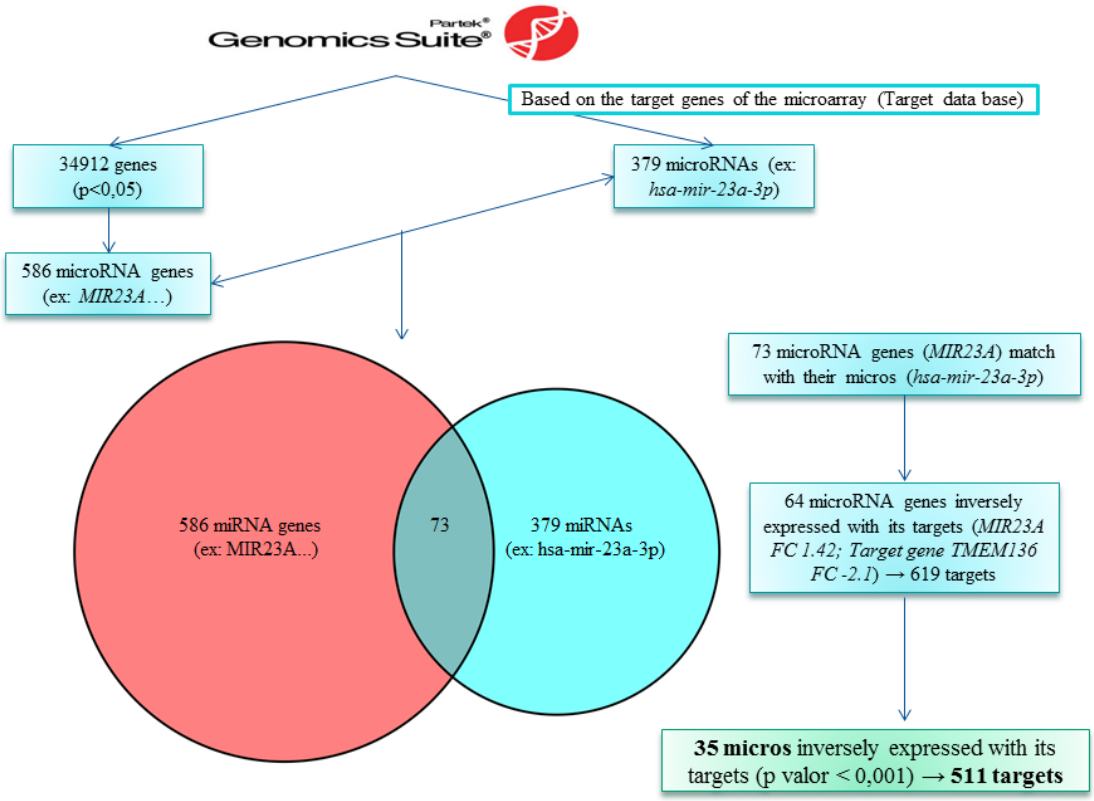

Figure 15. Scheme of the steps followed for the first bioinformatics analysis and selection of the different miRNAs.

Next, we carried out an over-representation analysis using the g: Profiler software, with aiming to see, based on the altered targets, which pathways the 35 miRNAs could be involved in. Thus, as observed in the following Manhattan plot (Figure 16), we selected the information from the Reactome biological pathway database.

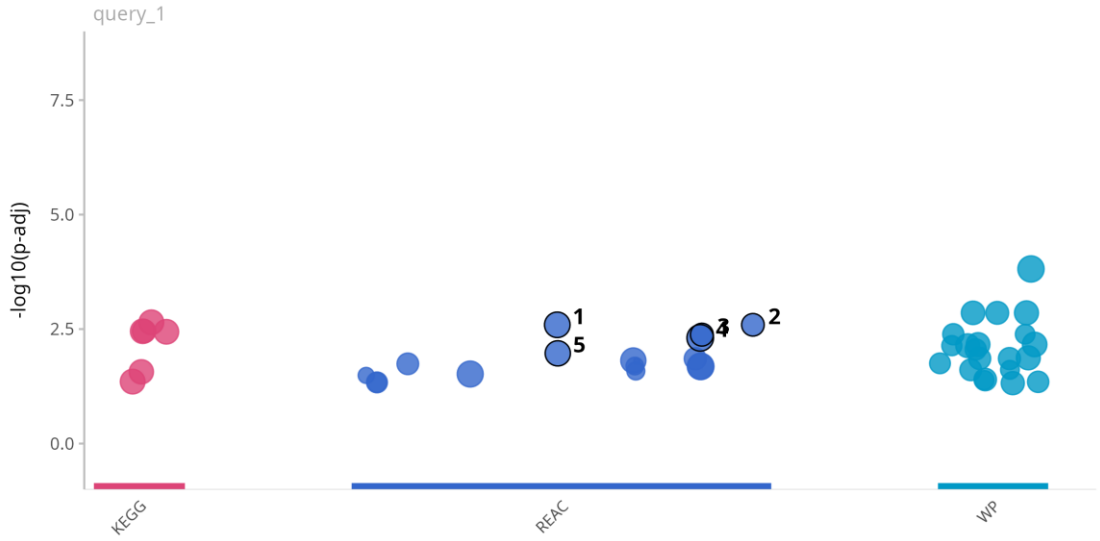

id	source	term_id	term_name	term_size	p_value
1	REAC	REAC:R-HSA-5683057	MAPK family signaling cascades	308	2.6e-03
2	REAC	REAC:R-HSA-4420097	VEGFA-VEGFR2 Pathway	94	2.6e-03
3	REAC	REAC:R-HSA-194138	Signaling by VEGF	104	4.2e-03
4	REAC	REAC:R-HSA-9006934	Signaling by Receptor Tyrosine Kinases	486	4.9e-03
5	REAC	REAC:R-HSA-5684996	MAPK1/MAPK3 signaling	269	1.1e-02

g:Profiler (biit.cs.ut.ee/gprofiler)

Figure 16. **Manhattan plot of different databases**. The x axis represents functional annotations that are grouped and colored according to the sources: KEGG: Kyoto Encyclopedia of Genes and Genomes; REAC: Reactome database; WP: WikiPathways. The y-axis shows the adjusted p values in the negative log 10 scale. Each circle consists of one annotation and is sized according to the number of genes involved.

The following cord plot (Figure 17) is a graphical representation of the results from the Reactome database. Above are represented most of the 35 miRNAs altered after treatment of U87 cells with prelatent AT, and below are the 5 most overrepresented altered pathways in Reactome. The wider the connection between the miRNA and the pathway, the more altered targets the miRNA has in this specific route. As shown in Figure 17, two of the most altered pathways are related to the VEGFA pathway. Therefore, the final selection was based on the following criteria: none of the 3 microRNAs had previously been related to GBM and, while miR-A and miR-C were selected for having the most altered targets in the VEGF pathways, miR-B was selected for being the miRNA whose gene expression was most altered in the expression array (FC miR-A: 1.61; FC miR-B: 2.54; FC miR-C: 1.22).

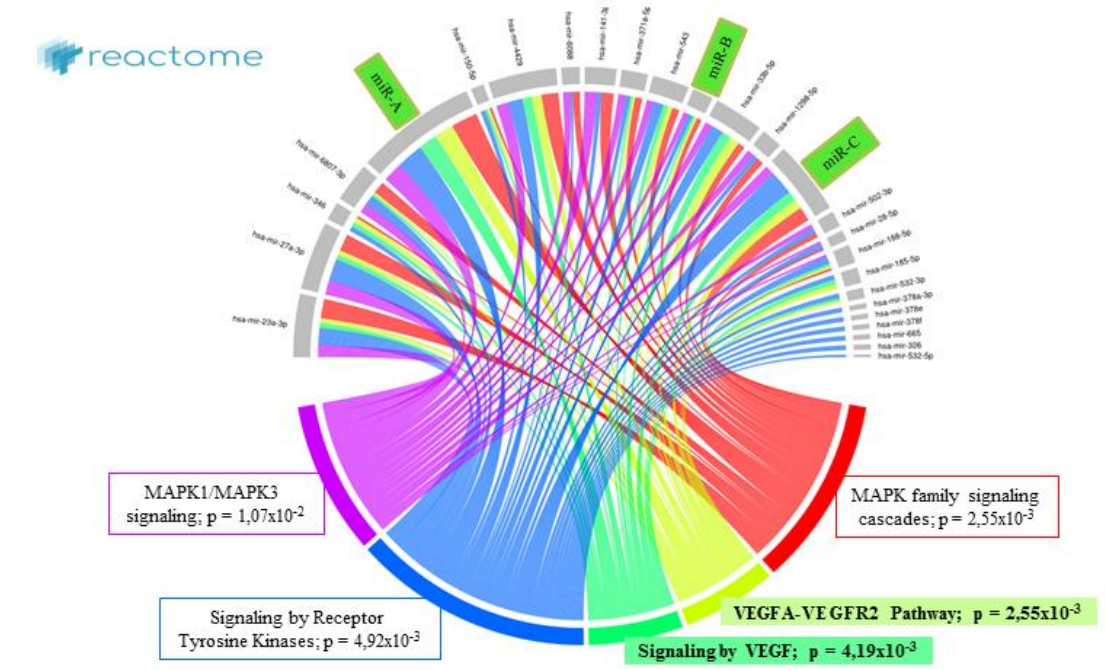

Figure 17. **Cord plot representation of the Reactome database results**. Above, there are 35 miRNAs, and below, the 5 most overrepresented altered pathways. The 3 selected miRNAs are marked as "microRNA-A, -B or –C". The wider the connection between the miRNA and the pathway, the more altered target this miRNA has in this specific route.

To demonstrate the role of these 3 miRNAs in inhibiting angiogenesis, we transfected U87 cells with each microRNA individually and together. First of all, we confirmed the high transfection efficiency of the miRNAs individually by measuring their expression in the transfected cells (Figure 18). However, transfection of the miRNAs together decreased the efficiency by more than half for miR A- and C- (Figure 18).

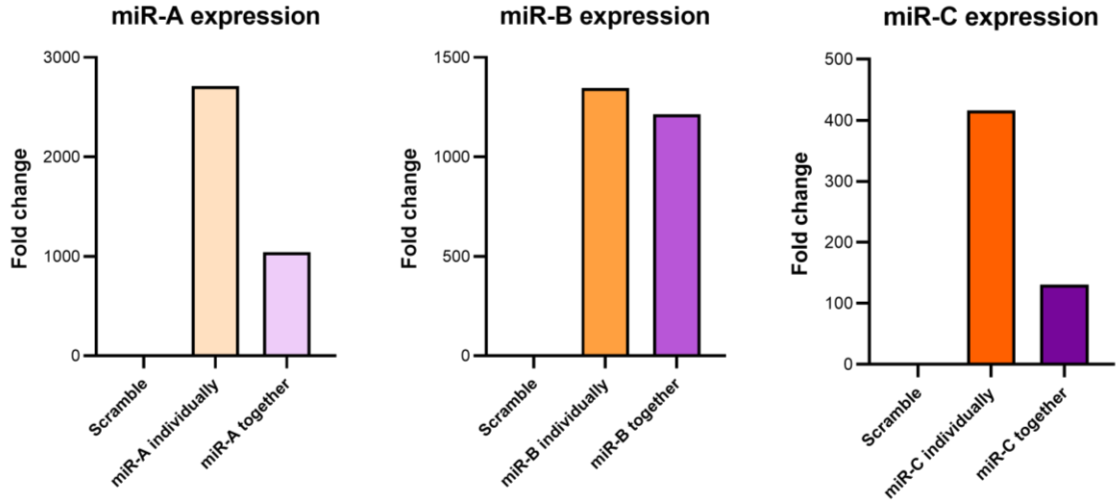

Figure 18. Measurement of miRNAs expression by qRT-PCR after transfection with miRNA mimics. miR-A, miR-B and miR-C levels were quantitated by qPCR following either transfection in U87 cells. Results are represented as changes relative to the values of the cells transfected with the scramble, taken as 100%.

After validating the transfection efficiency (Figure 18), the angiogenesis was evaluated after co-culturing the U87-transfected cells with endothelial cells. Unexpectedly (Figure 19), despite the precise criteria explained above that were followed to select the 3 miRNAs, we did not obtain a reduction in endothelial vessel formation, assessed as total length (sum of length of segments, isolated elements and branches in the analysed area), either after independently or together miRNAs transfection. However, a reduction in angiogenesis can be noticed in the microscopy images with miR-A (Figure 19C), as smaller vessels are observed and most of them not fully formed compared to the positive control (Figure 19A). This could be due to the design of the macro used for the analysis of the images (Angiogenesis Analyzer, Fiji) because, as showed in Figure 19B, it identifies endothelial vessel formation even in the negative control, when no vessels are formed in this control (Figure 19B). Therefore, these results will be repeated either by using another analysis or by selecting other miRNAs from our microarray results also involved in the VEGFA/angiogenesis pathways.

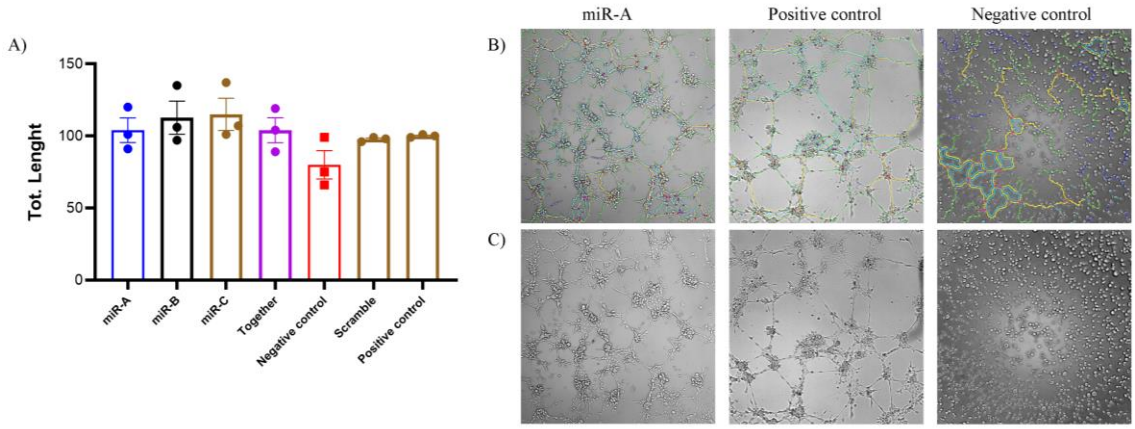

Figure 19. **Effect of the selected miRNA expression on angiogenesis in endothelial cells.** Images were recorded with a Leica microscope at 5×, and ImageJ Angiogenesis Analyzer was used to analyze angiogenesis. A) The results are represented as Total length. B) Representative images of the Angiogenesis Analyzer outcome. C) Representative images of the angiogenesis assay after transfecting U87 cells with miR-A, and in comparison with a scramble (positive control) and D,L sulforaphane (negative control).

3.3 Cell cycle and proliferation assay

Glioma tumors have a highly proliferative phenotype, principally due to the loss of multiple cell-cycle inhibitors and to increased signaling from multiple growth factor receptors that positively regulates the cell cycle[102]. After prelatent AT treatment of U87

cells, we observed that different cyclin genes and regulatory proteins involved in the cell cycle progression were inhibited (Table 3).

Table 3. Altered genes after treatment with prelatent (prelat.) antithrombin (AT) which were related to cell cycle. Results were obtained by using Parket Genomics Suite software.

Table 3. Microarray expression altered genes related to cell cycle after treatment with prelatent antithrombin.			
Gene symbol	**Gene name**	***p*-value** (prelat. *vs* control)	**Fold-change** (prelat. *vs* control)
CCND3	*Cyclin D3*	8.46×10^{-5}	-1.65
CCNE1	*Cyclin E1*	3.99×10^{-4}	-1.62
CCNE2	*Cyclin E2*	2.65×10^{-6}	-2.06
CDK1	*Cyclin dependent Kinase 1*	2.36×10^{-6}	-2.47
CDK4	*Cyclin-dependent kinase 4 or cell division protein kinase 4*	2.60×10^{-5}	-1.64
CDK6	*Cyclin-dependent kinase 6*	4.72×10^{-3}	-1.55
E2F1	*E2F Transcription Factor 1*	6.47×10^{-6}	-1.87
E2F3	*E2F Transcription Factor 3*	7.11×10^{-6}	-1.94
E2F4	*E2F Transcription Factor 4*	1.09×10^{-7}	-2.03
RAD51	*DNA repair protein RAD51 homolog 1*	4.97×10^{-5}	-2.09
RB1	*Retinoblastoma protein*	1.37×10^{-6}	-1.58

Therefore, we studied the effect of native and prelatent conformations (2.16 µM) on the cell cycle and proliferation processes of U87 and U251 cells by measuring 7-AAD and BrdU incorporation by flow cytometry. In U87 cells, we observed that either native or prelatent AT inhibited both S-phase of the cell cycle (53%, p=0.0003 control *vs*. prelatent AT; 64%, p=0.0001 control *vs.* native AT) and cell proliferation (70%, p=0.015 control *vs*. native AT) by more than half, with the native conformation being the most effective form (Figure 20A). Furthermore, both conformations induced an increase in the quiescent cellular phase G0-G1 (p=0.0009 control *vs*. prelatent AT; p=0.0002 control *vs*. native AT). In contrast, neither native nor prelatent AT had significant effects on U251 cells, although a S-phase and proliferation non-statistically reduction can also be observed when are treated with native AT (Figure 20B).

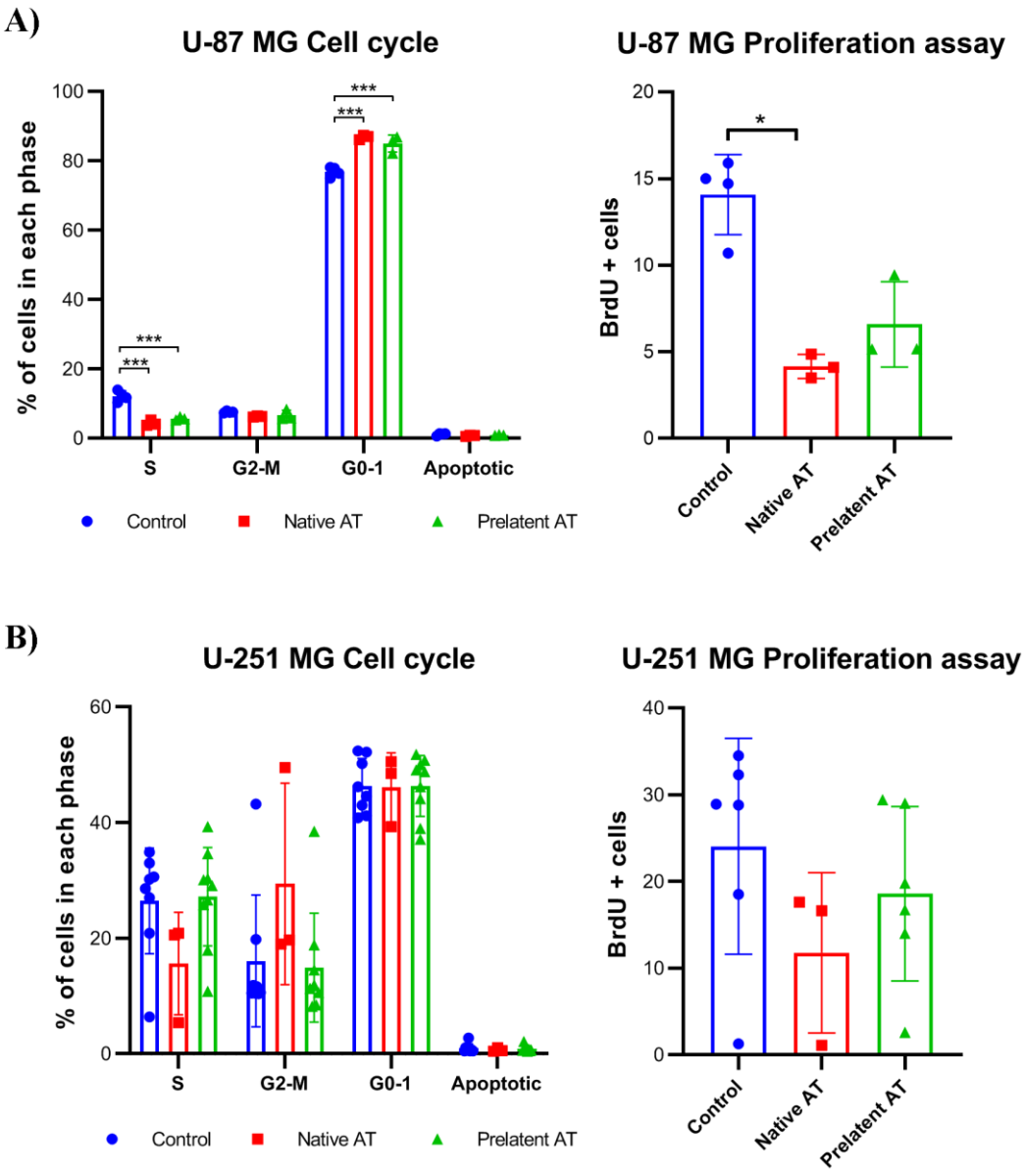

Figure 20. Effect of native and prelatent antithrombin (AT) on cell cycle (left) and proliferation (right) in U87 (A) and U251 (B) glioblastoma cell lines. * $p<0.05$, *** $p<0.0001$.

After these results, we validated the expression of different cell cycle proteins by western blot (pRb, CCNE2, CDK4, E2F4 and cyclin D1), and we determined that native AT was able to inhibit E2F4 factor ($p=0.04$) and Rb phosphorylation ($p=0.03$), both of which are involved in the entry of cells into the S phase of the cell cycle (Figure 21).

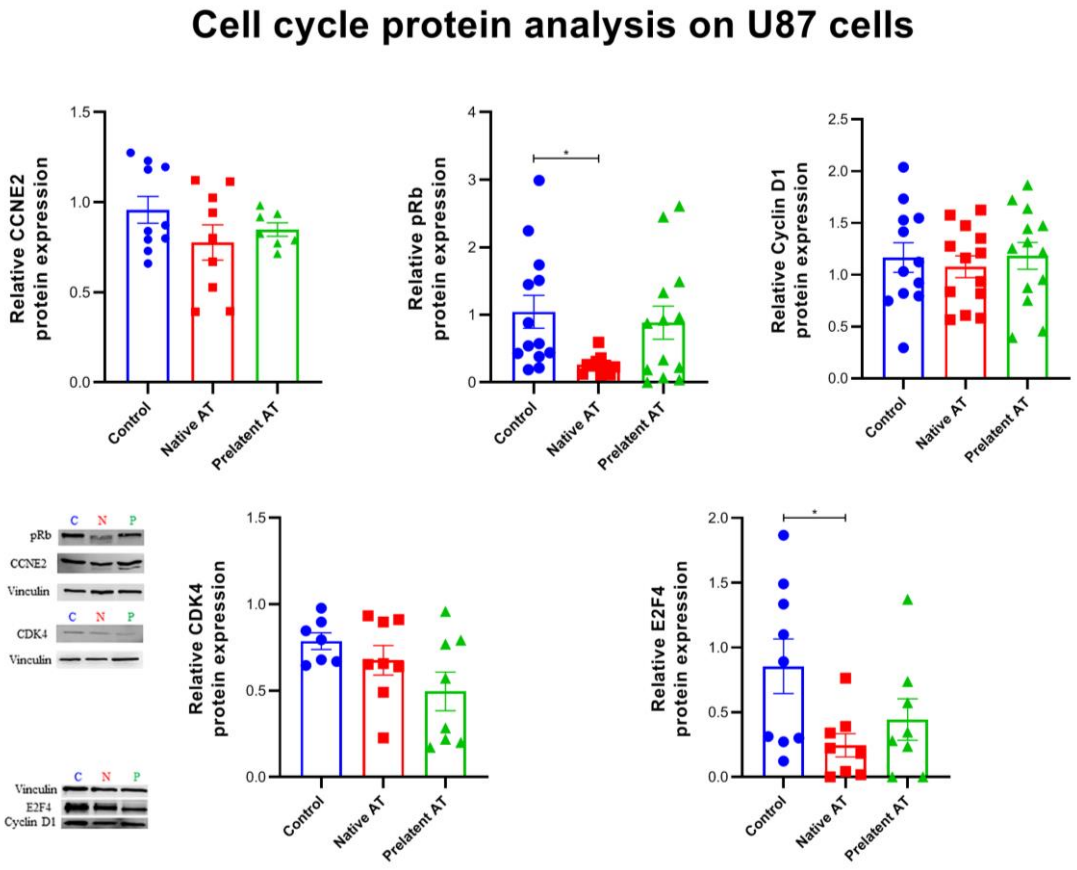

Figure 21. Cyclins and regulatory proteins involved in the cell cycle progression expressed on U87 glioblastoma cells after treatment with antithrombin (AT). Electrophoresis and western blot of cyclin E2 (CCNE2), pRb, cyclin d1, CDK4 and E2F4 proteins in lysates of U87 cells treated with buffer A (C, control), prelatent AT (P) or native AT (N). Vinculin expression was detected as loading control. * $p < 0.05$.

According to previous cell cycle results, we did not observe inhibition of any of these proteins after AT treatment of the U251 cell line (Figure 22).

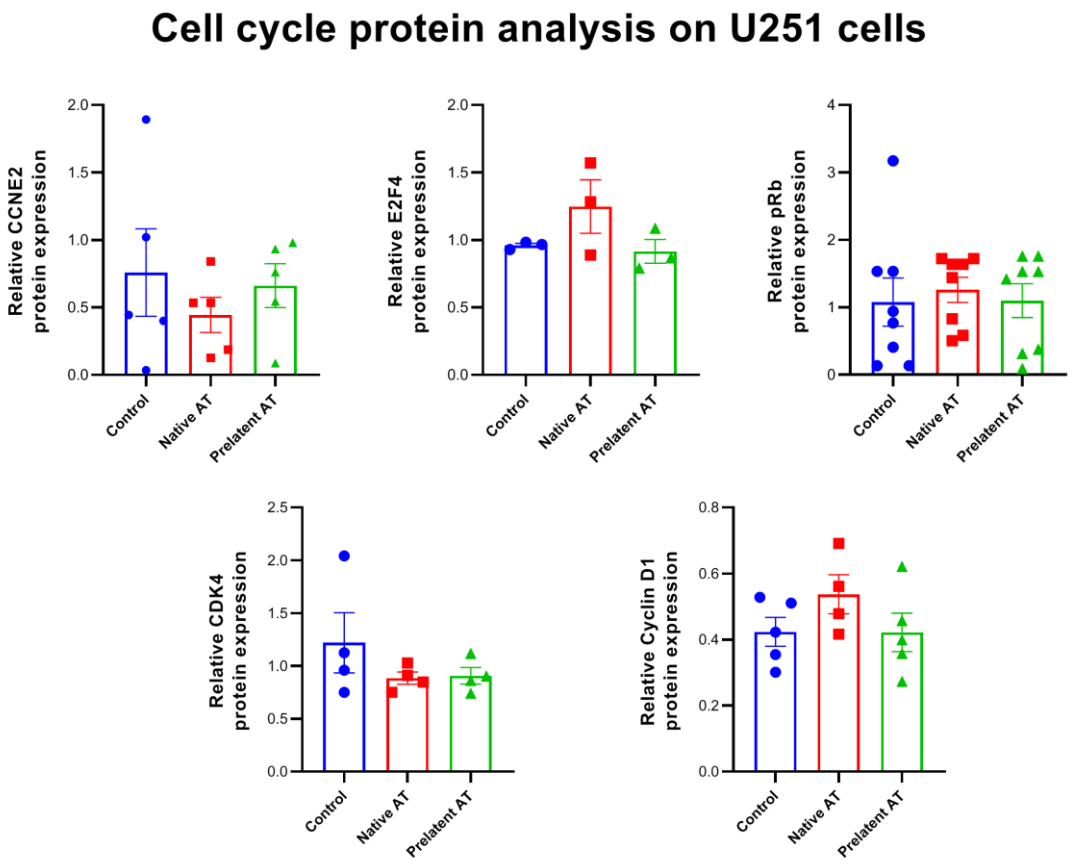

Figure 22. Cyclins and regulatory proteins involved in the cell cycle progression expressed on U251 glioblastoma cells after treatment with antithrombin (AT). Electrophoresis and western blot of cyclin E2 (CCNE2), pRb, cyclin d1, CDK4 and E2F4 proteins in lysates of U251 cells treated with buffer A (C, control), prelatent AT (P) or native AT (N). Vinculin expression was detected as loading control.

4. Discussion

As mentioned earlier, angiogenesis is an important process in the progression of GBM. Tumor cells secrete significant amounts of proangiogenic molecules to support the constant influx of nutrients and oxygen for further growth, resulting in aberrant microenvironments and stimulating angiogenesis. Several studies have shown that angiogenesis in GBM is significantly greater than in low-grade cancers. Therefore, the discovery of new mechanisms involved in the progression of this process is necessary to develop new antiangiogenic therapies[103]. Among the molecules that we have studied and that are involved in GBM angiogenesis are miRNAs. MiRNAs are small non-coding RNAs consisting of 20–22 nucleotides that participate in the post-translational regulation of gene expression through RNA interference processes. Each miRNA has the potential to regulate about 200 target genes[104]. Several miRNAs have been demonstrated to be dysregulated in GBM, with most of them being up-regulated compared to normal brain samples. For instance, it has been shown *in vitro* that overexpression of miR-221, miR-222 or miR-378, among others, promotes the progression of angiogenesis in different GBM cell lines[105].

Our previous results showed that the antiangiogenic function of AT is related to both the inhibition of VEGFA and by direct interaction with different proteins expressed in endothelial cells[15,80], but AT also regulates the expression of different microRNAs involved in this pathway. MiRNAs may become a promising therapeutic target due to their ability to target multiple genes. Our results suggest an antiangiogenic role for miR-A in GBM, as its overexpression promotes a reduction in the formation of new vessels by endothelial cells co-cultured with transfected-U87 cells.

The use of synthetic exogenous oligonucleotides, also known as miRNA-mimics, which have the same sequence as the corresponding endogenous miRNAs, are being tested *in vitro* as antitumor therapy in GBM[106]. However, this novel therapy has several challenges related to its administration. It must be organ-specific, off-targets effects, able to cross the BBB, and its intravascular degradation must be avoided, among other factors. Therefore, different delivery technologies are being developed, such as virus-based delivery, or nanoparticles loaded with nucleic acids, which penetrate the GBM cells and release their contents by endocytosis and transcytosis. The use of lentiviruses, adenoviruses and adenoassociated viruses as carriers allows the corresponding miRNA

therapy to reach the cell nucleus protected from degradation by nucleases, thus increasing the half-life of the miRNA in blood. In addition, viral capsid proteins can be modified to increase their affinity for tumor cells. On the other hand, the use of nanoparticles is also being developed. As with viral therapies, it also protects miRNAs from degradation and also allows their delivery into the nucleus or cytoplasm. However, unlike the first therapy, it does not cause high immunogenicity or toxicity, but it presents lower transfection efficiency and shorter duration of target gene expression. In addition, a great advantage of the use of nanoparticles is their controlled and tissue-specific administration[107].

On the other hand, our results also show the effect of AT in the cell cycle and proliferation of U87 cells. The cell cycle consists of DNA replication in S phase and the generation of 2 identical daughter cells in M phase. For the proper progress of this process, there are 3 checkpoints: one near the end of G1 phase, one during G2/M phase and one on the metaphase to anaphase transition, which are controlled by different proteins. The first checkpoint, which ensures proper cell growth and DNA integrity, involves the retinoblastoma protein (Rb), whose activity is regulated by several molecules such as p16, cyclin-dependent kinases 4 and 6, cyclin D and the transcription factor E2F. In addition, when DNA damage is noticed, several proteins are also activated, including p53, which mediates cell cycle arrest to allow the DNA to repair itself or the cell to enter senescence or cell death[98].

In GBM, different mutations have been observed in different checkpoints leading to cell cycle dysregulation. In up to 78-79% of cases, *RB1* has been found to be altered, and deletion or mutations are present in 7.6-11% of GBM patients[49]. pRb is considered as a tumor suppressor protein, as it inhibits the cell cycle entry at the G1-S phase. In G0 and early G1, Rb forms a growth repressor complex with different members of the E2Fs family, thus preventing E2Fs from regulating the expression of several genes involved in the progression of the G1-S stage of the cell cycle. In contrast, cyclin-dependent kinases (e.g. cyclins D and E) and cyclin-dependent kinases (e.g. CDK4, 6 and 2) phosphorylate Rb late in G1, promoting dissociation of hyperphosphorylated Rb from E2F, allowing E2F-mediated transcription activation and entry into S-phase[108,109]. In fact, Palbociclib, an inhibitor of CDK4/6 that prevents the downstream inhibition of pRb, has been shown to inhibit the growth of intracranial GBM xenograft tumors in mice[110].

The activity of E2Fs is mediated by interactions with negative regulators, the pocket proteins known as pRB, p107 and p130. While E2F1-3 preferentially binds to pRB, E2F4 can bind to all of them, although it is primarily regulated by p107 and p130. Thus, E2Fs have been classified as transcriptional activators (E2F1-3) or transcriptional repressors (E2F4-8) and are thus predicted to play a dual role in human cancers[108]. The transcription factor E2F4 is a member of the E2F family and plays a pro- or anti-tumorigenic role in various types of cancer, as it may have both gene activation and repression functions. For example, while E2F4 represses the MAPK signaling pathway, thereby inhibiting the progression of acute myeloid leukemia, it also accelerates the progression of colorectal cancer cells[111]. Regarding its relationship to GBM, E2F4 has been identified as an unfavorable prognostic factor for glioma patients, since the higher the WHO classification of glioma, the higher the expression of E2F4, suggesting that this factor may play a role in the malignant progression of gliomas[111]. In a study searching for the role of GSCs in tumor progression, they performed a single-cell RNA sequencing comparing 53,586 adult GBM cells *vs* 22,637 normal human fetal brain cells to compare the transcriptomic development of these tumor cells. In this research, they observed that in GSCs, the E2F4 pathway was the most significant altered. Moreover, its overexpression had previously been demonstrated in GBM cell lines. Therefore, its inhibition was tested with HLM006474, a small molecule that prevents E2F4 binding to DNA, and observed a reduction in the proliferation and survival of progenitor GSCs[112]. Finally, and according to our results, in U87 cells it has already been shown that inhibition of CDK4 and E2F4 is associated with an arrest of the G2/M phase and a decrease of the S phase of the cell cycle[113]. Moreover, the cyclin D1 (CCND1)/CDK4/6–CDKN2A (p16INK4A)–Rb axis is altered in more than half of GBM cases[114]. Finally, inhibition of the DNA repair protein RAD51, crucial for homologous recombination, has been shown to favor the sensitization of GSCs to radiation[115].

In summary, in this second chapter we have shown that both native and prelatent AT are able to inhibit the entry of U87 cells into the S phase of the cell cycle. This mechanism could be mediated by the inhibition of pRb phosphorylation and E2F4 expression. In addition, the expression of different transcripts involved in the cell cycle are altered after treatment of U87 cells with prelatent AT. Therefore, although at the protein level some of the inhibitions were not statistically significant, we can hypothesize that the

antiproliferative effect of native and prelatent AT could result from the reduction of the expression of different cyclins or cycle-regulatory proteins, as shown by the results of the expression array.

Additionally, AT treatment did not have the same effect on the U251 cell line, where no antitumor effects have yet been observed. The explanation to the different behavior of U87 and U251 GBM cells under treatment with AT could be the differences in protein expression between the two cells lines, as it has been previously reported[116]. In fact, although it is only a speculation, the potential receptor of AT in U87 cells could be absent in U251 cells.

To end, as discussed above, angiogenesis is a process that, among other mechanisms, involves cell proliferation for the formation of new vessels. Besides glioblastoma, breast cancer and colorectal cancer are two highly angiogenic tumors[17]. Therefore, since it has been demonstrated that antithrombin is able to inhibit in vitro both cell proliferation and angiogenesis, its antitumor role could also be explored in these tumours, once the potential antitumor receptor for antithrombin has been identified.

CHAPTER 3. Identification of the potential receptor of antithrombin in glioblastoma multiforme cells and validation of the in vitro results in a preclinical model based on the use of organoids and in samples of glioblastoma multiforme patients.

1. Introduction 78

2. Material and methods 84

2.1 Crosslinking and immunoprecipitation assay 84

2.2 Proteomic analysis by TripleTOF 6600 LC-MS/MS System 84

2.2.1 Protein digestion 84

2.2.2 Protein Quantification by SWATH-MS (Sequential Window Acquisition of all Theoretical Mass Spectra) Analysis 84

2.3 Receptor blocking: cytometry 85

2.4 Organoids generation 86

2.5 Glioma stem cells generation 87

2.6 *In vitro* 3D invasion assay 88

2.7 Validation of dystonin expression by Real-Time qPCR 88

3. Results 89

3.1 Identification of the receptor of AT on GBM cells: Dystonin 89

3.2 Native and prelatent antithrombin can inhibit 3D glioblastoma-neurospheres invasion on human brain organoids 94

3.3 Validation of dystonin expression in glioblastoma cell lines and patients' samples 95

4. Discussion 97

1. Introduction

As described in previous chapters, AT exerts an antitumor effect on GBM cells, a mechanism that seems to be partly independent of its serine protease inhibitory activity. This mechanism could depend on its interaction with a cellular receptor that mediates these effects. Some receptor has already been described for AT. For example, the interaction between AT and syndecan-4, a transmembrane heparin sulfate proteoglycan present on the surface of endothelial cells, is crucial for the anti-inflammatory effect of AT. When AT binds to the heparin sulfate chains of syndecan-4, the release of PGI2 is triggered, which is a potent anti-inflammatory and vasodilatory molecule[26]. Syndecan-4 and β-AT's interaction also inhibits the NF-κB signaling pathway, as the degradation of IκB (the inhibitor of NF-κB) is impaired. This keeps NF-κB sequestered in the cytoplasm and prevents its translocation to the nucleus[28]. Additionally, LRP1 (low-density lipoprotein receptor-related protein 1) is a cell surface receptor that plays a role in various cellular processes, including endocytosis, cell signaling, and the clearance of proteins from the circulation. The interaction between AT and LRP1 occurs through the heparin-binding site of AT, and it leads to the internalization of the AT-LRP1 complex into the cell through clathrin-coated pits by endocytosis. Once inside the cell, AT is directed to lysosomes for degradation[117,118]. However, to date, the receptor by which AT exerts its antitumor role in GBM is unknown. Therefore, the identification of the receptor of AT would not only provide us with information about the mechanism underlying its antitumor role, but it would also provide a potential prognostic biomarker to add to the diagnostic repertoire and justify its therapeutic role.

In addition, although in this doctoral thesis has been demonstrated the anti-tumour effect of AT in the U87 GBM cell line, this tumour has certain characteristics that could hamper the extrapolation of the results to the clinic such as the high inter- and intra-tumour heterogeneity or the lack of an adequate experimental methodology encompassing all the characteristics of GBM.

It is important to take into account some peculiarities of this tumor. The classification of gliomas is crucial for patient management and histopathological diagnosis is the gold standard, as this technique provides important prognostic information. Large biopsies often show a gradual transition from normal appearance of gray or white matter to a lesion with grayish discoloration and blurring of pre-existing anatomical structures,

consistent with the presence of a diffuse glioma. In this context, necrosis indicates high-grade malignancy, especially in patients who have not previously received radio- or chemotherapy. However, microscopic analysis is required to perform the WHO classification of grades I-IV. Regarding GBM, there are different phenotypic variants. The most frequent variants are giant cell GBM (with predominantly multinucleated giant tumor cells), small cell GBM (with small, relatively monomorphic tumor cells and little cytoplasm) and gliosarcoma (with a broad sarcomatoid phenotype). To classify gliomas into WHO grades, the histological features of nuclear atypia, mitotic activity, necrosis and florid microvascular proliferation are used (Table 4). The histological diagnosis of GBM is characterized by the presence of necrosis and/or florid microvascular proliferation, and a mitotic activity of 10% (whereas in lower grade gliomas it is usually less than 5%), while nuclear atypia is more significant in low-grade gliomas[43].

Table 4. Grading of diffuse gliomas according to histological features. Image adapted from Wesseling, P., *et al*[43].

Table 4. Grading of diffuse gliomas according to histological features.		
ASTROCYTIC	***OLIGOASTROCYTIC***	**OLIGODENDROGLIAL**
Low grade +/- nuclear atypia	***Low grade*** +/- nuclear atypia	***Low grade*** +/- nuclear atypia
Anaplastic nuclear atypia + brisk mitotic activity	***Anaplastic*** nuclear atypia + brisk mitotic activity +/- florid microvasc. prolif.	***Anaplastic*** nuclear atypia + brisk mitotic activity +/- florid microvasc. prolif. +/- necrosis
Glioblastoma nuclear atypia + mitotic activity + necrosis and/or florid microvasc. prolif.	***Glioblastoma*** ***+ oligo-component*** nuclear atypia + mitotic activity + necrosis +/- florid microvasc. prolif.	

Nevertheless, histological classification is limited by the biological diversity of gliomas and by inter-observer variability. For example, the O-6-Methylguanine-DNA Methyltransferase protein, encoded by the *MGMT* gene, is a DNA repair protein that eliminates toxicity by alkylating agents. In this sense, the *MGMT* promoter methylation is associated with better response to alkylating chemotherapy, as it reduces DNA repair, and with longer survival of GBM patients treated with radiotherapy combined with

concurrent and adjuvant temozolomide. Another example are the *IDH1/IDH2* mutations. They are rare in primary GBM, while in secondary GBM (low-grade diffuse astrocytoma or anaplastic astrocytoma that progress to GBM), usually manifested in younger patients, are widely common and are associated with better prognosis[101]. In Figure 23 are represented the most frequent molecular alterations in astrocytic, oligodendroglial, and oligoastrocytic gliomas.

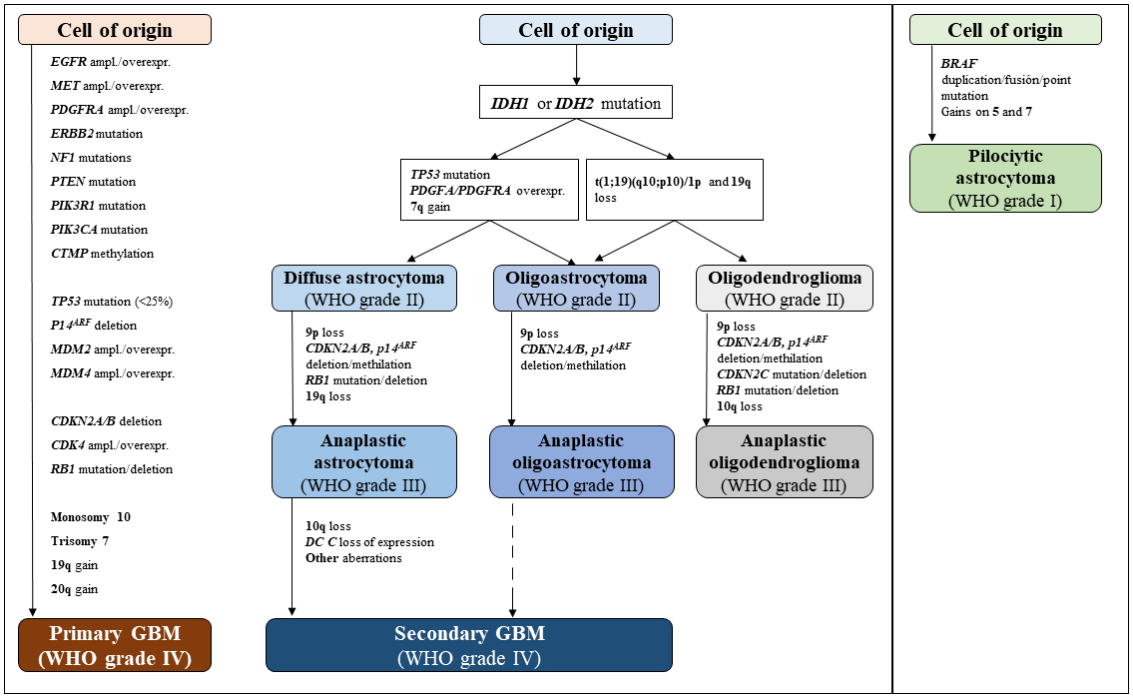

Figure 23. Summary of most frequent molecular alterations in gliomas. GBM: glioblastoma; Ampl.: amplification; Overexpr.: overexpression; WHO: World Health Organization. Image adapted from Riemenschneider, M.J., *et al*[101].

Furthermore, primary GBM has been classified into different subtypes based on transcription profiles, genetic alterations, and DNA methylation, in order to develop more personalized treatments[48] (Figure 24).

Still, there is a need for molecular markers that not only provide a specific classification but also information related to prognosis and a personalized response to therapy. In GBM diagnosis, few biomarkers provide this combined information.

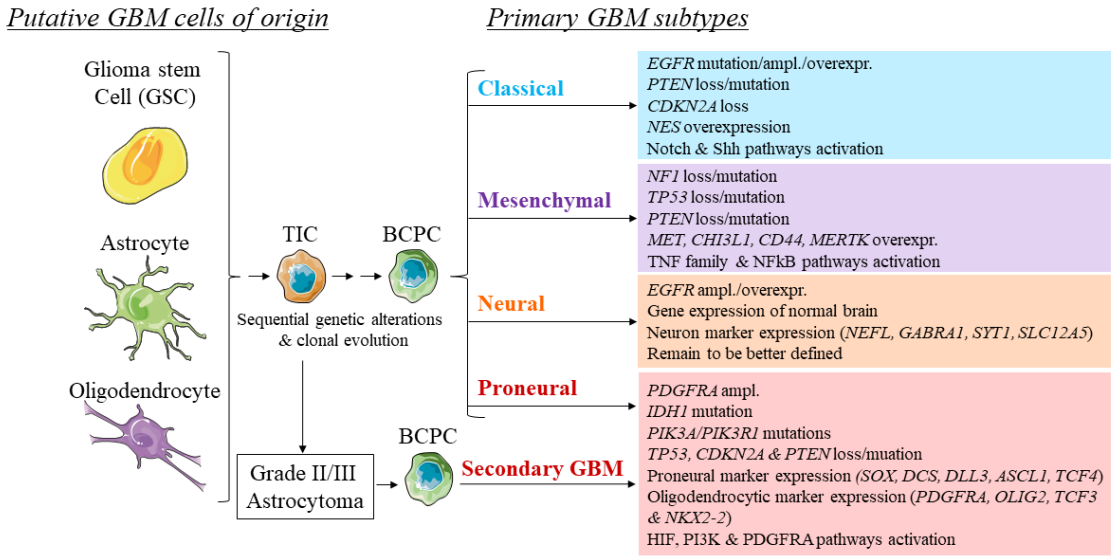

Figure 24. Subclassification of primary glioblastoma (GBM) based on sequential genetic changes observed in the pathogenesis. TIC: tumor–initiating cells; BCPC: brain cancer–propagating cells. Image adapted from Van Meir, E.G., *et al*[48].

On the other hand, GBM is characterized for presenting GSCs. These GSCs have a crucial role in the infiltrative capacity of the tumor, as well as in the high heterogeneity that characterizes this tumor[119]. Unfortunately, the involvement of these cells in the GBM progression has not been considered in most of the experiments conducted to investigate this tumor. Therefore, a precise experimental design is needed to adequately recapitulate both the heterogeneity and the invasive behavior of this tumor and, particularly, of these GSCs.

The study with immortalized cells lines conducted in research laboratories for many years has several limitations. This is due to the fact that these studies do not allow replication of the architecture, spatial heterogeneity, and interactions with the stroma of the tumor. Moreover, U87 cells, the most widely used cells to study GBM, have been assimilated into the mesenchymal subtype of The Cancer Genome Atlas Network classification, despite exhibiting differences in some proteases and mesenchymal genes[120,121]. To date, the models for the study of GBM consist of 2D cell culture in media containing fetal bovine serum and animal models. These models provide information on expression patterns, mutational status, drug response, resistance mechanisms, and insights into new biological pathways, thus greatly contributing to the understanding of GBM. However, they have their drawbacks. For example, the main problem with 2D cultures is that, with continuous passages, specific genetic clones end up being selected, thereby losing the heterogeneity that characterizes this tumor.

Additionally, cells also end up developing their own mutations and phenotypes. Furthermore, these cells are typically cultured as adherent monolayers in medium containing fetal serum, which does not truly represent the characteristics of the tumor microenvironment[122]. An example related to these issues is the U251 cell line used in this doctoral thesis, as mentioned above. This cell line was initially commercialized as U-373 MG. However, after observing changes in its phenotype, an analysis of short tandem repeats showed that, although it was still related to GBM, it had mutated significantly, and had to be renamed as a new cell line, U251[123]. Therefore, in this final chapter of this doctoral thesis, two GBM patient biopsy-derived cell lines harboring GSCs cells and cultured in a defined neurobasal medium have been used, as they more closely mirror the phenotype and genotype of the primary tumor compared to commercialized cell lines cultured with fetal bovine serum. In addition, we have adapted these cells to 3D neurospheres, which have already been shown to maintain a certain degree of heterogeneity and, when intracranially implanted in immunodeficient rodents, retain invasion patterns, a feature that is lost with conventional cell lines. On the downside, these cells are also maintained long-term in culture, so it has also been shown that they eventually undergo clonal selection[124].

As for the shortcomings of animal models, they are time-consuming, labor-intensive, require immunodeficient strains to simulate the immunosuppressive microenvironment found in GBM, have their own genetic variability, and therefore do not reproduce the cellular heterogeneity seen in human GBM tumors[125]. Therefore, we have generated human healthy brain organoids, a technique that is now emerging as a promising tool. Organoids are defined as self-organized, 3D, organotypic structures that recapitulate the original composition of an organ *in vitro*. Two approaches to investigate GBM using organoids have been established: On one hand, there are tumor-derived organoids or tumoroids, which are cultured from patient biopsies in a defined medium, allowing them to maintain both the patient's own heterogeneity and tumor microenvironment, thus enabling personalized therapy studies. However, these models are still being optimized as many of the organoids eventually lose their vasculature and immune cells. Moreover, they do not interact with non-tumor cells and are complex to manipulate. Therefore, it is not the ideal model to investigate the invasion pattern of GSCs[126]. The second approach, which has been employed in this doctoral thesis, is to generate human brain organoids established from induced pluripotent stem cells (iPSCs). These iPSCs

are derived from healthy skin fibroblasts that have been reprogrammed to an embryonic-like pluripotent state by transfection with a cocktail of retroviral vectors expressing *OCT4*, *SOX2*, *KLF4*, and *MYC*. These 4 transcription factors, also known as OSKM or Yamanaka factors, are cellular reprogramming factors involved in maintaining the embryonic state of stem cells and inducing pluripotency in fibroblasts[127]. Briefly, first of all, transfected-iPSCs are aggregated into embryoid bodies and incubated in a medium that allows them to differentiate into neuroectoderm cells. Next, the neuroectoderm forms neuroepithelia that organize radially in rosettes similar to ventricular zones, that expand and form various brain structures using a neurobasal differentiation medium (referred to in this thesis as organoid medium) supplemented with different factors such as B27 (for neuronal differentiation and survival), 2-mercaptoethanol and insulin (for neural stem cell maintenance), among others as will be detailed below. Once the organoid has been formed, it is incubated in agitation to favor the correct diffusion of oxygen and nutrients[128]. These organoids recapitulate many aspects of healthy human brain development and function. However, they lack underlying meninges, vasculature and immune cells. Still, the combined application of these organoids and GBM neurospheres containing GSCs allows, compared to animal models, a decrease in cost and time, while maintaining some degree of heterogeneity, thus providing an ideal microenvironment to recapitulate the invasion behavior of GSCs[129,130].

One of the barriers that has persisted over time in the therapeutic advancement of GBM has been the lack of an adequate experimental system that recapitulates both the molecular heterogeneity of this tumor and the microenvironment and invasive behavior of GSCs. In this sense, in collaboration with Dr. Jay Gopalakrishnan's lab at the University of Düsseldorf (Germany), we used a 3D model to study the invasiveness of GSCs in healthy human brain organoids, established from iPSCs, and 3D neurospheres, established from cell lines derived from biopsies of a GBM patient harboring GSCs and cultured in a defined neurobasal medium. This 3D experiment allows studying the role of GSCs in GBM invasion, partially reproducing the tumor microenvironment, and preserving some of the heterogeneity of GBM cells[131].

In this chapter, our main objective was to elucidate the potential receptor of AT in GBM cells. Identifying this receptor would not only provide us with information about the mechanism by which AT exerts its antitumor function in GBM, but it would also

provide a potential prognostic biomarker to add to the diagnostic repertoire and justify its therapeutic role. Additionally, by using an organoid model and evaluating the invasive effect of tumor GSCs, we aim to corroborate the antitumor effect of AT. Once identified the receptor for AT, the final aim of this chapter was to evaluate the expression of this potential receptor in GBM cells, in cells from a patient with GBM and in biopsies from patients with GBM.

2. Material and methods

2.1 Crosslinking and immunoprecipitation assay

Crosslinking assay was performed following the procedure for intra- and extra-cellular protein crosslinking given by the manufacturer (ThermoScientific, sulpho-EGS, 21566). Briefly, $5x10^5$ U87 cells were cultured in a polystyrene microplate 6-well (Falcon, 353934). Then, cells were detached, suspended and 3-times washed with cold PBS (pH 8.0) and treated with 2.16 µM native or prelatent AT, or buffer A for 1 hour (n=2). Afterwards, 10 mM sulpho-EGS (ethylene glycolbis(sulfosuccinimidylsuccinate)) was added for 30 minutes at room temperature. Sulfo-EGS is used for crosslinking cell surface proteins, as it will not permeate the cell membrane. Finally, a 20 mM quenching solution (1M Tris, pH 7.5) was added to stop the reaction, for 15 minutes.

Next, cellular pellets were lysed and 8 µg of total protein were used. Dynabeads™ Protein A magnetic beads (ThermoFisher Scientific, 10001D) coupled with rabbit anti-human AT antibody (Sigma-Aldrich, A9522) were used following the user manual to immunoprecipitate all established AT covalent complexes. Anti-rabbit IgG (Sigma-Aldrich, I5006) was used as negative control.

2.2 Proteomic analysis by TripleTOF 6600 LC-MS/MS System

2.2.1 Protein digestion: After protein immunoprecipitation all conditions were loaded on a 10% SDS-PAGE gel. The run was stopped as soon as the front had penetrated 3 mm into the resolving gel. The resulting condensed protein bands underwent gel digestion using Trypsin and were processed as previously by our group[132,133].

2.2.2 Protein Quantification by SWATH-MS (Sequential Window Acquisition of all Theoretical Mass Spectra) Analysis: To build the MS/MS spectral

libraries, peptide solutions were analyzed by shotgun data-dependent acquisition using micro-LCMS/MS, as previously by our group[132,133]. The MS2 spectra (MS/MS spectra) of the identified peptides were then used to generate the spectral library for SWATH peak extraction using the add-in for PeakView Software (version 2.2, Sciex), MS/MSALL with SWATH Acquisition MicroApp (version 2.0, Sciex). Peptides with a confidence score >99% (obtained from the Protein Pilot database search) were included in the spectral library. For relative quantification by SWATH-MS analysis, SWATH-MS acquisition was performed on a TripleTOF 6600 LC-MS/ MS system (Sciex) using SWATH mode. The acquisition mode consisted of a 250 ms survey (MS scan) MS1 scan from 400 to 1250 m/z, followed by an MS2 (MS/MS) scan from 100 to 1500 m/z (25 ms acquisition time) of the top 65 precursor ions from the survey scan, for a total cycle time of 2.8 s. The fragmented precursors were then added to a dynamic exclusion list for 15 sec. Any singly charged ions were excluded from the (MS/MS analysis) MS2 analysis. Targeted data extraction from the SWATH MS runs was performed by PeakView v.2.2 (Sciex, USA) using the SWATH MS Acquisition MicroApp v.2.0 (Sciex, USA). Data were processed using the spectral library created from data-dependent acquisition. SWATH MS quantization was attempted for all proteins in the ion library that were identified by ProteinPilotTM 5.0.1 with a false discovery rate <1%. PeakView computed a false discovery rate and a score for each assigned peptide based on the chromatographic and spectra components: only peptides with a false discovery rate <1%, 10 peptides and 7 transitions per peptide were used for protein quantization. The integrated peak areas were processed by MarkerView software version 1.3.1 (Sciex, USA) for a data-independent method for relative quantitative analysis. A most likely ratio normalization was performed to control for possible uneven sample loss across the different samples during the sample preparation process. Unsupervised multivariate statistical analysis using PCA was performed to compare data across samples.

2.3 Receptor blocking: cytometry

$2.5x10^5$ U87 cells were grown in a polystyrene microplate 6-well (Falcon, 353934). Then, the following treatments were incubated for 11 hours (n=2/group): (1) Control: Buffer A, (2) 2.16 µM Native AT, (3) 2.16 µM Prelatent AT, (4) 2.16 µM Native AT + 1:200 anti-dystonin antibody (Merck, HPA030200), (5) 2.16 µM Native AT + 1:200 anti-dystonin antibody (Merck, HPA030200), (6) 1:200 anti-dystonin antibody (Merck, HPA030200). Afterwards, cells were labeled with 10 µM 5-Bromo-20-deoxyuridine

(BrdU) (BD Biosciences, 552598) for 4 hours. Then, the APC BD BrdU flow kit (552598, BD Biosciences) was used to fix and permeabilize cells prior to DNAse treatment and staining with anti-BrdU-APC. Total DNA was stained with 7-aminoactinomycin D to evaluate cell death. Finally, data were obtained using a BD Accuri C6 flow cytometer device (Ann Arbor) and analyzed with FlowJo 10.3 software. The experiment was performed in triplicate.

2.4 Organoids generation

Commercial iPSCs transfected with red fluorescence protein (RFP) (Coriell Institute for Medical Research, AICS-0031-035) were used to generate healthy human brain organoids, following the protocol described by Goranci-Buzhala, G. *et al*[131]. First, iPSCs were grown on 35 mm plates (ThermoFisher, 150460) pre-treated with 1X Geltrex (a compound like matrigel but with reduced growth factors, to favor only iPSC growth and not fibroblast growth; Gibco, A14133-01) diluted with DMEM/F12 medium (Gibco, 31331028), and were checked for appropriate stem cell morphology. mTesR medium (basal medium for iPSCs cell spreading, Stem cell technologies, 05850) supplemented with 0.1% LIF (Leukemia inhibitory factor, inhibits differentiation of iPSCs, Peprotech, 300-05) was daily renewed until the colonies were 70-80% confluent. At that point, iPSCs were detached with ReLeSR (Stemcell technologies, 05872) and re-cultured at least twice before organoids generation. When iPSCs colonies were 70-80% confluent, iPSCs were detached and disaggregated as single cells with Accutase (reagent equivalent to trypsin but less toxic and only used with cells grown in serum-free medium, Sigma-Aldrich, A6964-100ML) for 5 min at 37ºC. Next, $3x10^5$ total iPSCs in 100 µl were centrifuged at 193 *g* for 8 minutes in a 96-well V-shaped-bottom plate (Thermo scientific, 277143) to obtain immature organoids. From here, cells were incubated at 37ºC and 5% CO_2 and half of the medium was renewed for 5 days using neural induction medium (NIM, Stemcell Technologies, 05835) and 10 µM ROCK inhibitor Y-27632 2HCl (improves viability of colonies, Selleckchem, S1049). NIM medium allows the iPSCs to differentiate into spheres of the neuroectoderm. After 5 days, the organoids were collected using 100 µm filters (VWR European, 732-2759), washed with DMEM/F12 medium and incubated with organoid medium and agitation at 37ºC and 5% CO_2 for 4 additional days, until they were considered mature organoids on day 9. Organoid medium was composed by the following compounds: 50% neurobasal medium (basal medium for neural stem cell spreading, Gibco, 21103049) and 50%

DMEM/F12 supplemented with 1X L-glutamine (Thermo scientific, 25030081), 1X non-essential amino acids (Thermo scientific, 11140050), 1X penicillin-streptomycin (Thermo scientific, 15140-122), 0.05 mM β-mercaptoethanol (reducing agent that prevents toxic levels of oxygen free radicals, Gibco, 31350-010), 0.5X B27 (hormone mix that promotes proliferation of neuronal cell lines, Thermo scientific, 12587010), 0.5X N2 (supplement for neuron differentiation and survival, Thermo scientific, 17502048) and insulin (primary cell antimicrobial, Sigma-aldrich, I3536-100MG). At this point, the inhibitors SB431542 (receptor kinase inhibitor, Selleckchem, S1067) and dorsomorphin (BMP and AMPK inhibitor, Sigma-aldrich, 866405-64-3) were added. Thereafter, the medium was renewed once a week, and mature organoids can be used at any time. This shift to organoid medium supplemented with various factors allows the neuroectoderm to form radially organized neuroepithelia that expand and form various brain structures such as ventricles, while supplementation promotes neuronal differentiation and the maintenance of neural stem cells. Agitation is important for proper diffusion of oxygen and nutrients.

2.5 Glioma stem cells generation

The 275 and 275-BIS cell lines were supplied by Dr. Roberto Pallini's and Dr. Jay Gopallakirhsnan's lab. These cells, which contain GSCs[131], were obtained from the biopsy at diagnosis of a patient with GBM, denominated 275, while 275 BIS cells were obtained from the biopsy at relapse of the same patient. The cells were then transfected with lentiviral particles for green fluorescent protein (GFP) expression. 3D neurospheres were generated with 275 primary and 275-BIS recurrent cell lines as previously described[131]. Briefly, the cells were grown on matrigel hESC-qualified matrix (contains various extracellular matrix proteins to simulate the cell basement membrane and to promote cell culture and differentiation, Corning, 354277) in an incubator at 37°C, 5% CO_2 with neurocult NS-A basal medium (basal medium for neural stem cells spreading, Stemcell technologies, 05750) supplemented with 1X B27, 1X N2, 1X glutamax (Gibco, 35050-061), 100 µg/ml primocin-antibiotic (primary cell antimicrobial, Invivogen, ant-pm-05), 0.0075% bovine serum albumin (Sigma-Aldrich, A1595), 10 ng/ml epidermal growth factor (EGF, general cell growth, Peprotech, 100-15) and 10 ng/ml basic fibroblast growth factor (bFGF, general cell growth, Peprotech, 100-18B) To notice, heparin is normally used in this medium as it, together with the epidermal growth factor, promotes the maturation of neural stem cells. However, this

component was not added to our media to study the native and prelatent conformations of AT as they could become activated. Cells were then detached with Accutase, and $1x10^4$ cells were centrifuged in a low-adherent 96-well U-shaped-bottom plate (Thermo scientific, 15227905). Finally, the 3D neurospheres were allowed to grow for at least 48h before its use.

2.6 *In vitro* 3D invasion assay

Primary and recurrent patient neurospheres and 25 days old organoids were co-cultivated and treated for 10 alternating days with 10 µM native or prelatent AT or buffer A (control). The anti-invasive AT effect was evaluated by fluorescence microscopy (LSM 880, ZEISS) and the results were measured using the Fiji Software. These experiments were performed in technical triplicates.

2.7 Validation of dystonin expression by Real-Time qPCR

U87 and U251 cell lines were purchased from ATCC, 275 and 275 BIS cell lines were kindly provided by Prof. Roberto Pallini and Dr. Jay Gopalakrishnan, and formalin-fixation and paraffin embedding tissues from 10 patients with grades I and II (low grades), and III and IV (high grades) were obtained from the national Biobank of the Instituto de Salud Carlos III and sliced in four 10 µm each slides per sample. Then, total RNA was isolated using the PureLink™ FFPE Total RNA Isolation Kit (Invitrogen, K1560-02). The RNA concentration and 260/280 ratio were determined by using a NanoDrop spectrophotometer (Thermo Scientific). From total RNA, a 50-ng sample was reversetranscribed to cDNA according to the manufacturer's instructions (SuperScript First Strand, Invitrogen). PCR reactions were carried out using TaqMan® Gene Expression primers and probes, designed as follow in Table 5:

Table 5. Primers and probes for *DST* isoforms detection.

Table 5. Primers and probes for *DST* isoforms detection			
Gene isoform	**Forward**	**Reverse**	**Probe**
DST a1, b1	GTTACCTCTCCCCTGC TGC	TCTGAACTTTGTCCCG TTCATCT	AGTATCTCCAGGCCTA CGAGG
DST a2, b2	GCTTTCCTCGTCTTGC TGAG	CCAGCAGCAGAAGAA GACGA	TGTGCCCTCTTCCTCT TGTTG
DST a3, b3	TGGGGAATGTCTGTG GATGTG	TTTTCTTCCAGGAGAG TATTTTTCAGG	GAAGAACAATATGTA GATCCTGCCAAAAC

A pre-amplification PCR reaction (Table 6) was performed on an Eppendorf MasterCycler Nexus SX1 thermal cycler (Eppendorf), and a following qPCR (Table 7) reaction was performed on a QuantStudio™ 5 Real-Time PCR System (ThermoFisher), in technical duplicate for each sample. VIC-ACTB_PL (Hs01060665_g1, 11917021, ABI Applied Biosystems) probe expression was used as the endogenous reference control. The fold difference for each sample was obtained using the comparative CT (ΔΔCT) method.

Table 6 Pre-amplification PCR run method.

Table 6 Pre-amplification PCR run method			
Step	**Temperature**	**Time**	**Ramp rate**
Denaturation	95ºC	10’	2.73ºC/s
Amplification x15 cycles	95ºC	15’’	2.73ºC/s
	60ºC	4’	2.11ºC/s
Cooling	4ºC	∞	

Table 7. qPCR run method.

Table 7 qPCR run method			
Step	**Temperature**	**Time**	**Ramp rate**
Denaturation	95ºC	20’’	2.73ºC/s
Amplification x15 cycles	95ºC	1’’	2.73ºC/s
	60ºC	20’’	2.11ºC/s

3. Results

3.1 Identification of the receptor of AT on GBM cells: Dystonin

Once the *in vitro* antitumor role of AT on GBM cells was confirmed, we aimed to identify the receptor that AT is binding to in order to exert all these effects. To this end, after treating U87 cells with native or prelatent AT, or buffer A (control), we performed a crosslinking assay using the sulpho-EGS compound and following immunoprecipitation to obtain the covalent AT complexes formed. Samples were analyzed by quantitative proteomics. As shown in the PCA (Figure 25), samples incubated with native or prelatent AT were differentiated in a distinct cluster than the control samples, confirming the distinction between the different populations. Furthermore, as presented in Table 8, we identified dystonin as the receptor of AT in

U87 cells with a high specific interaction with both prelatent (p-value: $1.04x10^{-10}$, FC: 139.80) and native AT (p-value: $1.32x10^{-7}$, FC: 145.40) compared to control samples.

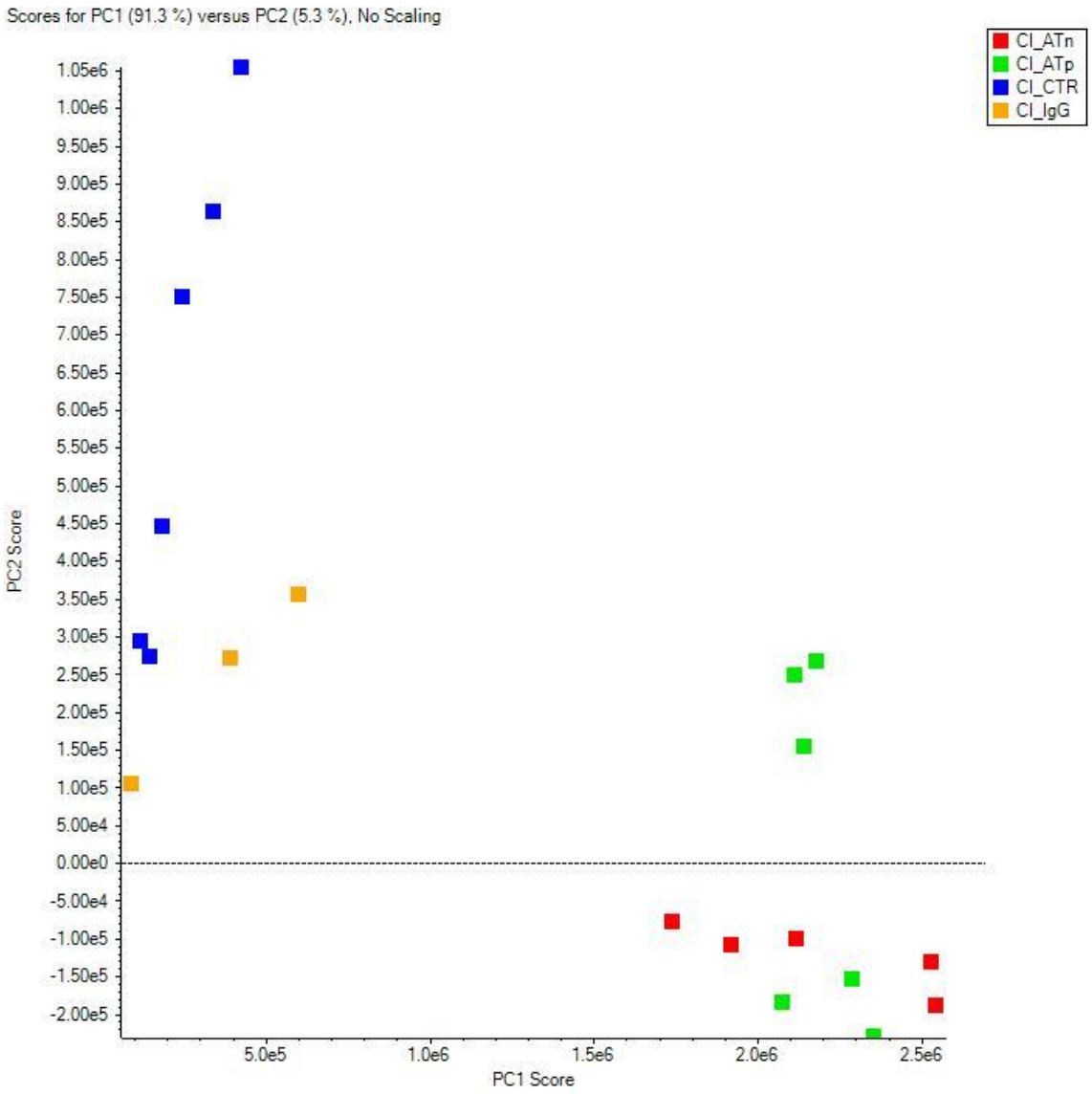

Figure 25. Principal component analysis (PCA) plot illustrating the protein relationship between U87 immunoprecipitated samples incubated with native or prelatent antithrombin (AT) *vs*. controls. The PCA was obtained using samples first crosslinkated and then immunoprecipitated with native AT (ATn, red squares), prelatent AT (ATp, green squares), buffer A (CTR, blue squares) or IgG antibody (IgG, yellow squares).

Table 8. Proteomics study. Results obtained by SWATH-MS of crosslinked and immunoprecipitated U87 lysates incubated with native antithrombin, prelatent or buffer A (control samples).

Table 8. Prelatent AT vs Control		
Protein	***p*-value**	**Fold-change**
Dystonin	**$1{,}04\times10^{-10}$**	**139,80**
Immunoglobulin gamma-1 heavy chain	$1{,}05\times10^{-11}$	103,37
Immunoglobulin kappa variable 3-20	$5{,}30\times10^{-7}$	29,14
Antithrombin-III	**$2{,}34\times10^{-7}$**	**16,89**
Immunoglobulin kappa variable 3D-7	$6{,}07\times10^{-8}$	10,68
Immunoglobulin heavy constant gamma 4	$1{,}03\times10^{-2}$	8,60
Immunoglobulin kappa variable 4-1	$2{,}79\times10^{-6}$	6,18
Bone morphogenetic protein 1	$9{,}67\times10^{-3}$	5,95
Immunoglobulin kappa variable 1D-12	$2{,}13\times10^{-4}$	5,49
Immunoglobulin kappa variable 1-33	$9{,}10\times10^{-3}$	4,95
Peptidyl-prolyl cis-trans isomerase A	$1{,}33\times10^{-3}$	4,74
…	…	…
Native AT vs Control		
Protein	***p*-value**	**Fold-change**
Dystonin	$1{,}32\times10^{-7}$	145,40
Immunoglobulin gamma-1 heavy chaim	$1{,}90\times10^{-9}$	99,19
Immunoglobulin kappa variable 3-20	$8{,}72\times10^{-4}$	21,26
Immunoglobulin heavy constant gamma 4	$1{,}05\times10^{-3}$	15,97
Antithrombin-III	$5{,}18\times10^{-7}$	14,64
Immunoglobulin kappa variable 3D-7	$2{,}51\times10^{-9}$	11,85
E3 ubiquitin-protein ligase MARCHF6	$1{,}85\times10^{-2}$	9,70
Bone morphogenetic protein 1	$8{,}09\times10^{-3}$	5,93
Immunoglobulin kappa variable 4-1	$1{,}53\times10^{-7}$	5,65
Immunoglobulin kappa variable 1D-12	$1{,}26\times10^{-4}$	4,38
Immunoglobulin kappa variable 1-33	$2{,}70\times10^{-2}$	3,86
…	…	…

Dystonin is a cytoskeletal protein belonging to the spectraplakin family. The dystonin gene, *DST* or *BPAG1*, presents tissue-specific promoters and several exons that are alternatively spliced, resulting in differentially expressed protein isoforms that localize to distinct cellular regions (muscular, neuronal and epithelial) where they perform unique cellular functions (isoforms a1, a2, a3, b1, b2, b3 or e)[134] (Figure 26)[134].

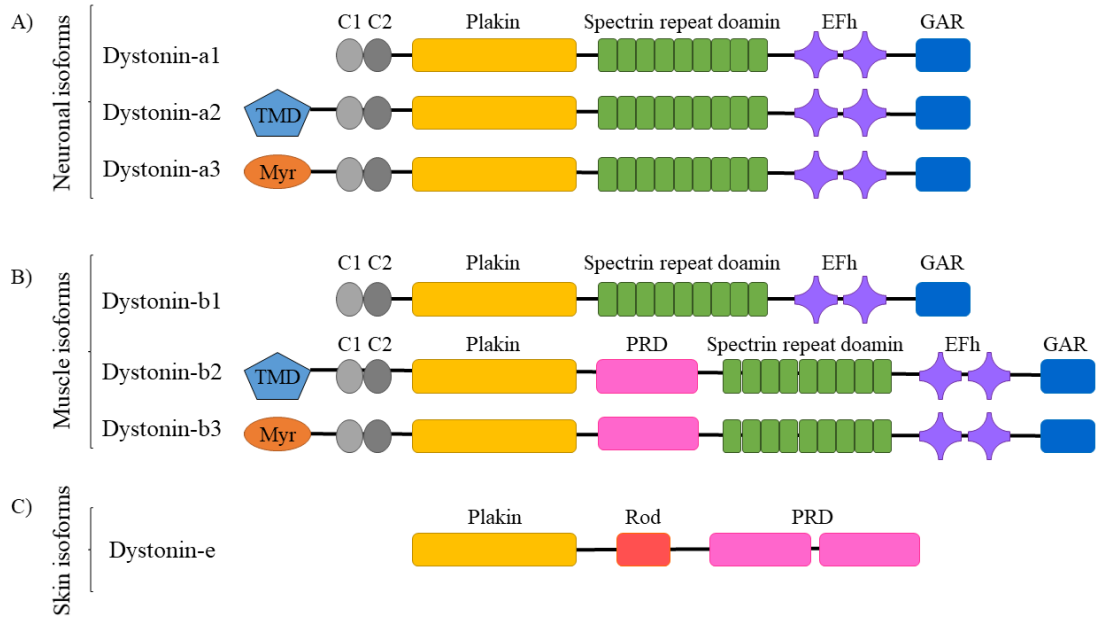

Figure 26. Schematic representation of the predominant *DST* isoforms. Neuronal (A) and muscle (B) dystonin isoforms possess actin binding domains at their N-termini (calponin homology domains, C1 and C2), and C-termini microtubule binding domains (EF-hands and a growth arrest-specific 2 related domain (GAR) domain), while skin (C) dystonin isoform doesn't. Because of the plakin repeat domain (PRD), muscle isoforms present a molecular weight of 834 kD, while neuronal isoforms are ~615 kD. The differences in splice variants is largely restricted to the N-termini, whereby dystonin-a/b1 contains an actin binding domain, dystonin-a/b2 has a transmembrane domain (TMD) preceding the actin binding domain, and dystonin-a/b3 contains a putative myristoylation motif (Myr) that precedes a single calponin homology domain. (C) The skin epithelial isoform dystonin-e is smaller (302 kD) and presents a N-terminus plakin domain, a Rod domain that is unique to this isoform, followed by 2 plakin repeat domains that are involved in intermediate filament binding. GAR =Image adapted from Lynch-Godrei, A. *et al*[135].

In order to validate that AT could be exerting its antiproliferative effect through specific dystonin interaction, we blocked the AT-dystonin binding using a polyclonal anti-dystonin antibody, and assessed the cell cycle and proliferation of U87 cells.

First of all, no differences were observed in the inhibition of the S phase (Figures 27A and 27C) exerted by the anti-dystonin antibody alone or in the presence of AT. There was also no difference in the effect produced by the anti-dystonin antibody in the presence or absence of AT in the G2-M (Figure 27D) and G0-1 (Figure 27E) phases of the cell cycle and compared to the control. These results suggest that the inhibitory effect of antithrombin on the cell cycle might not be mediated by the binding of the protein to dystonin. However, a greater effect of cell apoptosis was observed only in the presence of the anti-dystonin antibody (Figure 27F).

Regarding cell proliferation (Figure 27B), the addition of the anti-dystonin antibody alone exerted the same anti-proliferative effect as AT and compared to the control. In fact, such inhibition was slightly greater than that exerted by AT alone. This could indicate that dystonin blockade is involved in anti-proliferative effect exerted by AT.

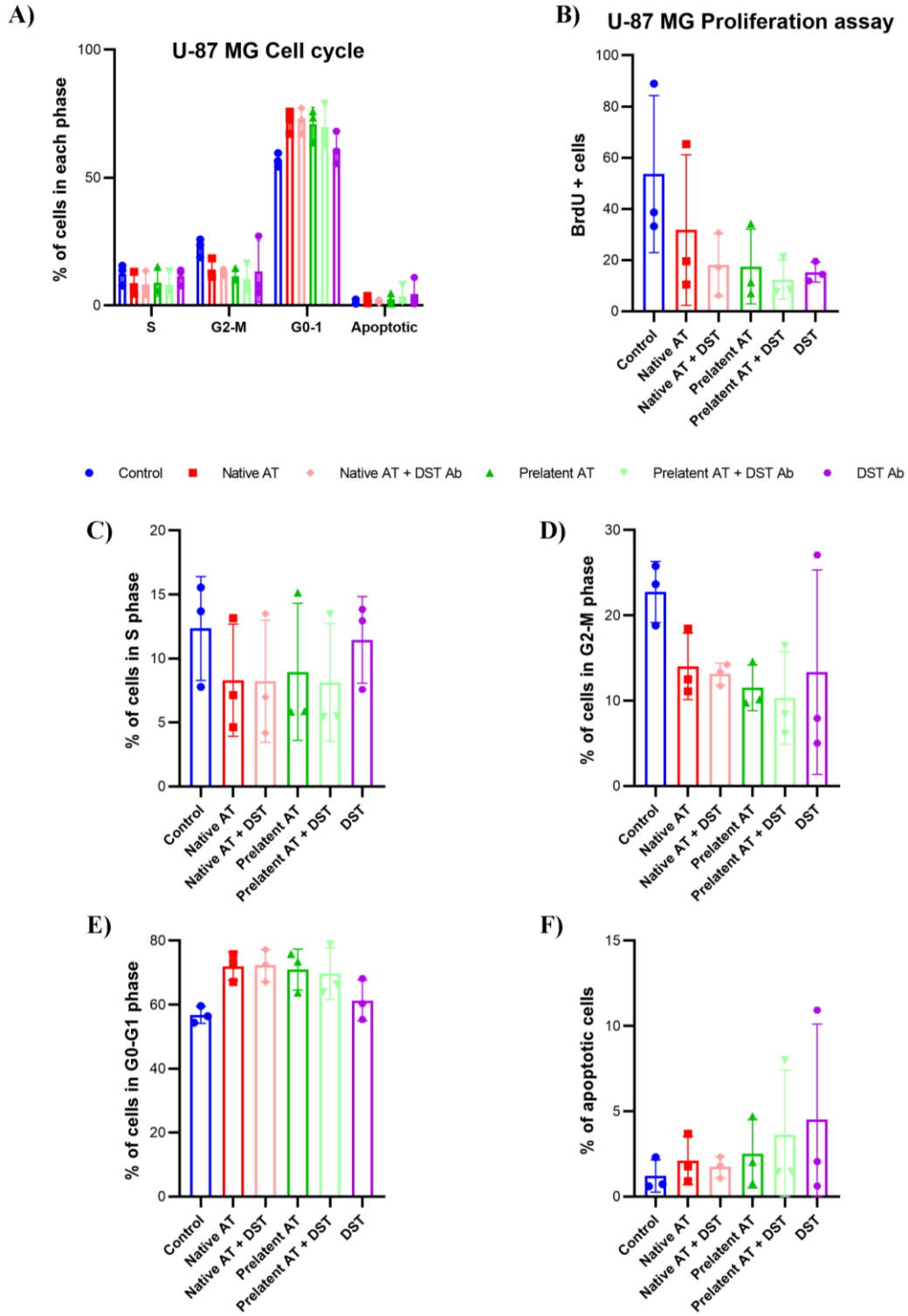

Figure 27. Effect of native and prelatent antithrombin (AT) in the presence or absence of anti-dystonin antibody (DST) and compared to control on cell cycle (A, C-F) and proliferation (B) in U87 cell line.

3.2 Native and prelatent antithrombin can inhibit 3D glioblastoma-neurospheres invasion on human brain organoids

As previously described[131], the organoids showed developmental patterns such as the presence of rosettes, indicating that the neuroectoderm has formed radially organized neuroepithelia in rosettes similar to ventricles zones (Figure 28, pointed by arrows).

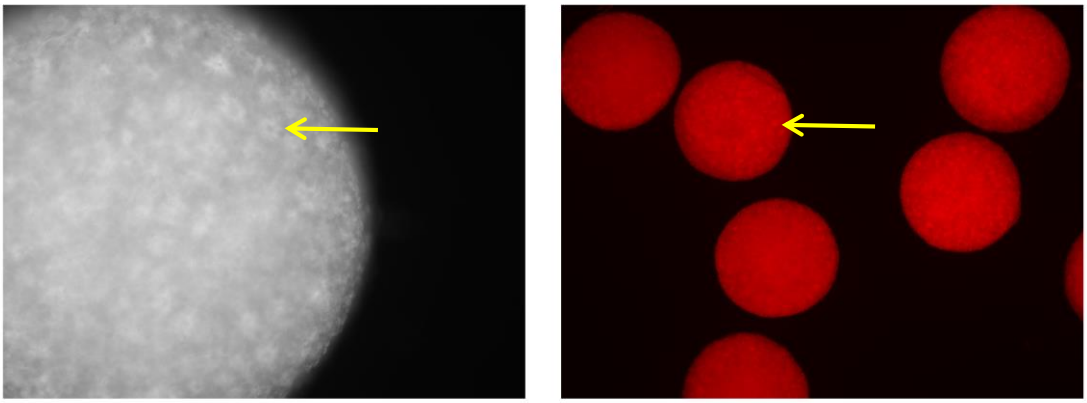

Figure 28. **Organoids development**. Microscopy images showing organoids at day 5 of development. Arrows highlight the rosettes resembling brain ventricles.

Organoids (25 days old) and neurospheres were treated for 10 alternating days with 10 µM native or prelatent AT, or buffer A (control). Although the following results are preliminary and need to be repeated for confirmation, as shown in Figure 29A, while the 275 control neurospheres were completely inside the organoid, part of the 275 neurospheres treated with native and prelatent AT were outside the organoid. The results obtained with the 275 BIS neurospheres were even more surprising (Figure 29B), as none of the neurospheres treated with native or prelatent AT could invade the organoid, whereas the untreated neurospheres completely invaded the organoids.

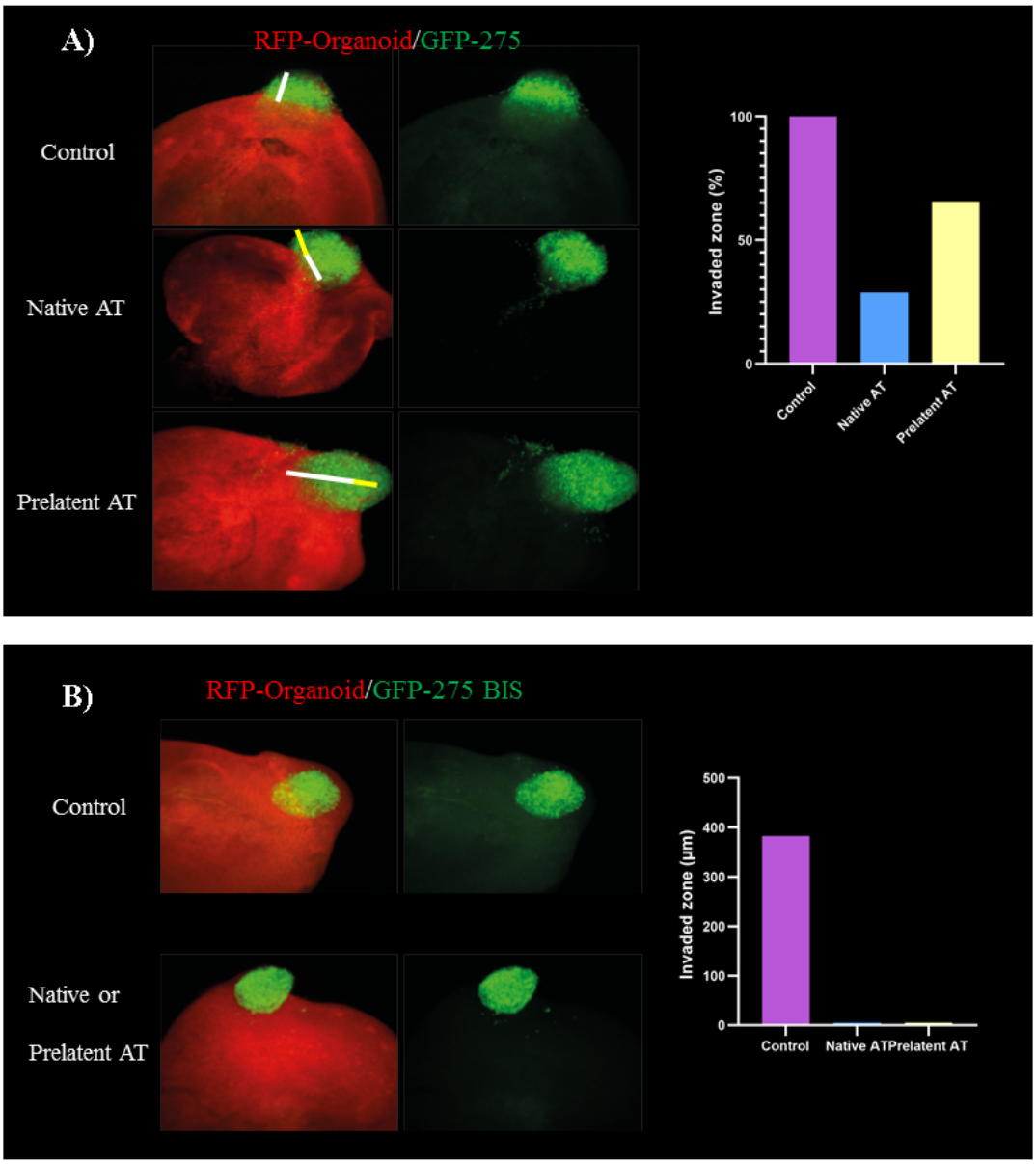

Figure 29. **Three-dimensional model of glioblastoma multiforme invasion to test the antitumor effect of antithrombin (AT)**. In green, 275-neurospheres (A) or 275 BIS-neurospheres (B) generated from primary tumor cells of a GBM patient are shown. In red, human brain organoides generated from induced pluripotent stem cells are shown. On the left, representative fluorescence images of the results are shown. On the right, the percentage of invasion of each neurosphere is represented.

3.3 Validation of dystonin expression in glioblastoma cell lines and patients' samples

We observed a greater effect of AT on U87 *vs.* U251, and in the cells extracted from the patient with GBM, the effect was greater in the relapsed line 275 BIS versus 275. Therefore, we performed a RT-qPCR with the aim of determining the expression of

dystonin in these cell lines.

Furthermore, we evaluated the expression of the different dystonin isoforms in 5 samples from patients with low-grade gliomas (I-II) and in 5 samples from patients with high-grade gliomas (III-IV), with the aim of determining whether dystonin expression could be used as a prognostic marker (Figure 30).

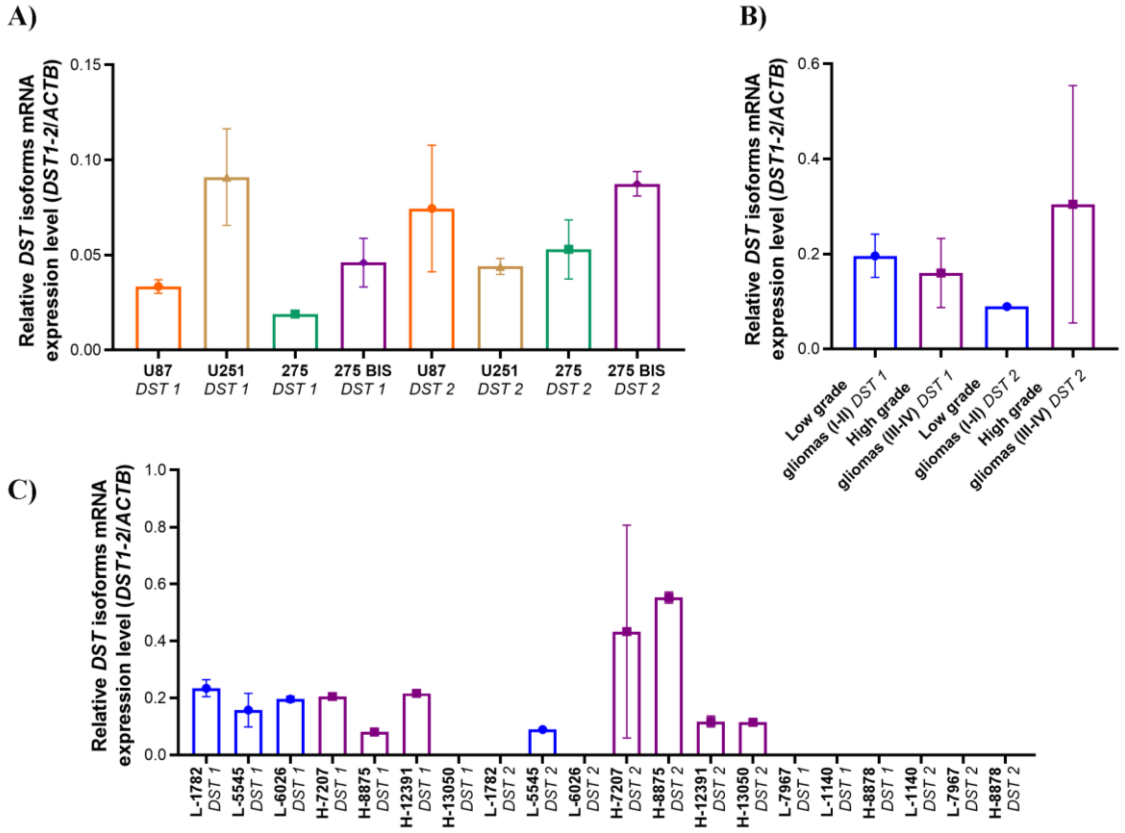

Figure 30. **Dystonin isoforms expression**. Relative expression of dystonin isoforms 1 (*DST 1*) and 2 (*DST 2*) to *ACTB* mRNA (2-ΔCt) in U87, U251, 275 and 275 BIS cell lines (A), and in glioma patient samples represented as average (B) or individually (C). Samples with no expression (0) indicates no amplification. Each condition was evaluated in duplicate.

First of all, it should be noted that no amplification of dystonin isoform 3 was obtained in any of the cell lines or patient samples (data not shown), confirming the low expression of this isoform in GBM samples. However, consistent with our hypothesis, Figure 30A shows that expression of isoform 2 is higher in U87 and 275 BIS cell lines than in U251 and 275, which reinforces our previous hypothesis that AT may be binding with greater affinity or exerting a greater effect by interacting with dystonin isoform 2. Regarding the samples with patients with different grade gliomas, we found

several challenges (Figure 30C). Two samples from each group did not amplify for any of the isoforms, and some samples only amplified for one of the isoforms and not for the other, which leads us to hypothesize that RNA degradation could be affecting the measure of expression, or these samples express little or none dystonin. Furthermore, and in line with the main characteristic of GBM, we identified a high inter- and intra-tumoural heterogeneity, since according to the calculated average (Figure 30B) it could be inferred that isoform 2 is expressed much more in patients with high-grade gliomas, but when observing the results individually, while samples 7207 and 8875 express a high amount of isoform 2, the same does not occur with samples 12391 and 13050. Anyway, these results encourage us to increase the sample size to elucidate if isoform 2 could discriminate those GBM patients which could benefit from AT treatment.

4. Discussion

Despite the complexity of the underlying disease, the identification of the potential receptor of AT in this tumor would help the selection of patients who could benefit from AT's treatment. Importantly, AT could even be used as a drug in those pathologies where this receptor is expressed. Dystonin, also known as bullous pemphigoid antigen 1, is a cytoskeleton and cytoskeletal linking protein that belongs to the spectraplakins family, which are adhesion proteins between the cytoskeleton and other junctional complexes. Like spectrin, it binds actin filaments to membrane receptors, while as a plakin, it is a component of desmosomes and hemidesmosomes where it connects adhesion receptors to intermediate filaments. Dystonin, is encoded by the *DST* gene, and is a large protein (~300-800 kDa) that, as shown in Figure 26, presents several plakin domains and different structural domains (e.g. actin-binding domain, spectrin-repeat-containing rod domain, and microtubule-binding domain), allowing the protein to cross-link cytoskeletal filaments or to link filaments to junctional complexes and organelles. Plakin family members are commonly found in tissues that undergo mechanical stress, such as epithelial and muscle tissues, and peripheral nerves. Within epithelial cells, some plakins such as dystonin can localize to both intermediate filaments and filament attachment sites, which are situated at the plasma membrane, and in turn provide the cell structural stability. *DST* gene is characterized for presenting tissue-specific promoters and an abundance of exons that are alternatively spliced yielding differentially expressed protein isoforms that localize to distinct cellular

regions where they perform unique cellular functions, in fact, dystonin has 3 tissue-specific isoforms: neural, muscular and eptihelial[134]. The epithelial isoform of dystonin is associated with the autoimmune disease bullous or bullous pemphigoid, in which the immune system attacks the skin, usually causing large, pruritic blisters with areas of inflamed skin. In fact, the knockout of this gene isoform (*BPAG1e*) leads to skin fragility syndrome and dystonia. *BPAG1e* is mainly expressed in the epidermis, cornea and bladder. The neural (BPAG1a) and muscle isoforms (BPAG1b) are two large proteins with a predicted molecular mass of 625 kDa and of 834 kDa, respectively. In addition, the muscular and neural isoforms can each present 3 isoforms that differ in their N-terminus (a1, a2, a3 or b1, b2, b3) (Figure 26)[136].

Regarding the relationship of dystonin with cancer, although little is known, different studies suggest that dystonin could exert pro- or antitumoral effects depending on the altered isoform. For instance, in breast cancer, the epithelial isoform has been shown to play an antitumor role, as its high expression has been associated with better prognosis and immune infiltration[137], and with less tumourigenesis[138]. However, in melanoma, it has been observed that dystonin is overexpressed, thus favoring tumor proliferation, while its lower expression has been related to better survival on these patients[139]. In our study we have demonstrated for the first time the benefit of dystonin blockade in U87 GBM cells, as it provoked a significant decrease in both S-phase of the cell cycle and cell proliferation, as well as a slight increase in cell apoptosis. However, the antibody used does not block a specific isoform. Therefore, having confirmed the antiproliferative role of dystonin blockade, we decided to evaluate each neural isoform. Since there is no permeabilization step during the crosslinking and immunoprecipitation assay, according to the RT-qPCR results, we hypothesized that AT would be interacting with some of the isoforms that have membrane-binding domains. Specifically, dystonin-a1 encodes a short N-terminal domain that includes an actin-binding domain, whereas dystonin-a2 possesses a transmembrane domain and dystonin-a3 possesses a putative myristoylation domain, which has been shown to aid its localization to the nuclear envelope membrane and perinuclear membranes and plasma membrane, respectively. We cannot rule out the possibility that AT is also endocytosed by tumor cells and once inside endosomes or multivesicular bodies, interacts with dystonin. This endocytosis could be mediated by LRP1[140,141], which is expressed in these tumor cells (data obtained from our proteomic experiment).

The main limitation of this chapter was the measurement of the different dystonin isoforms in samples from patients with gliomas of different grades. The quantitative PCR as well as digital PCR are highly sensitive and reliable techniques. However, quantitative PCR requires technique and endogenous control optimisation, which impaired the correct amplification of the samples. Meanwhile, digital PCR not only yields more precise results, but also allows us not to use an endogenous control, which would allow us to better optimise the experiment[142]. Therefore, this experiment should be repeated using the digital PCR technique.

In recent years, several studies have shown that the use of 3D organoids and neurospheres from patients allows preservation of histological architectures and genetic profiles of their parental tumours, even after long-term culture, and are suitable for biomarker identification and high-throughput in vitro drug screening. In particular, the 3D system employed in this doctoral thesis based on the use of neurospheres from GBM patients and organoids from healthy human brain, provides several advantages such as preserving the heterogeneity, invasion patterns of GSCs, and tumour microenvironment of the GBM, and can be used as a preclinical study model that allows personalized therapy studies[143]. Although the results shown require validation, both the native and prelatent forms of AT showed an anti-invasive effect on cell lines 275 and 275 BIS, especially on recurrent patients. However, the 3D model, although a great advance, does not yet allow us to replace animal experimentation. Therefore, it will be necessary to demonstrate these results in an *in vivo* model in which the potential bleeding risk that could be involved in the administration of AT should be evaluated. Eight-40% of GBM patients suffer from venous thromboembolism (VTE), and there is an increased risk of VTE after surgery and compared to other tumors. In addition, these patients suffer intracranial hemorrhages due to the high vascularization characteristic of this tumor. In fact, 0.5-3.4% of patients debut with this symptom, while 2-8% suffer from this symptom during the course of the disease. In addition, 8% of patients suffer spontaneous or post-operative hemorrhages. However, as we have already mentioned that these patients are also at risk for VTE, anticoagulation prophylaxis is hesitant in these patients[144]. In fact, there is no effective thromboprophylactic strategy for these patients[145]. The administration of AT, especially the prelatent conformation, would not only provide the antitumor function demonstrated in this doctoral thesis, but could also provide an antithrombotic effect that would not be as hazardous as the administration of

heparin. Therefore, since these patients are at risk of bleeding in the first month after tumor resection, which is also the time between the surgery and the start of radiochemotherapy, our aim would be to administer AT once this bleeding risk has gone[144]. Bevacizumab slightly increases the risk of both thrombosis and bleeding[146,147]. Given that prelatent AT represses VEGFA while retaining its anticoagulant capacity, its *in vivo* interaction with bevacizumab should be the subject of a separate analysis in the future. Furthermore, in the *in vivo* experiments, it will be necessary to determine the type and doses of administration of AT. In fact, there are currently different and novels methods of chemotherapy administration in GBM such as the convection-enhanced delivery, implanted reservoirs, or intra-arterial delivery[68,148].

CONCLUSIONS

1. Prelatent antithrombin, as well as the native conformation, is able to inhibit enteropeptidase, a serine protease involved in tumorigenesis. However, prelatent antithrombin exerts anti-tumour effects that seem to be independent of the inhibition of serine proteases. Thus, prelatent antithrombin is able to significantly reduce migration and invasion of U87 glioblastoma cells and, in the case of migration, more efficiently than the native form. These effects of prelatent antithrombin are not enhanced by the presence of heparin.

2. Prelatent antithrombin is able to regulate VEGFA expression in U87 cells, showing surprisingly versatile antitumor mechanisms related to the inhibition of angiogenesis processes. In fact, prelatent antithrombin regulates the expression of several microRNAs involved in the VEGFA signalling pathway. These results enhance the potential use of synthetic miRNA mimics as antitumor therapy.

3. Prelatent antithrombin reduces the expression of STAT3 and the phosphorilation of pSTAT3α and pERK1/2, which has been associated with the inhibition of the VEGFA expression and with reduced resistance to treatment, which is one of the main complications of this tumour.

3. Native and prelatent antithrombin inhibit the S-phase of the cell cycle as well as the proliferation of U87 cells by inhibiting phosphorylation of pRb and reducing E2F4 expression.

4. The antitumor effects of antithrombin are not observed in the U251 glioblastoma cell line, possibly due to differences in protein expression compared to the U87 cell line.

5. We have identified dystonin, a protein member of the plakin family, as the receptor of antithrombin in U87 glioblastoma cells, which is is involved in the antiproliferative effect exerted by antithrombin. Although it is necessary to increase the sample size, dystonin isoform 2 seems to be overexpressed in high-grade gliomas compared to low-grade gliomas. If confirmed, the identification of dystonin as a biomarker and

therapeutic target could open up new treatment strategies in GBM and other tumours, as well as to identify those patients who could benefit from antithrombin treatment.

6. Native and prelatent antithrombin preliminary are able to inhibit tumour invasion in a preclinical model based on the use of 3D human healthy brain organoids and neurospheres from a glioblastoma patient. These results were more relevant when evaluating the inhibition of invasion of the neurospheres obtained from the patient's relapsed biopsy. These differences in the effect of antithrombin between biopsies at diagnosis and at relapse, as well as with the U87 and U251 cell lines, highlight the great heterogeneity that characterises this tumour and the relevance of using a proper preclinical model to find new therapies for treating glioblastoma, as well as it emphasis the need to identify new therapies and biomarkers able to provide more personalised treatments for these patients.

BIBLIOGRAPHY

1. Versteeg HH, Heemskerk JWM, Levi M, Reitsma PH. New Fundamentals in hemostasis. *Physiol. Rev.* 2013;93(1):327–358.
2. Rezaie AR, Giri H. Anticoagulant and signaling functions of antithrombin. *J. Thromb. Haemost.* 2020;18(12):3142–3153.
3. Martińez-Martínez I, Navarro-Fernández J, Østergaard A, et al. Amelioration of the severity of heparin-binding antithrombin mutations by posttranslational mosaicism. *Blood*. 2012;120(4):900–904.
4. Águila S, Izaguirre G, Martínez-Martínez I, et al. Disease-causing mutations in the serpin antithrombin reveal a key domain critical for inhibiting protease activities. *J. Biol. Chem.* 2017;292(40):16513–16520.
5. Corral J, de la Morena-Barrio ME, Vicente V. The genetics of antithrombin. *Thromb. Res.* 2018;169:23–29.
6. Águila S, Navarro-Fernández J, Bohdan N, et al. Role of the C-sheet in the maturation of N-glycans on antithrombin: functional relevance of pleiotropic mutations. *J. Thromb. Haemost.* 2014;12(7):1131–1140.
7. Águila S, Noto R, Luengo-Gil G, et al. N-Glycosylation as a Tool to Study Antithrombin Secretion, Conformation, and Function. *Int. J. Mol. Sci.* 2021;22(2):1–12.
8. Silverman GA, Bird PI, Carrell RW, et al. The serpins are an expanding superfamily of structurally similar but functionally diverse proteins. Evolution, mechanism of inhibition, novel functions, and a revised nomenclature. *J. Biol. Chem.* 2001;276(36):33293–33296.
9. Olson ST, Shore JD. Demonstration of a two-step reaction mechanism for inhibition of alpha-thrombin by antithrombin III and identification of the step affected by heparin. *J. Biol. Chem.* 1982;257(24):14891–14895.
10. Roth R, Swanson R, Izaguirre G, et al. Saturation Mutagenesis of the Antithrombin Reactive Center Loop P14 Residue Supports a Three-step Mechanism of Heparin Allosteric Activation Involving Intermediate and Fully Activated States. *J. Biol. Chem.* 2015;290(47):28020–28036.
11. Kearon C, Akl EA, Comerota AJ, et al. Antithrombotic therapy for VTE disease: Antithrombotic Therapy and Prevention of Thrombosis, 9th ed: American College of Chest Physicians Evidence-Based Clinical Practice Guidelines. *Chest*. 2012;141(2 Suppl):e419S-e496S.
12. Whisstock JC, Bottomley SP. Molecular gymnastics: serpin structure, folding and misfolding. *Curr. Opin. Struct. Biol.* 2006;16(6):761–768.
13. de la Morena-Barrio M, Sandoval E, Llamas P, et al. High levels of latent antithrombin in plasma from patients with antithrombin deficiency. *Thromb. Haemost.* 2017;117(5):880–888.
14. O'Reilly MS, Pirie-Shepherd S, Lane WS, Folkman J. Antiangiogenic activity of the cleaved conformation of the serpin antithrombin. *Science (80-.).*

1999;285(5435):1926–1928.
15. Larsson H, Åkerud P, Nordling K, et al. A Novel Anti-angiogenic Form of Antithrombin with Retained Proteinase Binding Ability and Heparin Affinity. *J. Biol. Chem.* 2001;276(15):11996–12002.
16. Richard B, Swanson R, Schedin-Weiss S, et al. Characterization of the conformational alterations, reduced anticoagulant activity, and enhanced antiangiogenic activity of prelatent antithrombin. *J. Biol. Chem.* 2008;283(21):14417–14429.
17. Liu ZL, Chen HH, Zheng LL, Sun LP, Shi L. Angiogenic signaling pathways and anti-angiogenic therapy for cancer. *Signal Transduct. Target. Ther.* 2023;8(1):198.
18. Martinelli I, Mannucci PM, De Stefano V, et al. Different Risks of Thrombosis in Four Coagulation Defects Associated With Inherited Thrombophilia: A Study of 150 Families. *Blood*. 1998;92(7):2353–2358.
19. H Barnes D. Antithrombin deficiency. *Medscapescape*. 2022;
20. Yang L, Dinarvand P, Qureshi SH, Rezaie AR. Engineering D-Helix of Antithrombin in Alpha-1-proteinase Inhibitor Confers Antiinflammatory Properties on the Chimeric Serpin. *Thromb. Haemost.* 2014;112(1):164–175.
21. Warren BL, Eid A, Singer P, et al. High-Dose Antithrombin III in Severe Sepsis: A Randomized Controlled Trial. *JAMA*. 2001;286(15):1869–1878.
22. Hoffman JN, Wiedermann CJ, Juers M, et al. Benefit/risk profile of high-dose antithrombin in patients with severe sepsis treated with and without concomitant heparin. *Thromb. Haemost.* 2006;95(5):850–856.
23. Kienast J, Juers M, Wiedermann CJ, et al. Treatment effects of high-dose antithrombin without concomitant heparin in patients with severe sepsis with or without disseminated intravascular coagulation. *J. Thromb. Haemost.* 2006;4(1):90–97.
24. Horie S, Ishii H, Kazama M. Heparin-like glycosaminoglycan is a receptor for antithrombin III-dependent but not for thrombin-dependent prostacyclin production in human endothelial cells. *Thromb. Res.* 1990;59(6):895–904.
25. Harada N, Okajima K, Kushimoto S, Isobe H, Tanaka K. Antithrombin Reduces Ischemia/Reperfusion Injury of Rat Liver by Increasing the Hepatic Level of Prostacyclin. *Blood*. 1999;93(1):157–164.
26. Kaneider NC, Reinisch CM, Dunzendorfer S, Römisch J, Wiederman CJ. Syndecan-4 mediates antithrombin-induced chemotaxis of human peripheral blood lymphocytes and monocytes. *J. Cell Sci.* 2002;115(Pt 1):227–236.
27. Bae JS, Rezaie AR. Mutagenesis studies toward understanding the intracellular signaling mechanism of antithrombin. *J. Thromb. Haemost.* 2009;7(5):803–810.
28. Oelschläger C, Römisch J, Staubitz A, et al. Antithrombin III inhibits nuclear factor κB activation in human monocytes and vascular endothelial cells. *Blood*. 2002;99(11):4015–4020.
29. Praveen P, Madlen R, Femke DH, et al. A human antithrombin isoform dampens inflammatory responses and protects from organ damage during bacterial infection. *Nat. Microbiol.* 2019;4(12):2442–2455.

30. Huang C-Y, Sheen-Chen S-M, Ho H-T, Tang R-P, Eng H-L. Antithrombin-III attenuates hepatocyte apoptosis in bile duct ligated rat: a striking cellular change. *Surg. Innov.* 2010;17(2):132–135.
31. Guerrero JA, Teruel R, Martínez C, et al. Protective role of antithrombin in mouse models of liver injury. *J. Hepatol.* 2012;57(5):980–986.
32. Geiben-Lynn R, Brown N, Walker BD, Luster AD. Purification of a modified form of bovine antithrombin III as an HIV-1 CD8+ T-cell antiviral factor. *J. Biol. Chem.* 2002;277(44):42352–42357.
33. Elmaleh DR, Brown N V., Geiben-Lynn R. Anti-viral activity of human antithrombin III. *Int. J. Mol. Med.* 2005;16(2):191–200.
34. Asmal M, Seaman M, Lin W, et al. Inhibition of HCV by the serpin antithrombin III. *Virol. J.* 2012;9(1):1–10.
35. Prox D, Becker C, Pirie-Shepherd SR, et al. Treatment of human pancreatic cancer in mice with angiogenic inhibitors. *World J. Surg.* 2003;27(4):405–411.
36. O'Reilly MS. Antiangiogenic antithrombin. *Semin. Thromb. Hemost.* 2007;33(7):660–666.
37. Luengo-Gil G, Calvo MI, Martín-Villar E, et al. Antithrombin controls tumor migration, invasion and angiogenesis by inhibition of enteropeptidase. *Sci. Rep.* 2016;6(1):1–14.
38. Zhang W, Swanson R, Izaguirre G, et al. The heparin-binding site of antithrombin is crucial for antiangiogenic activity. *Blood*. 2005;106(5):1621–1628.
39. Larsson H, Sjöblom T, Dixelius J, et al. Antiangiogenic effects of latent antithrombin through perturbed cell-matrix interactions and apoptosis of endothelial cells - PubMed. *Cancer Res.* 2000;60(23):6723–6729.
40. Zhang W, Chuang Y-J, Jin T, et al. Antiangiogenic antithrombin induces global changes in the gene expression profile of endothelial cells. *Cancer Res.* 2006;66(10):5047–5055.
41. Zhang W, Swanson R, Xiong Y, Richard B, Olson ST. Antiangiogenic antithrombin blocks the heparan sulfate-dependent binding of proangiogenic growth factors to their endothelial cell receptors: Evidence for differential binding of antiangiogenic and anticoagulant forms of antithrombin to proangiogenic hepa. *J. Biol. Chem.* 2006;281(49):37302–37310.
42. Ostrom QT, Cioffi G, Waite K, Kruchko C, Barnholtz-Sloan JS. CBTRUS Statistical Report: Primary Brain and Other Central Nervous System Tumors Diagnosed in the United States in 2014-2018. *Neuro. Oncol.* 2021;23(12 Suppl 2):III1–III105.
43. Wesseling P, Kros JM, Jeuken JWM. The pathological diagnosis of diffuse gliomas: towards a smart synthesis of microscopic and molecular information in a multidisciplinary context. *Diagnostic Histopathol.* 2011;17(11):486–494.
44. Ferguson S, Lesniak MS. Percival Bailey and the classification of brain tumors. *Neurosurg. Focus*. 2005;18(4):.
45. Louis DN, Perry A, Burger P, et al. International Society of Neuropathology-Haarlem Consensus Guidelines for Nervous System Tumor Classification and

Grading. *Brain Pathol.* 2014;24(5):429–435.
46. Louis DN, Perry A, Reifenberger G, et al. The 2016 World Health Organization Classification of Tumors of the Central Nervous System: a summary. *Acta Neuropathol.* 2016;131(6):803–20.
47. Ohgaki H, Kleihues P. The definition of primary and secondary glioblastoma. *Clin. Cancer Res.* 2013;19(4):764–772.
48. Van Meir EG, Hadjipanayis CG, Norden AD, et al. Exciting New Advances in Neuro-Oncology: The Avenue to a Cure for Malignant Glioma. *CA. Cancer J. Clin.* 2010;60(3):166–193.
49. Pearson JRD, Regad T. Targeting cellular pathways in glioblastoma multiforme. *Signal Transduct. Target. Ther.* 2017;2(17040):.
50. Kreatsoulas D, Bolyard C, Wu BX, et al. Translational landscape of glioblastoma immunotherapy for physicians: guiding clinical practice with basic scientific evidence. *J. Hematol. Oncol.* 2022;15(80):.
51. A. McDowell K, J. Riggins G, L. Gallia G. Targeting the AKT Pathway in Glioblastoma. *Curr. Pharm. Des.* 2011;17(23):2411–2420.
52. Rong L, Li N, Zhang Z. Emerging therapies for glioblastoma: current state and future directions. *J. Exp. Clin. Cancer Res.* 2022;41(1):142.
53. Yang L-J, Zhou C-F, Lin Z-X. Temozolomide and radiotherapy for newly diagnosed glioblastoma multiforme: a systematic review. *Cancer Invest.* 2014;32(2):31–36.
54. Cruz Da Silva E, Mercier M-C, Etienne-Selloum N, Dontenwill M, Choulier L. A systematic review of glioblastoma-targeted therapies in phases II, III, IV clinical trials. *Cancers (Basel).* 2021;13(8):1–60.
55. Yung WK, Shapiro JR, Shapiro WR. Heterogeneous chemosensitivities of subpopulations of human glioma cells in culture. *Cancer Res.* 1982;42(3):992–998.
56. Iurlaro R, Waldhauer I, Planas-Rigol E, et al. A Novel EGFRvIII T-Cell Bispecific Antibody for the Treatment of Glioblastoma. *Mol. Cancer Ther.* 2022;21(10):1499–1509.
57. Bonavia R, Inda M-D-M, Cavenee WK, Furnari FB. Heterogeneity maintenance in glioblastoma: a social network. *Cancer Res.* 2011;71(12):4055–4060.
58. Cuddapah VA, Robel S, Watkins S, Sontheimer H. A neurocentric perspective on glioma invasion. *Nat. Rev. Neurosci.* 2014;15(7):455–465.
59. Vollmann-Zwerenz A, Leidgens V, Feliciello G, Klein CA, Hau P. Tumor Cell Invasion in Glioblastoma. *Int. J. Mol. Sci.* 2020;21(6):1932.
60. So J-S, Kim H, Han K-S. Mechanisms of Invasion in Glioblastoma: Extracellular Matrix, Ca2+ Signaling, and Glutamate. *Front. Cell. Neurosci.* 2021;15:663092.
61. Lathia JD, Mack SC, Mulkearns-Hubert EE, Valentim CLL, Rich JN. Cancer stem cells in glioblastoma. *Genes Dev.* 2015;29(12):1203–1217.
62. Ortensi B, Setti M, Osti D, Pelicci G. Cancer stem cell contribution to glioblastoma invasiveness. *Stem Cell Res. Ther.* 2013;4(1):18.
63. Koso H, Takeda H, Yew CCK, et al. Transposon mutagenesis identifies genes that transform neural stem cells into glioma-initiating cells. *Proc. Natl. Acad. Sci.*

U. S. A. 2012;109(44):E2998-3007.
64. Arvanitis CD, Ferraro GB, Jain RK. The blood–brain barrier and blood–tumour barrier in brain tumours and metastases. *Nat. Rev. Cancer*. 2019;20:26–41.
65. Agarwala SS, Kirkwood JM. Temozolomide, a novel alkylating agent with activity in the central nervous system, may improve the treatment of advanced metastatic melanoma. *Oncologist*. 2000;5(2):144–151.
66. Chen H-M, Teng H-W. The Advantage of Bevacizumab in Treating Colorectal Brain Metastasis. *J. Cancer Res. Pract.* 2014;1(2):146–151.
67. Sarkaria JN, Hu LS, Parney IF, et al. Is the blood-brain barrier really disrupted in all glioblastomas? A critical assessment of existing clinical data. *Neuro. Oncol.* 2018;20(2):184–191.
68. van Solinge TS, Nieland L, Chiocca EA, Broekman MLD. Advances in local therapy for glioblastoma - taking the fight to the tumour. *Nat. Rev. Neurol.* 2022;18(4):221–236.
69. Daniel J B, Amilcar C-S, Balveen K, Erwin G VM. Genetic and biologic progression in astrocytomas and their relation to angiogenic dysregulation. *Adv. Anat. Pathol.* 2002;9(1):24–36.
70. Sunit D, Philip A M. Angiogenesis in glioblastoma. *N. Engl. J. Med.* 2013;369(16):1561–1563.
71. Ahir BK, Engelhard HH, Lakka SS. Tumor Development and Angiogenesis in Adult Brain Tumor: Glioblastoma. *Mol. Neurobiol.* 2020;57(5):2461–2478.
72. Monteiro AR, Hill R, Pilkington GJ, Madureira PA. The Role of Hypoxia in Glioblastoma Invasion. *Cells*. 2017;6(4):45.
73. Seano G, Jain RK. Vessel co-option in glioblastoma: emerging insights and opportunities. *Angiogenesis*. 2020;23(1):9–16.
74. Bugge TH, Antalis TM, Wu Q. Type II transmembrane serine proteases. *J. Biol. Chem.* 2009;284(35):23177–23181.
75. Choi S-Y, Bertram S, Glowacka I, Park YW, Pöhlmann S. Type II transmembrane serine proteases in cancer and viral infections. *Trends Mol. Med.* 2009;15(7):303–312.
76. Makarova AM, Gorbacheva LR, Savinkova I V., et al. Effect of enteropeptidase on survival of cultured hippocampal neurons under conditions of glutamate toxicity. *Biochemistry. (Mosc).* 2010;75(9):1153–1159.
77. Karlsson G, Winge S. Separation of latent, prelatent, and native forms of human antithrombin by heparin affinity high-performance liquid chromatography. *Protein Expr. Purif.* 2004;33(2):339–345.
78. Karlsson G. Pasteurization of antithrombin without generation of the prelatent form of antithrombin. *Protein Expr. Purif.* 2004;35(2):381–386.
79. Shergalis A, Bankhead 3rd A, Luesakul U, Muangsin N, Neamati N. Current challenges and opportunities in treating glioblastomas. *Pharmacol. Rev.* 2018;70(3):412–445.
80. Peñas-Martínez J, Luengo-Gil G, Espín S, et al. Anti-Tumor Functions of Prelatent Antithrombin on Glioblastoma Multiforme Cells. *Biomedicines*. 2021;9(5):.

81. Bohdan N, Espín S, Águila S, et al. Heparanase Activates Antithrombin through the Binding to Its Heparin Binding Site. *PLoS One*. 2016;11(6):.
82. Mushunje A, Evans G, Brennan SO, Carrell RW, Zhou A. Latent antithrombin and its detection, formation and turnover in the circulation. *J. Thromb. Haemost.* 2004;2(12):2170–2177.
83. Langdown J, Belzar KJ, Savory WJ, Baglin TP, Huntington JA. The critical role of hinge-region expulsion in the induced-fit heparin binding mechanism of antithrombin. *J. Mol. Biol.* 2009;386(5):1278–1289.
84. Vleeschouwer S De, Bergers G. Glioblastoma: To Target the Tumor Cell or the Microenvironment? *Exon Publ.* 2017;315–340.
85. Kamal S S, Sherene L, Evandro de A, et al. Targeting the PI3K/AKT/mTOR and Raf/MEK/ERK pathways in the treatment of breast cancer. *Cancer Treat. Rev.* 2013;39(8):935–946.
86. Xie B, Zhang L, Hu W, et al. Dual blockage of STAT3 and ERK1/2 eliminates radioresistant GBM cells. *Redox Biol.* 2019;24(101189):.
87. Aigner P, Just V, Stoiber D. STAT3 isoforms: Alternative fates in cancer? *Cytokine*. 2019;118:27–34.
88. Zaragoza-Huesca D, Nieto-Olivares A, García-Molina F, et al. Implication of Hepsin from Primary Tumor in the Prognosis of Colorectal Cancer Patients. *Cancers 2022, Vol. 14, Page 3106*. 2022;14(13):3106.
89. Rodenas MC, Peñas-Martínez J, Pardo-Sánchez I, et al. Venetoclax is a potent hepsin inhibitor that reduces the metastatic and prothrombotic phenotypes of hepsin-expressing colorectal cancer cells. *Front. Mol. Biosci.* 2023;10:1182925.
90. Guilian N, Kenneth L W, Mei H, et al. Constitutive Stat3 activity up-regulates VEGF expression and tumor angiogenesis. *Oncogene*. 2002;21(13):2000–2008.
91. Chinot OL, Wick W, Mason W, et al. Bevacizumab plus radiotherapy-temozolomide for newly diagnosed glioblastoma. *N. Engl. J. Med.* 2014;370(8):709–722.
92. De Groot JF, Fuller G, Kumar AJ, et al. Tumor invasion after treatment of glioblastoma with bevacizumab: Radiographic and pathologic correlation in humans and mice. *Neuro. Oncol.* 2010;12(3):233–242.
93. Ouédraogo ZG, Biau J, Kemeny J-L, et al. Role of STAT3 in Genesis and Progression of Human Malignant Gliomas. *Mol. Neurobiol.* 2017;54(8):5780–5797.
94. Priego N, Zhu L, Monteiro C, et al. STAT3 labels a subpopulation of reactive astrocytes required for brain metastasis. *Nat. Med.* 2018;24(7):1024–1035.
95. de Groot J, Liang J, Kong LY, et al. Modulating antiangiogenic resistance by inhibiting the signal transducer and activator of transcription 3 pathway in glioblastoma. *Oncotarget*. 2012;3(9):1036–1048.
96. Han D, Yu T, Dong N, et al. Napabucasin, a novel STAT3 inhibitor suppresses proliferation, invasion and stemness of glioblastoma cells. *J. Exp. Clin. Cancer Res.* 2019;38(1):289.
97. Mason WP, Robles P de, Borodyansky L, et al. BBI608-201GBM: A phase Ib/II clinical study of napabucasin (BBI608) in combination with temozolomide

(TMZ) for adult patients with recurrent glioblastoma (GBM). *J. Clin. Oncol.* 2017;35(15_suppl):e13525–e13525.
98. Wang Z. Regulation of Cell Cycle Progression by Growth Factor-Induced Cell Signaling. *Cells*. 2021;10(12):3327.
99. Hanahan D, Weinberg RA. Hallmarks of cancer: the next generation. *Cell*. 2011;144(5):646–674.
100. Bertl E, Bartsch H, Gerhäuser C. Inhibition of angiogenesis and endothelial cell functions are novel sulforaphane-mediated mechanisms in chemoprevention. *Mol. Cancer Ther.* 2006;5(3):575–585.
101. Riemenschneider MJ, Jeuken JWM, Wesseling P, Reifenberger G. Molecular diagnostics of gliomas: state of the art. *Acta Neuropathol.* 2010;120(5):567–584.
102. Gladson CL, Prayson RA, Liu WM. The pathobiology of glioma tumors. *Annu. Rev. Pathol.* 2010;5:33–50.
103. Bouzari B, Mohammadi S, Bokov DO, et al. Angioregulatory role of miRNAs and exosomal miRNAs in glioblastoma pathogenesis. *Biomed. Pharmacother.* 2022;148:112760.
104. Zapata-Martínez L, Águila S, de los Reyes-García AM, et al. Inflammatory microRNAs in cardiovascular pathology: another brick in the wall. *Front. Immunol.* 2023;14:1196104.
105. Rezaei O, Honarmand K, Nateghinia S, Taheri M, Ghafouri-Fard S. miRNA signature in glioblastoma: Potential biomarkers and therapeutic targets. *Exp. Mol. Pathol.* 2020;117:104550.
106. Makowska M, Smolarz B, Romanowicz H. microRNAs (miRNAs) in Glioblastoma Multiforme (GBM)-Recent Literature Review. *Int. J. Mol. Sci.* 2023;24(4):3521.
107. Lei Q, Yang Y, Zhou W, et al. MicroRNA-based therapy for glioblastoma: Opportunities and challenges. *Eur. J. Pharmacol.* 2023;938:175388.
108. Attwooll C, Denchi EL, Helin K. The E2F family: specific functions and overlapping interests. *EMBO J.* 2004;23(24):4709–4716.
109. Burke JR, Liban TJ, Restrepo T, Lee H-W, Rubin SM. Multiple mechanisms for E2F binding inhibition by phosphorylation of the retinoblastoma protein C-terminal domain. *J. Mol. Biol.* 2014;426(1):245–255.
110. Michaud K, Solomon DA, Oermann E, et al. Pharmacologic inhibition of cyclin-dependent kinases 4 and 6 arrests the growth of glioblastoma multiforme intracranial xenografts. *Cancer Res.* 2010;70(8):3228–3238.
111. Sun Y-M, Zhang Y-M, Shi H-L, et al. Enhancer-driven transcription of MCM8 by E2F4 promotes ATR pathway activation and glioma stem cell characteristics. *Hereditas*. 2023;160(1):29.
112. Couturier CP, Ayyadhury S, Le PU, et al. Single-cell RNA-seq reveals that glioblastoma recapitulates a normal neurodevelopmental hierarchy. *Nat. Commun.* 2020;11(1):3406.
113. Yin D, Zhou H, Kumagai T, et al. Proteasome inhibitor PS-341 causes cell growth arrest and apoptosis in human glioblastoma multiforme (GBM). *Oncogene*. 2005;24(3):344–354.

114. Riess C, Irmscher N, Salewski I, et al. Cyclin-dependent kinase inhibitors in head and neck cancer and glioblastoma-backbone or add-on in immune-oncology? *Cancer Metastasis Rev.* 2021;40(1):153–171.
115. Tachon G, Cortes U, Guichet P-O, et al. Cell Cycle Changes after Glioblastoma Stem Cell Irradiation: The Major Role of RAD51. *Int. J. Mol. Sci.* 2018;19(10):3018.
116. Li H, Lei B, Xiang W, et al. Differences in Protein Expression between the U251 and U87 Cell Lines. *Turk. Neurosurg.* 2017;27(6):894–903.
117. Kounnas MZ, Church FC, Argraves WS, Strickland DK. Cellular internalization and degradation of antithrombin III-thrombin, heparin cofactor II-thrombin, and alpha 1-antitrypsin-trypsin complexes is mediated by the low density lipoprotein receptor-related protein. *J. Biol. Chem.* 1996;271(11):6523–6529.
118. Bres EE, Faissner A. Low density receptor-related protein 1 interactions with the extracellular matrix: More than meets the eye. *Front. Cell Dev. Biol.* 2019;7:31.
119. Yi Y, Hsieh I-Y, Huang X, Li J, Zhao W. Glioblastoma Stem-Like Cells: Characteristics, Microenvironment, and Therapy. *Front. Pharmacol.* 2016;7:477.
120. Verhaak RGW, Hoadley KA, Purdom E, et al. Integrated genomic analysis identifies clinically relevant subtypes of glioblastoma characterized by abnormalities in PDGFRA, IDH1, EGFR, and NF1. *Cancer Cell*. 2010;17(1):98–110.
121. Breznik B, Motaln H, Vittori M, Rotter A, Turnšek TL. Mesenchymal stem cells differentially affect the invasion of distinct glioblastoma cell lines. *Oncotarget*. 2017;8(15):25482–25499.
122. Lee J, Kotliarova S, Kotliarov Y, et al. Tumor stem cells derived from glioblastomas cultured in bFGF and EGF more closely mirror the phenotype and genotype of primary tumors than do serum-cultured cell lines. *Cancer Cell*. 2006;9(5):391–403.
123. Torsvik A, Stieber D, Enger PO, et al. U-251 revisited: genetic drift and phenotypic consequences of long-term cultures of glioblastoma cells. *Cancer Med.* 2014;3(4):812–824.
124. Gunti S, Hoke ATK, Vu KP, London NR. Organoid and Spheroid Tumor Models: Techniques and Applications. *Cancers (Basel).* 2021;13(4):874.
125. Silvia N, Dai G. Cerebral organoids as a model for glioblastoma multiforme. *Curr. Opin. Biomed. Eng.* 2020;13:152–159.
126. Klein E, Hau A-C, Oudin A, Golebiewska A, Niclou SP. Glioblastoma Organoids: Pre-Clinical Applications and Challenges in the Context of Immunotherapy. *Front. Oncol.* 2020;10:604121.
127. Cerneckis J, Cai H, Shi Y. Induced pluripotent stem cells (iPSCs): molecular mechanisms of induction and applications. *Signal Transduct. Target. Ther.* 2024;9(1):112.
128. Eichmüller OL, Knoblich JA. Human cerebral organoids - a new tool for clinical neurology research. *Nat. Rev. Neurol.* 2022;18(11):661–680.
129. Lancaster MA, Knoblich JA. Generation of cerebral organoids from human pluripotent stem cells. *Nat. Protoc.* 2014;9(10):2329–2340.

130. Sun N, Meng X, Liu Y, et al. Applications of brain organoids in neurodevelopment and neurological diseases. *J. Biomed. Sci.* 2021;28(1):30.
131. Goranci-Buzhala G, Mariappan A, Gabriel E, et al. Rapid and Efficient Invasion Assay of Glioblastoma in Human Brain Organoids. *Cell Rep.* 2020;31(10):.
132. Laso-García F, Casado-Fernández L, Piniella D, et al. Circulating extracellular vesicles promote recovery in a preclinical model of intracerebral hemorrhage. *Mol. Ther. Nucleic Acids*. 2023;32:247–262.
133. Pazos-Pérez A, Piñeiro-Ramil M, Franco-Trepat E, et al. The Hepatokine RBP4 Links Metabolic Diseases to Articular Inflammation. *Antioxidants (Basel, Switzerland)*. 2024;13(1):124.
134. Ferrier A, Boyer JG, Kothary R. Cellular and Molecular Biology of Neuronal Dystonin. *Int. Rev. Cell Mol. Biol.* 2013;300:85–120.
135. Lynch-Godrei A, Kothary R. HSAN-VI: A spectrum disorder based on dystonin isoform expression. *Neurol. Genet.* 2020;6(1):e389.
136. Künzli K, Favre B, Chofflon M, Borradori L. One gene but different proteins and diseases: the complexity of dystonin and bullous pemphigoid antigen 1. *Exp. Dermatol.* 2016;25(1):10–16.
137. Qiu X, Li X, Yan Y, et al. Identification of m6A-Associated Gene DST as a Prognostic and Immune-Associated Biomarker in Breast Cancer Patients. *Int. J. Gen. Med.* 2022;15:523–534.
138. Jain PB, Guerreiro PS, Canato S, Janody F. The spectraplakin Dystonin antagonizes YAP activity and suppresses tumourigenesis. *Sci. Rep.* 2019;9(1):1–17.
139. Leick KM, Rodriguez AB, Melssen MM, et al. The Barrier Molecules Junction Plakoglobin, Filaggrin, and Dystonin Play Roles in Melanoma Growth and Angiogenesis. *Ann. Surg.* 2019;270(4):712–722.
140. Fazavana JG, Muczynski V, Proulle V, et al. LDL receptor-related protein 1 contributes to the clearance of the activated factor VII-antithrombin complex. *J. Thromb. Haemost.* 2016;14(12):2458–2470.
141. Luengo-Gil G, García-Andreo AB, Ortega-Sabater C, et al. Antithrombin is incorporated into exosomes produced by antithrombin non-expressing cells. *Biochimie*. 2019;165:245–249.
142. Vellucci A, Leibovitch EC, Jacobson S. Using Droplet Digital PCR to Detect Coinfection of Human Herpesviruses 6A and 6B (HHV-6A and HHV-6B) in Clinical Samples. *Methods Mol. Biol.* 2018;1768:99–109.
143. Slika H, Karimov Z, Alimonti P, et al. Preclinical Models and Technologies in Glioblastoma Research: Evolution, Current State, and Future Avenues. *Int. J. Mol. Sci.* 2023;24(22):16316.
144. Kaptein FHJ, Stals MAM, Kapteijn MY, et al. Incidence and determinants of thrombotic and bleeding complications in patients with glioblastoma. *J. Thromb. Haemost.* 2022;20(7):1665–1673.
145. Perry JR, Rogers L, Laperriere N, et al. PRODIGE: A phase III randomized placebo-controlled trial of thromboprophylaxis using dalteparin low molecular weight heparin (LMWH) in patients with newly diagnosed malignant glioma. *J.*

Clin. Oncol. 2007;25(18_suppl):2011.
146. Nghiemphu P, Green RM, Pope WB, Lai A, Cloughesy TF. Safety of anticoagulation use and bevacizumab in patients with glioma. *Neuro. Oncol.* 2008;10(3):355–360.
147. Seidel C, Hentschel B, Simon M, et al. A comprehensive analysis of vascular complications in 3,889 glioma patients from the German Glioma Network. *J. Neurol.* 2013;260(3):847–855.
148. Brar HK, Jose J, Wu Z, Sharma M. Tyrosine Kinase Inhibitors for Glioblastoma Multiforme: Challenges and Opportunities for Drug Delivery. *Pharmaceutics*. 2022;15(1):59.